Improvement of Temperature Distribution across Thick Thermoset Composites Using Carbon Nanotubes

Pooya Rowghanian

A Thesis
in
The Department
of
Mechanical and Industrial Engineering

Presented in Partial Fulfillment of the Requirements
for the Degree of
Master of Applied Science (Mechanical Engineering) at
Concordia University
Montreal, Quebec, Canada

April 2012

CONCORDIA UNIVERSITY
School of Graduate Studies

This is to certify that the thesis prepared

By: **Pooya Rowghanian**

Entitled: **Improvement of Temperature Distribution across Thick Thermoset Composites Using Carbon Nanotubes**

and submitted in partial fulfillment of the requirements for the degree of

Master of Applied Science (Mechanical Engineering)

complies with the regulations of the university and meets the accepted standards with respect to originality and quality.

Signed by the final examining committee:

_____ Chair
Dr. Nadia Bhuiyan

_____ Examiner
Dr. Martin D. Pugh

_____ Examiner
Dr. Michelle Nokken
(Department of Building, Civil & Environmental Engineering)

_____ Supervisor
Dr. Suong Van Hoa

Approved by _____
Dr. A. K. Waizuddin Ahmed,
(MASc Program Director Department of Mechanical and Industrial Engineering)

_____
Dr. Robin Drew, (Dean of Faculty)

Date 17 April 2012

ABSTRACT

Improvement of Temperature Distribution Across Thick Thermoset Composites Using Carbon Nanotubes

POOYA ROWGHANIAN

The effect of adding carbon nanotubes (CNT) into epoxy on the temperature gradient in thick thermoset composites was studied and presented. Addition of CNT increases the thermal diffusivity of the resin and reduces the curing reaction speed. The latter slows down the rate of energy liberation, while the former helps to dissipate faster the released heat in the exothermic reaction. The results showed that the addition of up to 1 wt% CNT can reduce the difference between temperatures at the center and at the surface of 1.5-inch thick column of epoxy by 41%. Measured variations of heat capacity and thermal diffusivity by changes in both temperature and carbon nanotube contents as well as the empirically-evaluated cure kinetics of epoxy were used in a transient one-dimensional heat transfer finite difference model to determine the temperature distribution across thickness during the cure. Good agreement was obtained between calculated and experimental trends.

ACKNOWLEDGMENTS

I would like to express my sincere gratitude to Prof. Suong Van Hoa for introducing me to the world of composite materials. His availability, commitment and financial support throughout the course of this research were key factors to the realisation of this project, and his guidance helped me along my path to professional life.

I wish also to express my gratefulness to Dr. Iosif Daniel Rosca for his generosity in sharing knowledge and experience. Thanks are also due to Dr. Ming Xie and Mr. Heng Wang at CONCOM research group for sharing their expertise in laboratory works.

Special thanks to my life companion, Stephanie Brisson, for her courage and inspiration during the course of this research, and also, for proof reading the first draft of this thesis.

To my father

who taught me how to perceive,

and my mother

who taught me how to love.

TABLE OF CONTENTS

LIST OF FIGURES

LIST OF TABLES

NOMENCLATURE

c	Constant (K)
h	Convection heat transfer coefficient $(W/m^2.K)$
j	Imaginary unit $\sqrt{-1}$
k	Coefficient of thermal conductivity $(W/m.K)$
m	Order of reaction (unitless)
n	Order of reaction (unitless)
$\dot{q}_{gen}$	Rate of heat generation per unit volume (W/m^3)
t	Time variable (s)
$t_{T_{max}}$	The time at which maximum temperature occurs across the thickness of sample during the curing process (s)
$t_{\Delta T_{max}}$	The time at which the difference between the temperature of surface and midpoint of sample is maximum during the curing process (s)
x	Spatial variable (m)
B	Constant (unitless)
A_i	Frequency of pre-exponential factors for $i = 1, 2, 3$ $(1/s)$
Bi	Biot number (unitless)
C_p	Specific heat capacity $(J/kg.K)$
$E_{a,i}$	Activation energies for $i = 1, 2, 3$ (J/mol)
$\dot{E}_{gen}$	Rate of energy generation in a control volume (W)
$\dot{E}_{in}$	Rate of energy transfer input a control volume (W)
$\dot{E}_{st}$	Rate of change of energy stored within a control volume (W)

Fo Fourier number (unitless)

H_T Isothermal heat of reaction (J/kg)

H_t Generated heat in a reaction until time t (J/kg)

K_i Reaction rates as a function of temperature for $i = 1, 2, 3$ $(1/s)$

Q Instantaneous generated heat during isothermal scanning (J/kg)

R Universal gas constant (8.314 $J/mol.K$)

R_E Round-off error (K)

S Cross sectional area perpendicular to the thickness (m^2)

T Absolute temperature (K)

$\hat{T}$ Exact solution of the energy balance differential equation as a function of time and space (K)

T_∞ Absolute temperature of surrounding environment (K)

T_E truncation error (K)

T_m Absolute temperature at which the maximum curing rate occurs (K)

T_∞^p Absolute temperature of surrounding at time increment p (K)

T_i^p Absolute temperature of spatial increment i at time increment p (K)

T_{surf} Absolute temperature of surface of sample (K)

V Volume (m^3)

α Degree of cure (unitless)

α_i^p Degree of cure of spatial increment i at time increment p (unitless)

β Isothermal degree of cure (unitless)

γ Constant $(1/s)$

ε_i^p Error; difference between the solution of finite difference approximation

	and the exact solution of the differential equation at ith node and pth time increment (K)
λ	Thermal diffusivity (m^2/s)
ξ	Constant ($1/m$)
ρ	Density of the resin system (kg/m^3)
φ	Heating rate (K/s)
ΔH_R	Total heat of reaction (J/kg)
Δt	Duration of time increment (s)
Δx	Length of spatial increment (m)

Chapter 1: INTRODUCTION AND LITERATURE REVIEW

1.1. INTRODUCTION

The application of composite materials is expanding rapidly by the development of their manufacturing techniques. One of the limiting factors, however, in manufacturing thermoset composites is the exothermic chemical reaction which happens during the curing process between polymer, e.g. epoxy, and curing agent molecules. If the ratio between the exposed area of the laminate and the laminate volume is relatively large, the heat generated during the curing reaction will dissipate sufficiently fast to provide an acceptable uniform temperature distribution through the thickness of the laminate. On the other hand, if the laminate area to volume ratio is small, i.e. the laminate is considered thick, due to the low thermal conductivity of epoxy, the generated heat will not have enough time to exit the laminate, resulting in an increase in laminate temperature. Elevated temperatures will, in turn, accelerate the curing reaction which generates more heat. This chain of events can become a loop of heat generation leading to an uneven degree of cure distribution through the thickness. Residual stress is one of the direct consequences of non-uniform distribution of degree of

cure (Bogetti and Gillespie 1992). In the extreme scenario, heat accumulation in a laminate not only can result in internal degradation of material, but can also simply make the reaction run out of control.

The abovementioned problem is an important limiting factor for the thickness of the structures being manufactured from thermoset materials. However, if by some means, the thermal conductivity of the polymers can be improved so that they can dissipate the liberated heat during the curing process faster, this limiting factor can be pushed further back and structures with higher thickness can be designed and manufactured. This allows the remarkable properties of composites such as low specific weight to be applicable to a wider range of applications.

In recent years, the introduction of Carbon Nanotubes (CNTs) started to revolutionize the application of polymers due to their extraordinary properties and also by enabling researchers to modify the properties of polymers at the nano-scale. In particular, high thermal conductivity of carbon nanotubes is promising for enhancing the thermal conductivity of polymers. A recent comprehensive literature review on the main research works that studied the effect of CNTs on thermal conductivity of polymers supports this idea (Han and Fina 2011). For different materials, these studies have shown that although not as

significant as electrical conductivity, adding CNTs can enhance the thermal conductivity of polymers.

The potential for improving the thermal conductivity of thermosets by adding CNTs is the motivation of this thesis to take a deeper look into the introduction of CNTs in thermosets and their effects on temperature profile across the thickness of thick structures.

1.2. LITERATURE REVIEW

1.2.1. Synopsis

Energy generation happens because of the exothermic chemical reaction between the molecules of resin and curing agent during the curing process. Hence, the kinetics of this reaction needs to be understood. Section 1.2.2 is devoted to the literature about kinetics of curing reaction. Subsequently, studies on measurement and modeling of temperature profile through-the-thickness of thick thermoset laminates are reviewed in Section 1.2.3. Finally, the research works that considered the effects of CNTs on thermal conductivity and kinetics of curing process of epoxies are respectively explored in Sections 1.2.4 and 1.2.5.

1.2.2. Kinetics of curing reaction of epoxy

Understanding the cure kinetics of thermosetting materials has been of interest to researchers for many years. One of the most common methods to quantify the kinetics of curing reactions is by the Differential Scanning Calorimetry (DSC) test.

Many studies have focused on different types of thermosets and have tried different models to describe the cure kinetics to the best possible precision. Moreover, researchers have considered two major DSC data types: isothermal and dynamic tests. In an extensive study on Hercules 3501-6 which is a widely used resin in industry, the heat of reaction and degree of cure were measured using a differential scanning calorimeter. An expression based on Equation (1-1) was developed to correlate rate of cure, $d\alpha/dt$, and degree of cure, α, (Woo, Loos and Springer 1982).

$$\frac{d\alpha}{dt} = \begin{cases} (K_1 + K_2\alpha)(1-\alpha)(B-\alpha), & \alpha \leq 0.3 \\ K_3(1-\alpha), & \alpha > 0.3 \end{cases}$$
$$K_i = A_i e^{\left(-E_{a,i}/RT\right)}, \qquad i = 1, 2, 3 \tag{1-1}$$

In which, A_i are the pre-exponential factors, $E_{a,i}$ are the activation energies, R is the universal gas constant, B is a constant independent of temperature and T is absolute temperature. Additionally, viscosity of the resin was measured by a

plate-type viscometer and another expression was introduced to relate viscosity with degree of cure. In this study, both types of data from isothermal and dynamic scanning were used to determine the constants in Equation (1-1). The proposed model tends to predict the kinetics of the curing reaction rather close to the experimental values for Hercules 3501-6. The same authors, used this model in another study to develop a computer code for a flat-plate composite cured by a specified cure cycle, providing the temperature distribution, the degree of cure of the resin, the resin viscosity inside the composite, the void sizes, the temperatures and pressures inside voids, and the residual stress distribution after the cure (Loos and Springer 1983). The results of the model were in good agreement with the measurements of the temperature distribution in and the resin flow out of composites contracted from Hercules AS/3501-6 graphite epoxy prepreg tape.

Another study has considered Fiberite 976 resin and determined the heat of reaction, rate of cure and degree of cure, using isothermal scanning calorimetry (Dusi, et al. 1987). Here, dynamic scanning has been used to measure the total heat of reaction. The expression chosen to model the kinetics is shown in Equation (1-2) which is a generalized form of the autocatalytic reaction.

$$\frac{d\beta}{dt} = (K_1 + K_2\beta^m)(1-\beta)^n\,, \qquad K_i = A_i e^{\left(-\Delta E_i/RT\right)}, \qquad i = 1, 2 \tag{1-2}$$

Where, n and m are independent-of-temperature constants. $d\beta/dt$ is "isothermal" rate of cure which is defined as

$$\frac{d\beta}{dt} = \frac{1}{H_T}\left(\frac{dQ}{dt}\right)_T \tag{1-3}$$

In Equation (1-3), $\left(\frac{dQ}{dt}\right)_T$ is instantaneous rate of heat generation during isothermal scanning. The isothermal heat of reaction, H_T, is defined as the total amount of heat generated from initial time until no evidence is found of further reactions at a constant temperature. Isothermal rate of cure, $d\beta/dt$, is related to the rate of cure of reaction, $d\alpha/dt$, by Equation (1-4).

$$\frac{d\alpha}{dt} = \frac{H_T}{\Delta H_R}\frac{d\beta}{dt} \tag{1-4}$$

ΔH_R is the ultimate heat of reaction which is determined in a dynamic DSC test and is the total energy released from formation of bonds between all of the epoxy and curing agent chemical species. Here, the authors argue that the presence of catalysts in a resin system will not affect the type of model that quantifies the cure kinetics of the resin.

Similar research has been conducted on ICI Fiberite 977-3 and 977-2 thermosetting resins (Mantell, Ciriscioli and Almen 1995). However, here an n-th order model has been exploited for the curing kinetics, Equation (1-5).

$$\frac{d\alpha}{dt} = Ae^{\left(-E_a/RT\right)}(1-\alpha)^n \tag{1-5}$$

Where, A is pre-exponential factor and E_a is activation energy. In order to determine the constants of Equation (1-5) using several isothermal DSC tests (conventional thermal analysis), the authors suggested a method which requires only one DSC test run with a constant heating rate, yet is accurate.

In an extensive study, Málek et al. (1992) listed the most cited kinetic models and suggested an algorithm to select the most suitable model for a certain reaction. According to this study, a conventional thermal analysis method is reliable to determine the kinetic parameters especially for solid state transformation. Subsequently, the method proposed by Málek was validated for two different resin systems – diglycidyl ether of bisphenol A (DGEBA) and diglycidyl ether of hydroquinone (DGEHQ) with triethylenetetramine (TETA) as curing agent, using DSC tests with various heating rates (Roşu, et al. 2002). The agreement between the results predicted by the two-parameter autocatalytic model which was determined using these data and the experimental results from DSC

confirms Málek's approach in selecting the right model to describe cure kinetics.

One of the most cited methods using dynamic DSC test data to determine the constants of the autocatalytic kinetic model was proposed by Kissinger (1957). According to this method, the slope of $\ln(\varphi/{T_m}^2)$ versus $1/T_m$ relates to activation energy by Equation (1-6) in which φ is heating rate and T_m is the temperature at which the maximum curing rate occurs.

$$\frac{d\left(ln\frac{\varphi}{{T_m}^2}\right)}{d\left(\frac{1}{T_m}\right)} = -\frac{E_a}{R} \tag{1-6}$$

Kissinger's method has been verified in different studies for different epoxies, among all, for an epoxy-hexaanhydro-4-methylphthalicanhydride (MHHPA) system (Boey and Qiang 2000). Moreover, other research has shown that the error in calculating the activation energy using Kissinger's method will stay below 5% as long as the value of E_a/RT is greater than 10.0 (Criado and Ortega 1986).

Another research elaborated on the accuracy of different methods of determination of kinetic parameters (Sbirrazzuoli, Girault and Elégant 1995). An error was defined based on the difference between experimental and calculated

thermograms and was tried to be minimized in order to indicate the most accurate model.

For materials with temperature-dependent final degree of cure, e.g. AS4/3502 graphite/epoxy, the existing models were found to be inadequate (Shin and Hahn 2000). Instead, the authors introduce a technique which leads to more satisfactory results by normalizing the DSC data regardless of their type, i.e. isothermal or dynamic.

A more general procedure was considered in a different study which proposes using merely dynamic DSC data to determine the cure kinetics (Um, Daniel and Hwang 2002). It firstly suggests obtaining a relation between conversion and temperature at constant heating rate. According to the authors, it is easier to differentiate this relation with respect to time to determine the curing rate rather than using direct curve fitting among three variables (conversion, rate of cure and temperature).

Apart from this wide range of studies on modeling the cure kinetics, the American Society for Testing and Materials (ASTM) has regulated a remarkable series of test methods for typical materials. For instance, ASTM E 2070 indicates how to determine kinetic parameters using isothermal data (ASTM E 2070 2008)

or ASTM E 2041 has a procedure on estimating kinetic parameters using Borchardt and Daniels method (ASTM E 2041 2008).

1.2.3. Temperature profile of thick thermosets

Among the various studies on curing of thick thermoset composites, one research study combined a two-dimensional alternating direction explicit finite difference method with a generalized boundary condition formulation to predict temperature and degree of cure distributions as a function of the autoclave temperature history (Bogetti and Gillespie 1991). Here the authors could show the strong correlation between the spatial gradients in degree of cure and part geometry, thermal anisotropy, cure kinetics and the autoclave temperature cure cycle.

Another study considered glass-polyester and Hercules AS4/3501-6 graphite-epoxy composites (Yi, Hilton and Ahmad 1997, Yi and Hilton 1998). The curing kinetics for the latter was described by Equation (1-1) while a two-parameter autocatalytic model which formed the term of heat generation in the heat transfer equation was used for the former. Yi et al. (1997) used finite element analysis to solve this equation in three dimensions and develop a computer code which could take into account the temperature- and degree-of-cure-dependence of

material properties. Nevertheless, constant values were considered for material properties due to lack of experimental data in the studied cases. The researchers showed that temperature and degree of cure of thick laminates are considerably affected by the value of thermal conductivity. Therefore, thermal properties need to be measured accurately before being used in a numerical model.

Other investigators took advantage of well-developed pre- and post-processors of a general finite element software package (ANSYS) to prepare and demonstrate the user defined one-dimensional code which considered the tooling thickness as well as vacuum bagging thermal effect on the curing of thermosets (Guo, Du and Zhang 2005). In a parametric study, they considered the effect of convection coefficient of the autoclave air on temperature overshooting during the cure which showed that as the coefficient decreased, the temperature overshoot decreased while the time to reach the maximum temperature and the temperature difference from the autoclave air increased. A similar approach was taken by other researchers using a different general purpose finite element package (LUSYS) for a three-dimensional model (Joshi, Liu and Lam 1999). However, the kinetics of cure was expressed by an n-th order model similar to the one on Equation (1-5).

In another study, a finite element code was developed for the two-dimensional

cure simulation of thick composite structures (Park and Lee 2001). The obtained results were compared with the experimental results from Bogetti and Gillespie (1991) as well as Calius et al., (1990) and good agreement was observed. However, the overshoot was overestimated for cylinder and underestimated for flat plate in the cure simulation.

Yan also used a two-dimensional finite element model to simulate the curing of thick thermosets (2008). In this code, composite material was assumed to be transversely isotropic and the longitudinal and transverse thermal conductive coefficients were inserted into the code. The author argued that the heat transfer anisotropy had an important effect on temperature field. Moreover, a few numerical examples were given to prove the accuracy and effectiveness of the finite element formulation.

In another category of studies, the flow of the resin was considered at the same time to model the temperature and viscosity field of resin during the curing process. A study completed at Massachusetts Institute of Technology inspired a lot of similar studies in which the authors modelled resin flow using Darcy's Law for an anisotropic porous medium considering resin viscosity as a function of time only (Gutowski, Morigaki and Cai 1987). The model reflects three-dimensional flow and one-dimensional consolidation of the composite. They

applied the model to Compression Moulding and Bleeder Ply Moulding. A few years later, changes in viscosity with temperature change was considered in a one-dimensional finite difference model to simulate the flow of resin as well as temperature field for unidirectional Hercules AS-4/3501-6 graphite/epoxy composite laminates (Twardowski, Lin and Geil 1993).

Following many studies investigating the resin flow for different composite material process techniques, Davé proposed a model which could express the resin flow in the case of each technique; namely, autoclave processing, pultrusion and resin transfer moulding (1990). He showed that models for resin flow during composite processing in terms of Darcy's Law could be derived from a generalized theory which considers the effects of resin characteristics, porous media characteristics, and capillarity in porous media.

Considering the coupling between heat, cure kinetics, viscosity and flow, another study developed a model for the compression moulding technique (Hojjati and Hoa 1994). The authors achieved this goal by using squeezed sponge model to simulate the flow of resin in combination with heat conduction coupled with cure kinetics by the proposed model by Equation (1-1). They considered viscosity as a function of time and one spatial dimension and exploited a one-dimensional explicit finite difference method for their model.

Besides all these studies on temperature and flow field of thermosets during their curing process, there have been attempts to improve the problem of temperature overshooting in thick composite components. A typical approach has been modifying the curing cycle to minimize the peak temperature during the process. A manufacturing method called *continuous curing* was developed in which the material was cured continuously as it was laid up (Kim, et al. 1995). *Stage curing* was another technique studied shortly after, using the same concept of continuous curing technique with a slightly different method (White and Kim 1996). Steps of cooling and reheating were introduced into the curing cycle in another study which attempted to tackle the problem by trial and error (Kim and Lee 1997, Oh and Lee 2002).

A different approach was used to improve the temperature overshoot problem was to use on-line control systems to monitor the temperature or rate of curing, predict the maximum temperature and adjust the curing cycle in order for the peak temperature to stay an allowable range (Kalra, Perry and Lee 1992, Choi and Lee 1995, Parthasarathy, Mantell and Stelson 2004). In all these studies reducing the processing time has been of particular interest for researchers.

1.2.4. Effect of Carbon Nanotubes on thermal conductivity of polymers

Although the discovery date being a controversial issue among the scientists, carbon nanotubes became commercially available and attracted the attention of scientists and technologists from almost two decades ago (Monthioux and Kuznetsov 2006). Extraordinary properties of carbon nanotubes, e.g. high strength, high electrical and thermal conductivity, etc., explain the interest of researchers (Thostenson, Ren and Chou 2001).

Recently, there was a comprehensive review on thermal properties of carbon nanotubes and their polymer nano-composites (Han and Fina 2011). This review summarizes more than 300 different studies which have tried to deepen the understanding of thermal behaviour of carbon nanotubes. A quick assessment of this literature depicts a considerable scattering in the reported measurement data of thermal conductivity of polymers. Contradictory results are even found leading to the same scattering or to a contradiction in measurements of nano-composites thermal conductivity.

Different studies have shown that thermal conductivity of carbon nanotubes is exceptionally high, nevertheless, the scattering exists here, too. Berber et al.,

reported a very high value of 6600 *W/mK* for the thermal conductivity of an isolated nanotube at room temperature, comparable to the thermal conductivity of a hypothetical isolated graphene monolayer or diamond (Berber, Kwon and Tománek 2000). In another study, the thermal conductivity of a single wall carbon nanotube (SWCNT) was reported around 3500 *W/mK* at room temperature (Pop, et al. 2006).

Other researchers evaluated the thermal conduction mechanisms in carbon nanotube/epoxy composites (Gojny, et al. 2006). Instead of considering the phonon conduction mechanism inside carbon nanotubes, which is non-trivial, they simplified the heat conduction mechanism by assuming a general phonon mechanism to identify the general influential parameters on thermal conductivity of carbon nanotube/epoxy composites. Amongst all, authors studied the effect of different filler types as well as filler content on thermal conductivity of nano-composites. Figure 1-1 shows the result of this study in which EP, CB and DWCNT stand for epoxy, carbon black and double-wall carbon nanotube, respectively.

Gojny et al., also studied the effect of interfacial area between the fillers and epoxy on thermal conductivity. The overall size of the interface, the aspect ratio and the interfacial adhesion were identified as parameters dominating the

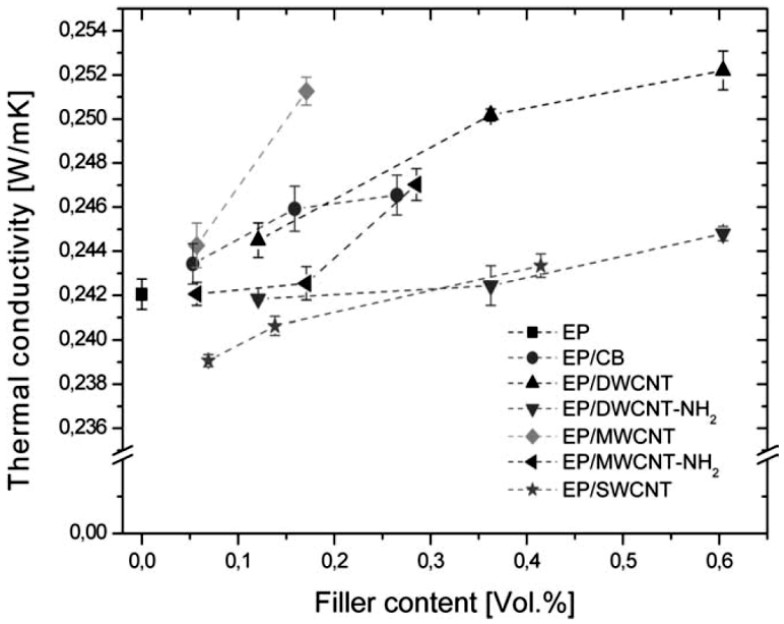

Figure 1-1: Thermal conductivity as function of filler content in vol% (Gojny, et al. 2006)

relative enhancement of the thermal conductivity.

Thermal conductivity of single and multiwall carbon nanotube/epoxy composites was studied elsewhere (Moisala, et al. 2006). The results are depicted in Figure 1-2. Introduction of MWCNTs in epoxy enhanced the thermal conductivity, however, SWCNTs tend to reduce the conductivity. Authors attributed this decrease in conductivity to a very large interface resistance to the heat flow associated with poor phonon coupling between the stiff nanotubes and the (relatively) soft polymer matrix.

However, these results from Moisala et al., contradicted another study which

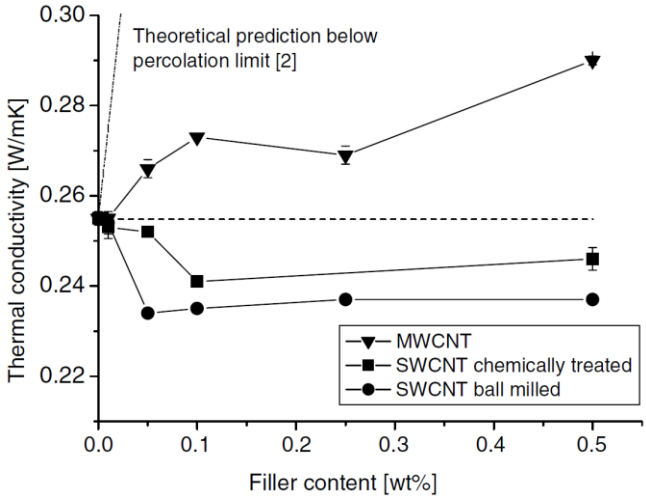

Figure 1-2: Thermal conductivity of composite materials as a function of carbon nanotube concentration. The dashed line represents the conductivity of pure epoxy (Moisala, et al. 2006)

showed the enhancement of thermal conductivity of carbon nanotube composites by adding SWCNTs (Biercuk, et al. 2002). Figure 1-3 illustrates that the thermal conductivity enhancement in single wall nanotube/epoxy samples rose more

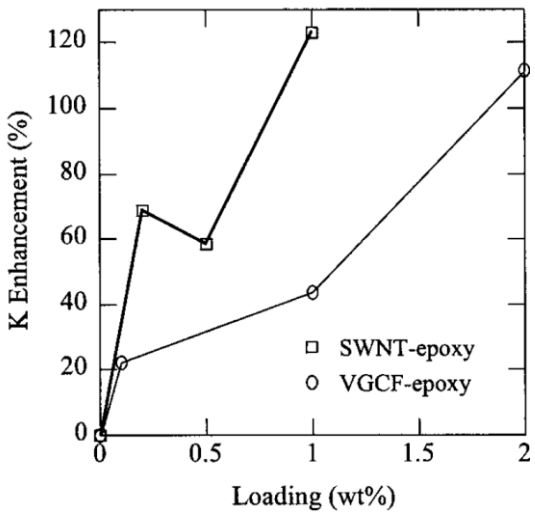

Figure 1-3: Enhancement in thermal conductivity relative to pristine epoxy as a function of SWNT and VGCF loading (Biercuk, et al. 2002)

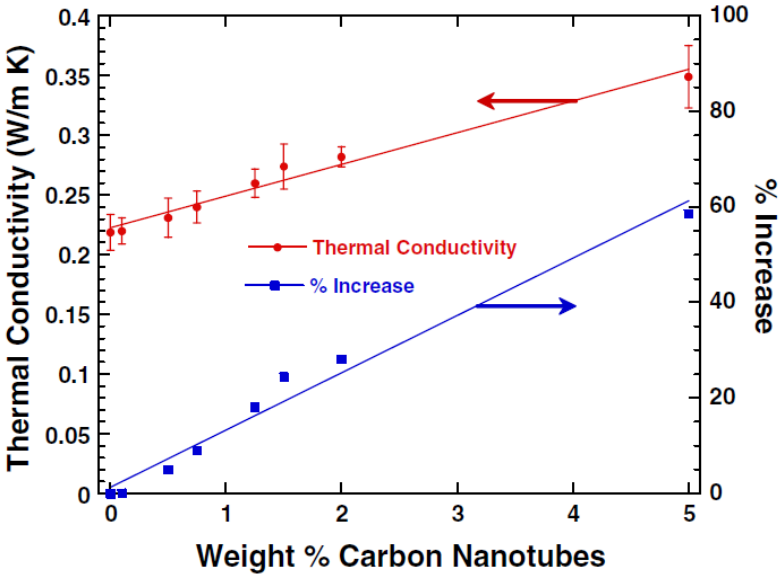

Figure 1-4: Influence of carbon nanotubes on composite thermal conductivity (Thostenson and Chou 2006)

rapidly than in vapour grown carbon fibers/epoxy samples by loading weight percentage.

Thostenson and Chou also investigated the influence of presence of carbon nanotubes in epoxy on thermal conductivity of the composite (2006). Figure 1-4 shows their results. The authors discuss that unlike electrical conductivity, where a sharp percolation threshold is seen, the increase in thermal conductivity with increasing nanotube concentration is nearly linear. The state of dispersion of carbon nanotubes in epoxy and its effect on thermal conductivity was also investigated. Authors used a calendaring technique to disperse carbon nanotubes in epoxy and showed that there was no statistical difference between the more highly dispersed and the agglomerated nano-composites. However,

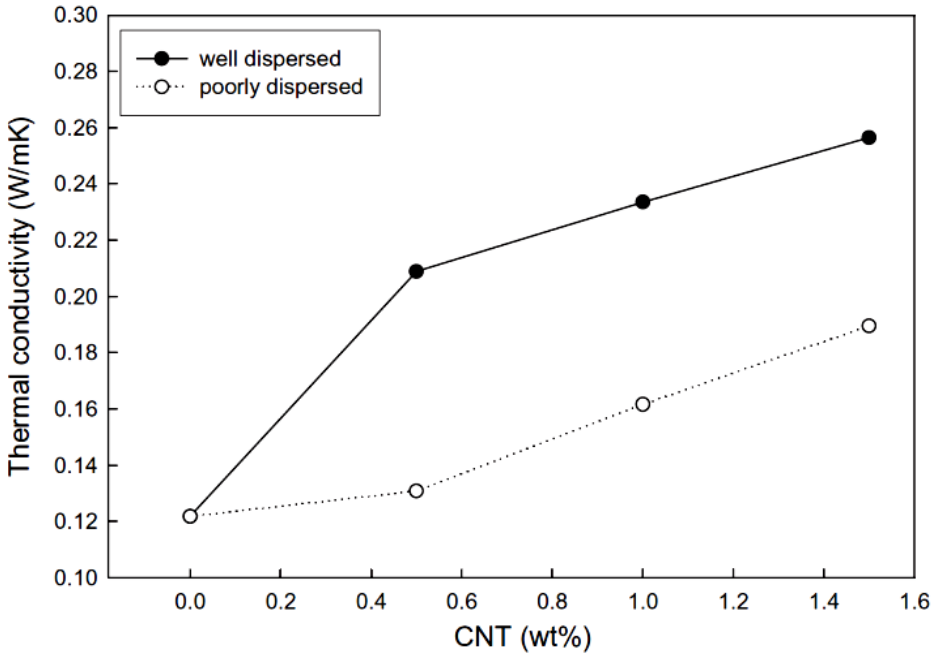

Figure 1-5: Thermal conductivity of the nano-composites with respect to carbon loading (Song and Youn 2005)

elsewhere the contrary was shown (Song and Youn 2005). Figure 1-5 illustrates these results. The dispersion technique in this study was a combination of sonication and the use of solvent for carbon nanotubes for well-dispersed samples. No solvent was used for poorly-dispersed ones. Absence of percolation threshold for thermal conductivity versus electrical conductivity was attributed to the ratio of electrical conductivity of carbon nanotubes to that of the polymer matrix, i.e. around 10^{15}, whereas this ratio is less pronounced for thermal conductivity (around 10^{4}).

The effect of purification of carbon nanotubes was also investigated in a different

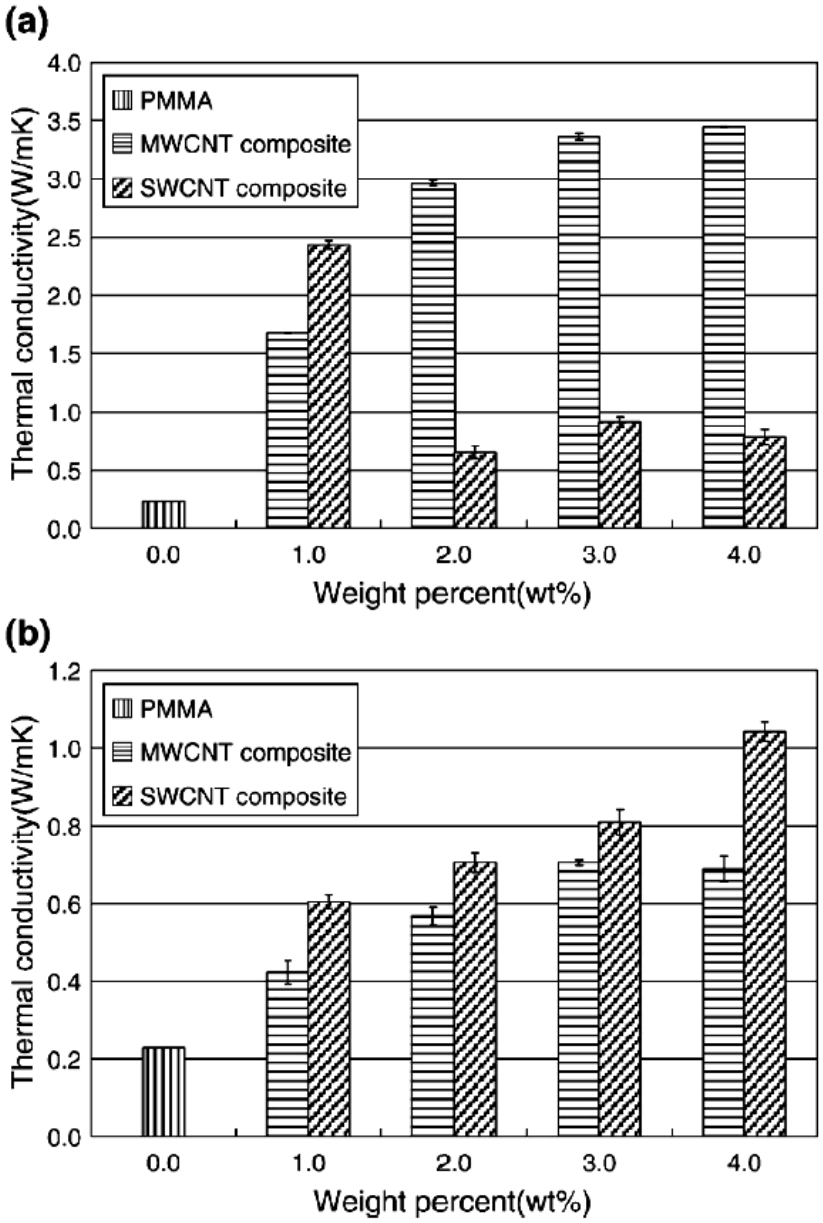

Figure 1-6: Thermal conductivity of PMMA-based composites reinforced with (a) unpurified CNTs, (b) purified CNTs (Hong and Tai 2008)

study (Hong and Tai 2008). According to this research, composites reinforced with the unpurified CNTs had higher thermal conductivity than that of the purified CNTs reinforced composite which was attributed to the generation of

defects on CNT surface during acid treatment, Figure 1-6.

The experimental results indicated enhancement of thermal conductivities over tenfold and near fifteen fold higher than PMMA for SWCNTs/PMMA and MWCNTs/PMMA composites, respectively. However, composites reinforced with acid-treated CNTs showed relatively low thermal conductivity.

In another attempt, carbon nanotubes were used to make a hybrid filler with graphite nanoplatelets (GNPs) to enhance the thermal conductivity of epoxy even more (Yu, et al. 2008). While compared to carbon black, SWNT and GNP alone, GNP/SWNT hybrid showed to be the most effective filler at 10 wt% loading among the other weight loadings, Figure 1-7.

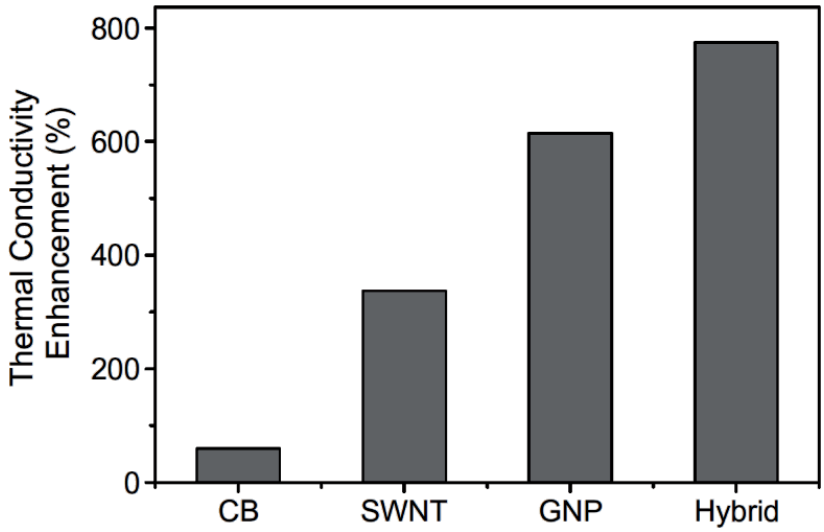

Figure 1-7: Thermal conductivity enhancement of epoxy composites for SWNT, GNP and GNP/SWNT hybrid filler at 10 wt % loading in comparison with carbon black (Yu, et al. 2008)

Mamunya et al., in another study, discussed the reason for very weak increase of the thermal conductivity of nano-composites with CNT volume concentration (2008, 1981-1988). According to them, in the system of polymer materials filled with conductive particles, the thermal conductivity value depends on relative concentrations of the polymer and filler. For the case of polymer/CNT composites for which formation of a conductive cluster at the percolation threshold of the electrical conductivity occurs at very small amounts of CNTs, this amount remains too small and exerts a rather weak effect on enhancement of thermal conductivity. In addition, considerable thermal resistance between matrix and filler phase is another reason explaining this modest enhancement.

1.2.5. Effect of Carbon Nanotubes on cure kinetics of thermosets

Although not known well enough yet, carbon nanotubes can affect the cure kinetics of the thermosetting materials. This can, in turn, influence the heat generation and the rate of it in the curing process. The available literature on the topic is not very extensive. Several contradictory results have also been reported.

Three different types of single wall carbon nanotubes were dispersed in epoxy system (EPIKOTE™ resin 862 and EPIKURE™ curing agent W) to investigate the curing process of epoxy resin based nano-composites (Tao, et al. 2006). The

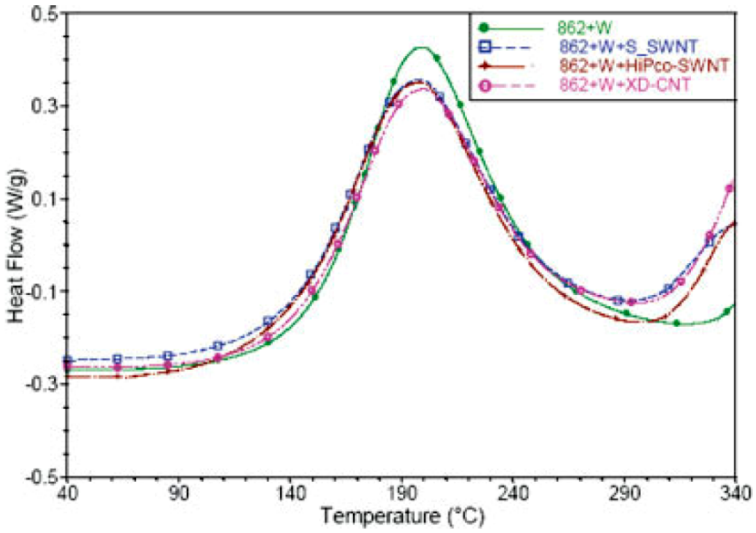

Figure 1-8: Dynamic DSC thermograms of the curing of the neat epoxy and epoxy nanocomposites (Tao, et al. 2006)

authors reported 6% decrease in total heat of reaction by adding 1 wt% XD-grade CNT which led to an overall slowdown in the curing process, Figure 1-8. A lower temperature at which the cure was initiated in the presence of carbon nanotubes compared to the pristine resin was also reported. According to this study, carbon nanotubes could reduce the glass transition temperature as well. This result contradicted another study which showed an increase of 40% in glass transition temperature by adding 1 wt% of multiwall carbon nanotubes (Jin, et al. 2001). This increase was reported elsewhere using functionalized multiwall carbon nanotubes (Velasco-Santos, et al. 2003).

In another attempt, a bisphenol-A type epoxy resin (YD114) and the curing agent KBH1089 were studied in combination with multiwall carbon nanotubes (Kim,

Lee and Park 2009). Results showed that addition of up to 0.5 wt% carbon nanotubes to epoxy resin reduced the total heat of reaction by about 30% which was explained by the fact that carbon nanotubes act as obstacles to the cross-linking reaction.

Cure kinetic of tetraglycidyl-4,4′-diaminodiphenylmethane (TGDDM) and 4,4′-diaminodiphenylsulfone (DDS) was studied as a curing agent in nano-composites with multiwall carbon nanotubes based on the autocatalytic model proposed by Kamal (Sourour and Kamal 1976), including the modifications of this model through the diffusion control function in the later stage of cure elsewhere (Xie, et al. 2004). The activation energy of nano-composites was observed to be lower than that of the neat resin. However, the initial reaction rate increased with adding carbon nanotubes while the time to reach the maximum rate decreased slightly in isothermal DSC tests, Figure 1-9. Additionally, the time to reach the maximum degree of cure decreased by addition of carbon nanotubes. These changes have been ascribed to the acceleration effect of carbon nanotubes.

In a different study, similar trends were observed by adding up to 10% of single wall carbon nanotubes into a diglycidyl ether of bisphenol A-based (DGEBA) epoxy resin (Puglia, Valentini and Kenny 2003). However, the decrease in total

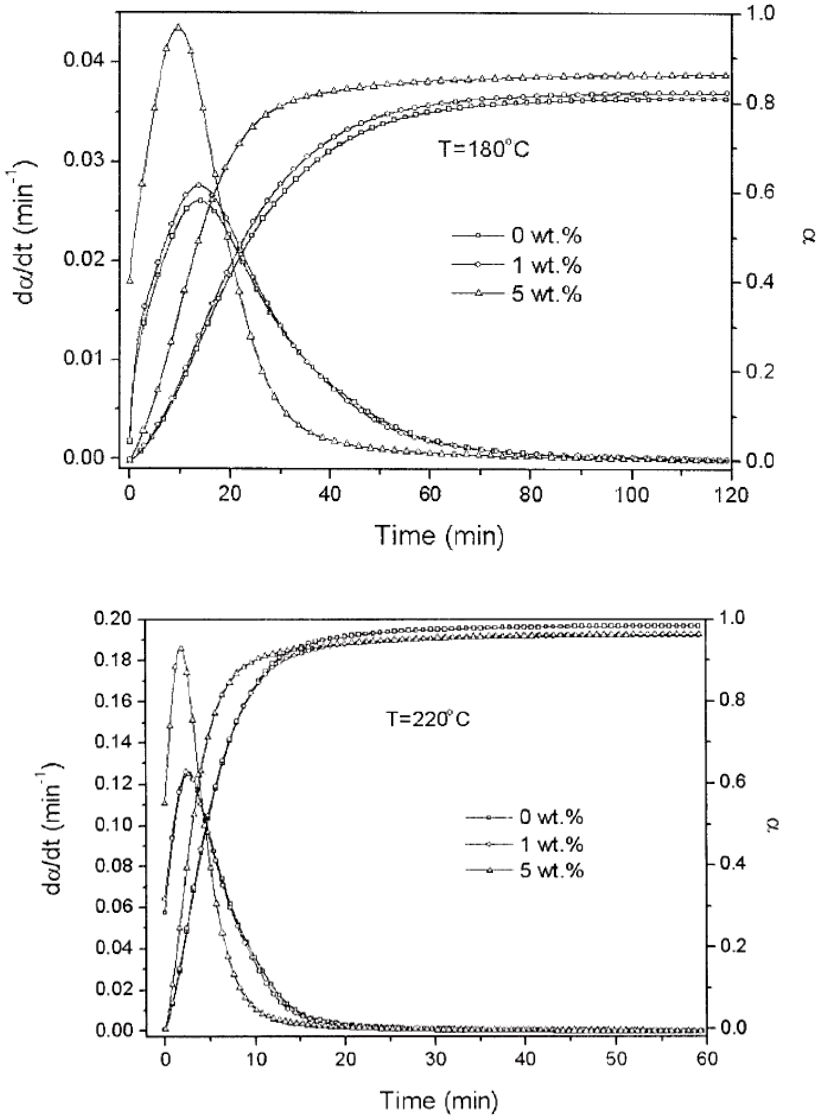

Figure 1-9: The reaction rate and extent of reaction of TGDDM/DDS epoxy and its nano-composites as a function of time at 180° C and 220° C (Xie, et al. 2004)

heat of reaction was directly ascribed to the proportional reduction of epoxy concentration in the composite. In addition, catalytic behaviour of single wall carbon nanotubes on the rate of reaction was more noticeable at low temperatures, Figure 1-10. The researchers attributed this accelerating effect on the curing kinetics to the extreme high thermal conductivity of carbon nanotubes

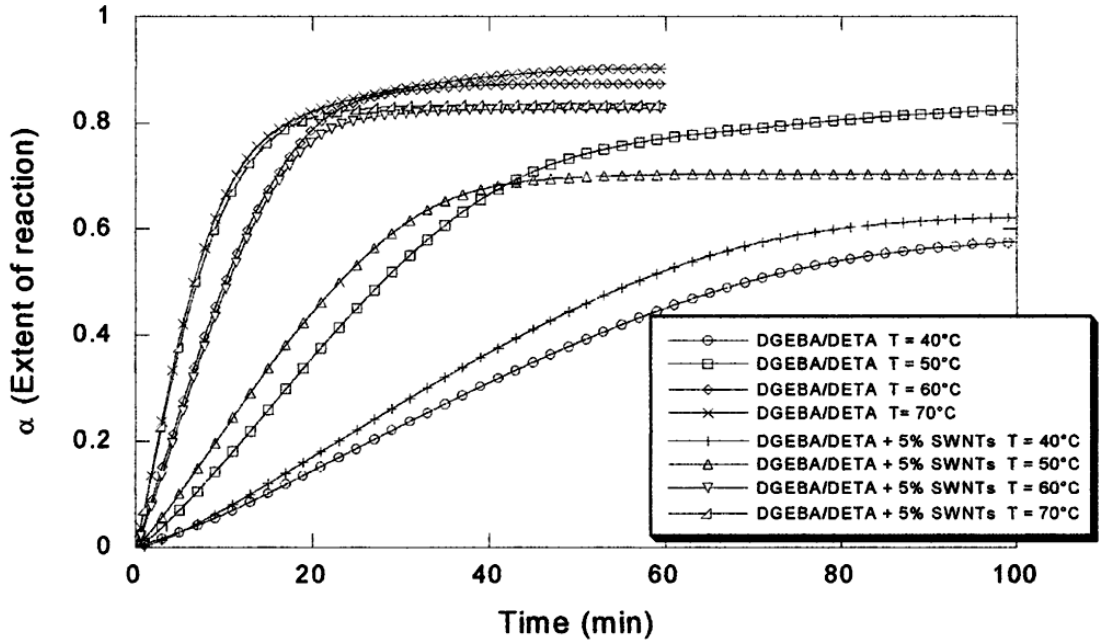

Figure 1-10: Extent of reaction versus time at different isothermal temperatures for DGEBA/DETA system and 5% DGEBA/DETA–SWNT composite (Puglia, Valentini and Kenny 2003)

and the ability of the epoxy resin to open and disperse the nanobundles, offering a higher surface for heat propagation. Nonetheless, this effect was reported at the lowest amount of carbon nanotubes studied with a marginal effect at higher concentrations, which indicates a saturation of the catalyzing action. This saturation was reported elsewhere for isotactic polypropylene (iPP) with different concentrations of multiwall carbon nanotubes in isothermal DSC tests (Xu and Wang 2008). The authors argued that for concentrations of carbon nanotubes below what they call the *critical gelation concentration*, carbon nanotubes mainly functioned as nucleating agents for crystallization to accelerate the cure rate. On the other hand, this rate was decelerated for the concentrations

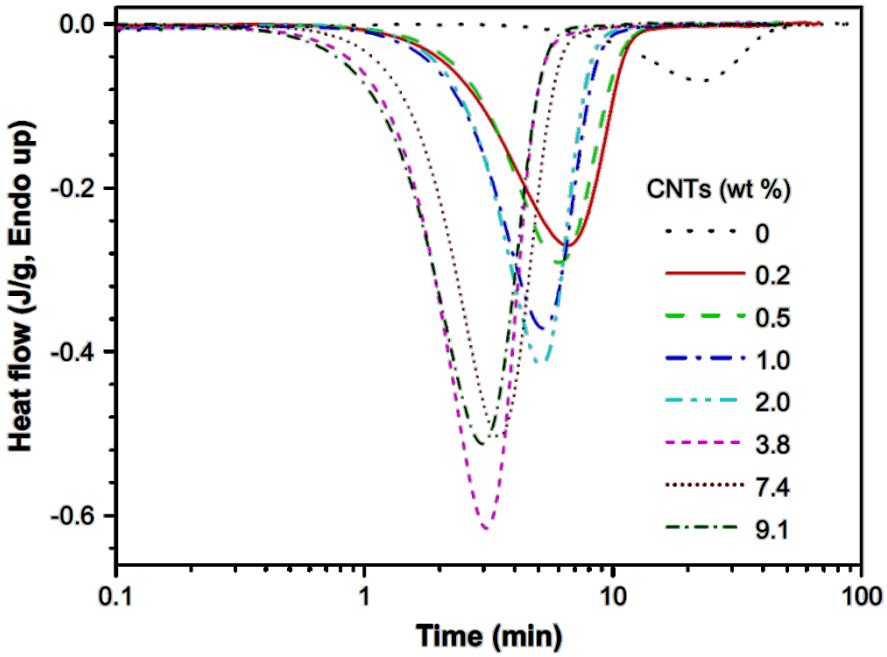

Figure 1-11: Heat flow curves of iPP/CNTs with different CNT concentrations during isothermal crystallization at 134° C (Xu and Wang 2008)

higher than critical gelation concentration due to the formation of carbon nanotube network which restricted mobility and diffusion of iPP chains to crystal growth fronts, Figure 1-11.

1.3. OBJECTIVE OF THE THESIS

The primary objectives of the present thesis are:

- To experimentally measure and numerically simulate the temperature distribution through-the-thickness of thick thermoset laminates during the curing process;
- To flatten the temperature profile across the thickness of thick thermoset

laminates during the curing process by introducing multiwall carbon nanotubes into the resin.

1.4. ORGANIZATION OF THE THESIS

The present chapter covers the problem statement as well as the previous works done on the cure kinetics of thermosets, different methods of temperature determination in thick thermoset laminates during the cure as well as temperature overshoot problem and eventually, effect of carbon nanotubes on both thermal conductivity and cure kinetics of polymers.

Chapter 2 introduces the experimental settings and test conditions, presenting the experimental results in the second section. With a similar approach, Chapter 3 discusses the theoretical aspects of the heat transfer, finite difference method and numerical stability. Then Kissinger's method is explained and applied to determine the constants of the cure kinetics model from DSC test data, followed by the results. And at the end, the results of the developed computer code to describe the temperature distribution are presented.

Chapter 4 mainly discusses the experimental and numerical results which are presented in Chapter 2 and 3, respectively. The thesis culminates with Chapter 5, highlighting conclusions, contributions and suggestions for future work.

Chapter 2: EXPERIMENTS AND RESULTS

In this chapter, the material used in the current study is firstly introduced. It is followed by a description of the procedures used for measuring the thermal properties. Subsequently, the sample preparation and measurement tool specifications for temperature measurements are explained. The results from the measurements of thermal properties as well as the temperature measurements are presented in the last section.

2.1. MATERIAL

The epoxy used in this study was EPON 862 (Diglycidyl ether of bisphenol F) which is very common in aerospace industry in combination with curing agent EPIKURE 3046 which is an amidoamine. They were both produced by Hexion Specialty Chemicals, Inc. According to the manufacturer recommendation, 47 parts of the curing agent were mixed with 100 parts of resin.

Carbon nanotubes were industrial grade MWCNTs from NanoLab Inc. and synthesized by catalytic vapour deposition. Their length and diameter range were 5 to 20 μm and 10 to 30 nm, respectively. According to the provider, the

Table 2-1: Calendaring procedure for dispersing CNT in epoxy

First gap (μm)	Second gap (μm)	Repetition
50	50	2
20	20	1
10	10	3

purity of MWCNTs was more than 85 wt% with impurities of iron and ceramic oxides. Both the MWCNTs and all the resin systems were used as received.

To disperse the carbon nanotubes in the epoxy a calendaring technique was used. For this purpose, a three-roll mill machine (EXAKT 80E) was used with the procedure indicated in Table 2-1. A three-roll mill or calendaring machine basically consists of three cylindrical rolls with adjustable gaps between them, each of which revolves at different speed and direction with respect to the adjacent one. The mixture of epoxy and carbon nanotubes is fed between the first two rolls and then is collected by a scraper blade in contact with the last roll. This configuration results in very high shear forces between the rolls applied to the mixture in a short time which prevents the breakage of individual carbon nanotubes. However, the period of application of the shear forces is large enough to break-up the agglomerated bundles of carbon nanotubes and result in a uniform dispersion of MWCNTs in epoxy (Thostenson and Chou 2006).

Four different types of samples were prepared: (a) pristine epoxy; (b) epoxy with 0.5 wt% CNTs; (c) epoxy with 1.0 wt% CNTs; and (d) epoxy with 1.5 wt% CNTs. However, due to high viscosity, high uncertainties in the preparation of samples with 1.5 wt% CNT concentration led to dismissing these samples from discussion, although the corresponding results are presented.

2.2. MEASUREMENT OF THERMAL PROPERTIES AND RESULTS

2.2.1. Characterization of the cure kinetics and results

A two-parameter autocatalytic model was used to characterize the cure kinetics. Equation (3-30) mathematically shows this model. There are four constants in this equation which should be determined empirically. For this purpose, Kissinger's method was used which has been validated for epoxy. Further elaboration on the cure kinetics model can be found in Section 3.2.4.

According to the Kissinger's method, several DSC test runs with different heating rate (φ) are required. For each of these runs the temperature at which maximum reaction rate occurs (T_m) should be recorded. Then, the activation energy can be calculated using Equation (1-6) from the slope of the plot of $\ln(\varphi/{T_m}^2)$ versus $1/T_m$. Subsequently, frequency of pre-exponential factor and orders of reaction are determined by a linear least square curve fitting on DSC

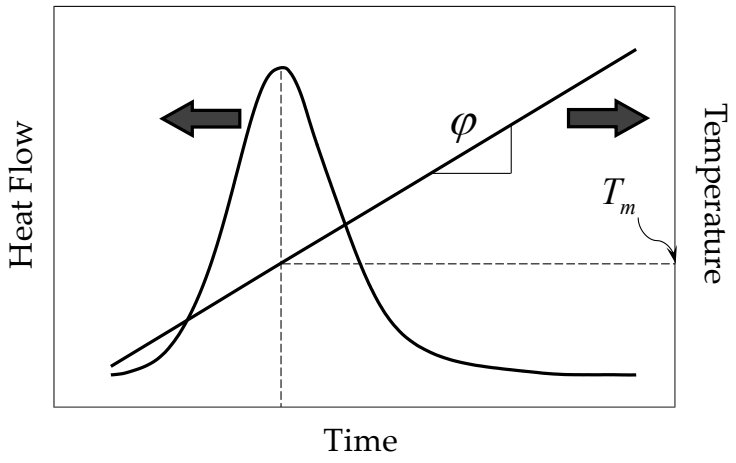

Figure 2-1: A typical DSC test run as well as the variations in the temperature with a constant heating rate

data for the linearized form of Equation (3-30). Figure 2-1 shows a typical DSC test run as well as the variations in the temperature with a constant heating rate.

Dynamic DSC tests with seven different heating rates were performed and each run was repeated three times. For this purpose, carbon nanotubes were dispersed in epoxy resin with desired concentration, using the calendaring machine according to the procedure described in Section 2.1. Then, curing agent was added with the ratio of 47 parts for 100 parts of epoxy and manually stirred for 5 minutes. DSC samples of weight of 10 ± 1 gr were subsequently prepared in Tzero™ pans and inserted into TA Instruments modulated DSC Q200 machine. Temperature was stabilized at 20°C and raised to 300°C with heating rates of 1, 2, 5, 7, 10, 15 and 20 °C/min.

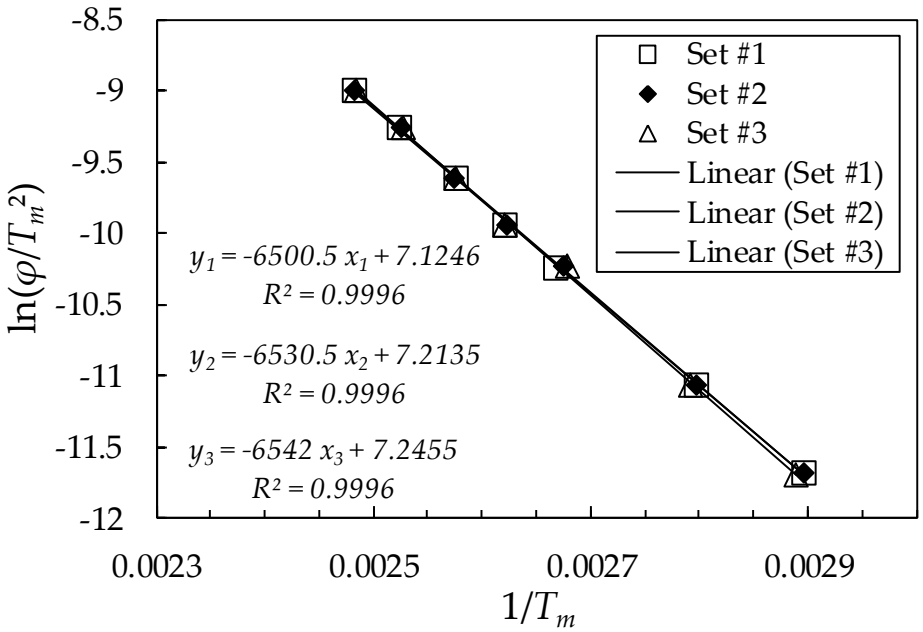

Figure 2-2:* $\ln(\varphi/T_m^2)$ *versus* $1/T_m$ *for three repetitions of DSC tests with heating rates of 1, 2, 5, 7, 10, 15 and 20* °C*/min for pristine resin

Plotting $\ln(\varphi/T_m^2)$ versus $1/T_m$, activation energy can be calculated for each set of runs from the slope of the graph using Equation (1-6). This plot is shown in Figure 2-2 for neat resin as well as the linear regressions for each of the sets. It is obvious that the variation in the results of the three runs is insignificant. The same trend was noticeable in the results of the samples with different concentrations of carbon nanotubes. The average value of activation energies obtained was similar for all the samples, namely pristine resin and samples with 0.5, 1.0 and 1.5 wt% of carbon nanotubes. Table 2-2 presents their standard deviations which are very small for all cases.

A linear least square curve fitting method was used to calculate the remaining

Table 2-2: The average value of activation energies and standard deviations for samples with different concentration of carbon nanotubes

CNT ($wt\%$)	Activation Energy (J/mol)	Std Dev.
0.0	54169.9	176.4
0.5	55027.5	235.7
1.0	55580.8	81.1
1.5	55394.1	55.8

constants in Equation (3-30), namely, frequency factor (A) as well as orders of reaction (m and n). For this purpose, Equation (3-30) was linearized as Equation (2-1).

$$\ln\left(\frac{\partial\alpha}{\partial t}\right) + \frac{E_a}{RT} = \ln A + n\ln(1-\alpha) + m\ln\alpha \tag{2-1}$$

Substituting j data points from DSC tests into Equation (2-1) with three unknown parameters yields an overdetermined system of equations which can be written in matrix form:

$$\boldsymbol{Mx} = \boldsymbol{b} \tag{2-2}$$

in which $\boldsymbol{M}$ is the matrix of coefficients, $\boldsymbol{x}$ is vector of unknowns and $\boldsymbol{b}$ is a known vector which are given in Equation (2-3). Vector of unknowns can be determined by Equation (2-4).

$$\boldsymbol{M} = \begin{bmatrix} 1 & \ln(1-\alpha_1) & \ln\alpha_1 \\ 1 & \ln(1-\alpha_2) & \ln\alpha_2 \\ \vdots & \vdots & \vdots \\ 1 & \ln(1-\alpha_j) & \ln\alpha_j \end{bmatrix}; \qquad \boldsymbol{b} = \begin{Bmatrix} \ln\left(\frac{\partial\alpha}{\partial t}\right)_1 + \frac{E_a}{RT_1} \\ \ln\left(\frac{\partial\alpha}{\partial t}\right)_2 + \frac{E_a}{RT_2} \\ \vdots \\ \ln\left(\frac{\partial\alpha}{\partial t}\right)_j + \frac{E_a}{RT_j} \end{Bmatrix}; \qquad \boldsymbol{x} = \begin{Bmatrix} \ln A \\ n \\ m \end{Bmatrix} \tag{2-3}$$

$$\boldsymbol{x} = (\boldsymbol{M}^T\boldsymbol{M})^{-1}\boldsymbol{M}^T\boldsymbol{b} \tag{2-4}$$

The aforementioned procedure was performed for three repetitions of each seven heating rate DSC runs (1, 2, 5, 7, 10, 15 and 20 °C/min), on every concentration of CNTs (zero, 0.5, 1.0 and 1.5 wt%). Values of A, m and n were determined. Then, the average of any of these constants was calculated from every set of seven heating rate runs for each of the CNT concentrations. At the end, the final value of each constant was determined by averaging the three repetitions of each set. These values, as well as corresponding standard deviations are shown in Table 2-3.

The same procedure was used to calculate the average of total heat of reaction which is the area under the heat flow diagram obtained from each DSC test runs. A typical DSC heat flow diagram is shown in Figure 2-3 for neat resin at heating rate of 7 °C/min. Average values of total heat of reaction as well as their corresponding standard deviations are listed in Table 2-3 for all of the studied cases.

Table 2-3: Mean values of constants of cure kinetics equation and total heat of reaction for different concentrations of CNT

CNT (*wt%*)		*A* (1/*s*)	*n*	*m*	ΔH_R (*J/g*)
0.0	Value	222000	2.07	0.32	400.4
	Std Dev	1200	0.03	0.02	2.4
0.5	Value	331000	2.27	0.37	408.4
	Std Dev	12200	0.06	0.02	0.5
1.0	Value	372000	2.36	0.36	413.0
	Std Dev	400	0.06	0.02	1.5
1.5	Value	387000	2.37	0.38	417.8
	Std Dev	7800	0.02	0.01	6.2

Degree of cure of the epoxy can be calculated from Equation (3-28) at each data point (typically more than 2000 points in one DSC run is recorded). The results are illustrated in Figure 2-3 for neat resin at heating rate of 7 °C/min.

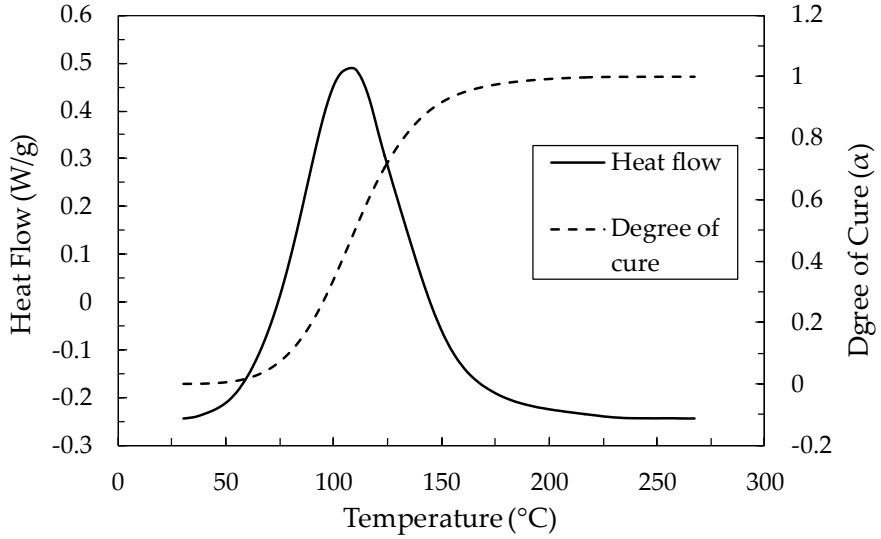

Figure 2-3: DSC thermogram (solid line) and calculated degree of cure (dashed line) for neat resin in a run with heating rate of 7 °C/min

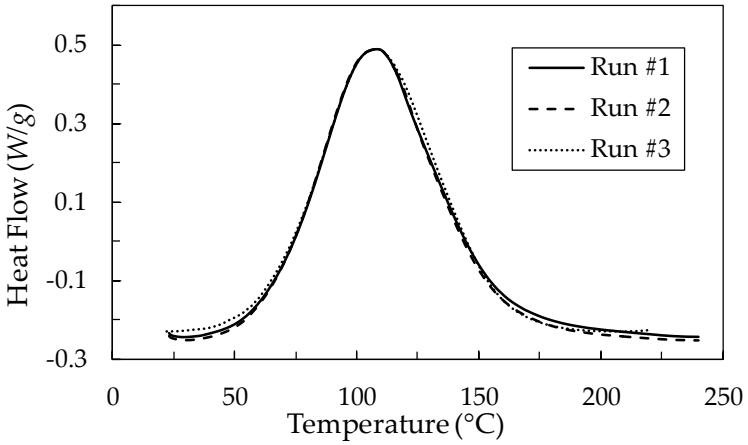

Figure 2-4: DSC thermograms of three runs with heating rate of 7 °C/min on neat resin

Figure 2-4 shows heat flow diagrams obtained from three different repetitions of DSC runs with heating rate of 7 °C/min on neat resin samples. It is evident that the variation between these three graphs is extremely small. The same trend was observed for all the other samples with different CNT contents. Insignificant standard deviation values for total heat of reactions presented in Table 2-3 is

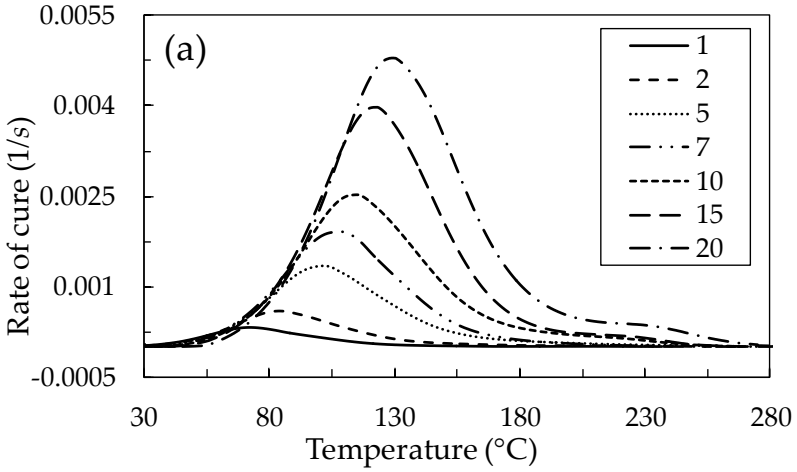

Figure 2-5: Rate of cure in DSC test runs with heating rates of 1, 2, 5, 7, 10, 15 and 20 °C/min for (a) pristine resin, (b) 0.5 wt%, (c) 1.0 wt% and (d) 1.5 wt% CNT contents (to be continued)

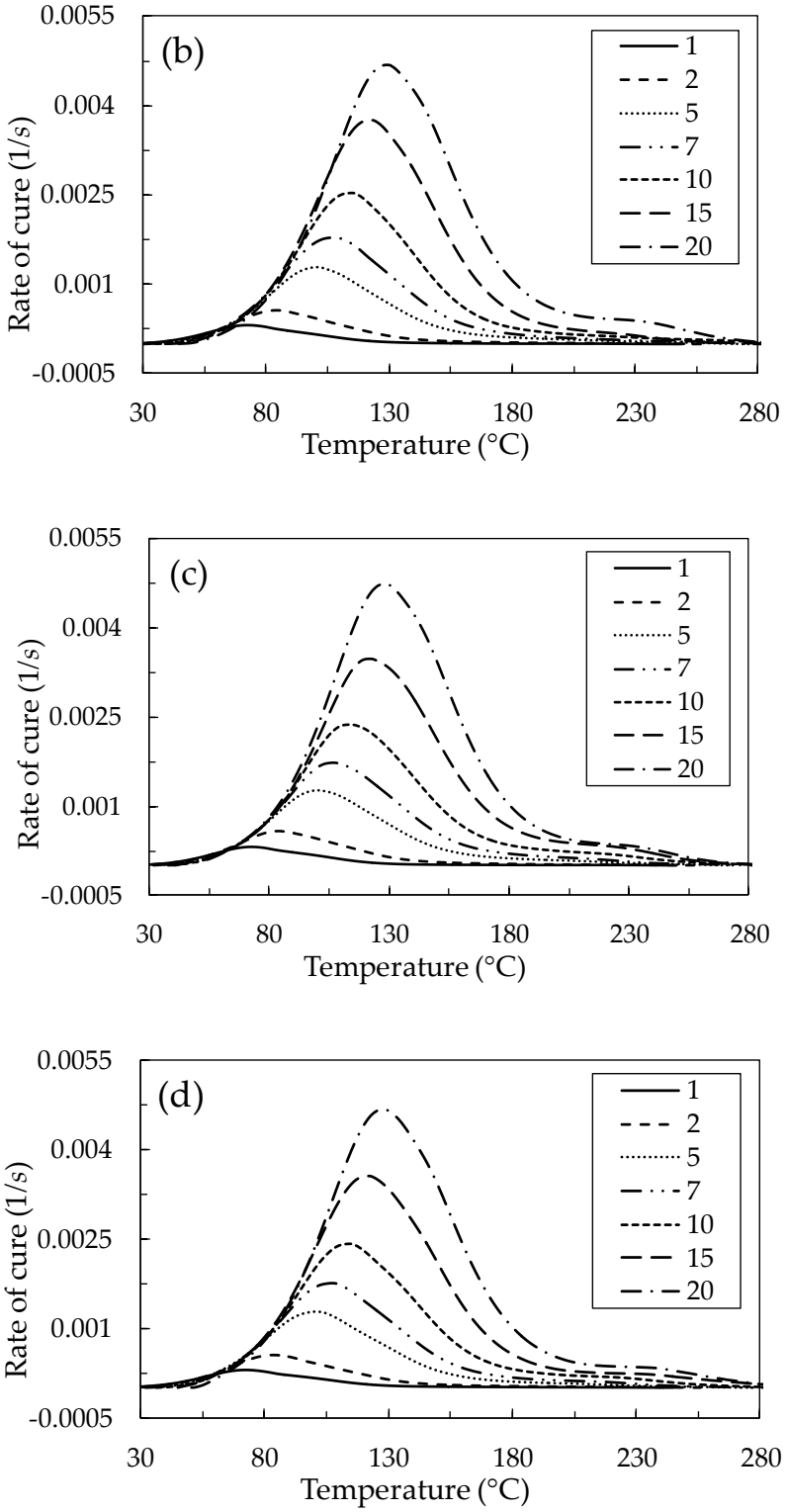

Figure 2-5: Rate of cure in DSC test runs with heating rates of 1, 2, 5, 7, 10, 15 and 20 °C/min for (a) pristine resin, (b) 0.5 wt%, (c) 1.0 wt% and (d) 1.5 wt% CNT contents
(Continued from the previous page)

observed, showing that the DSC tests are highly repeatable. Hence, for clarity of graphs, hereafter, solely the results of one of the repetitions among the three are shown and discussed for any CNT concentration.

Figure 2-5 and Figure 2-6 show the results of DSC tests. Rate of cure of epoxy is illustrated in Figure 2-5 for samples with different contents of CNT with different

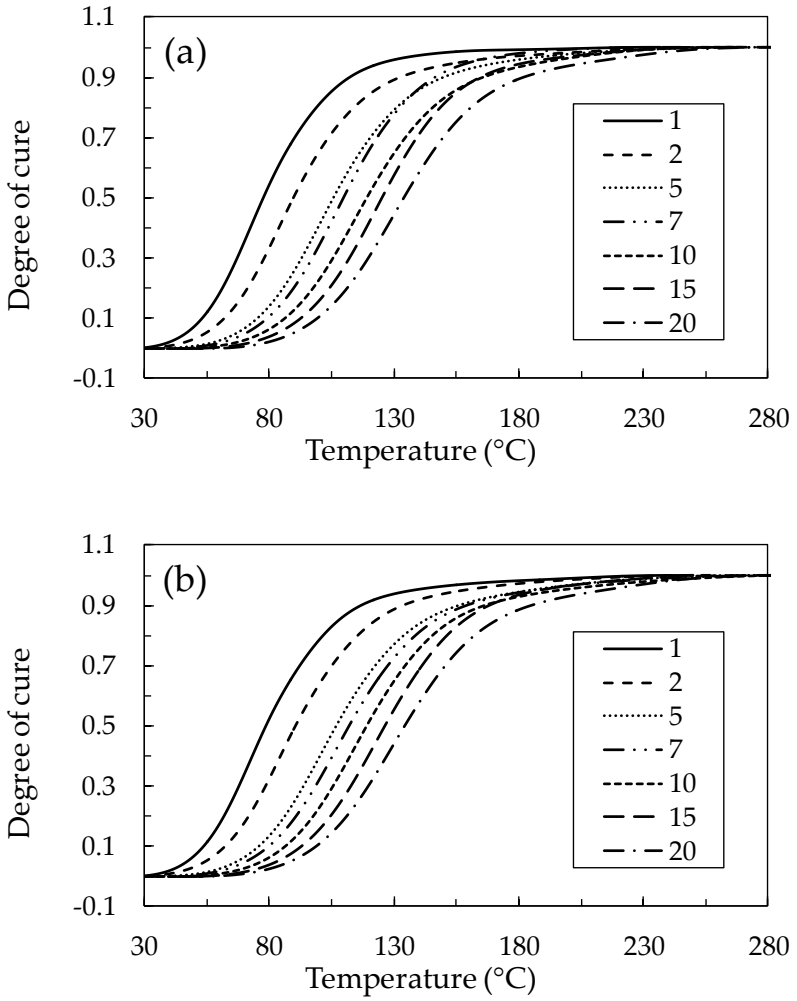

Figure 2-6: Degree of cure in DSC test runs with heating rates of 1, 2, 5, 7, 10, 15 and 20 °C/min for (a) pristine resin, (b) 0.5 wt%, (c) 1.0 wt% and (d) 1.5 wt% CNT contents (to be continued)

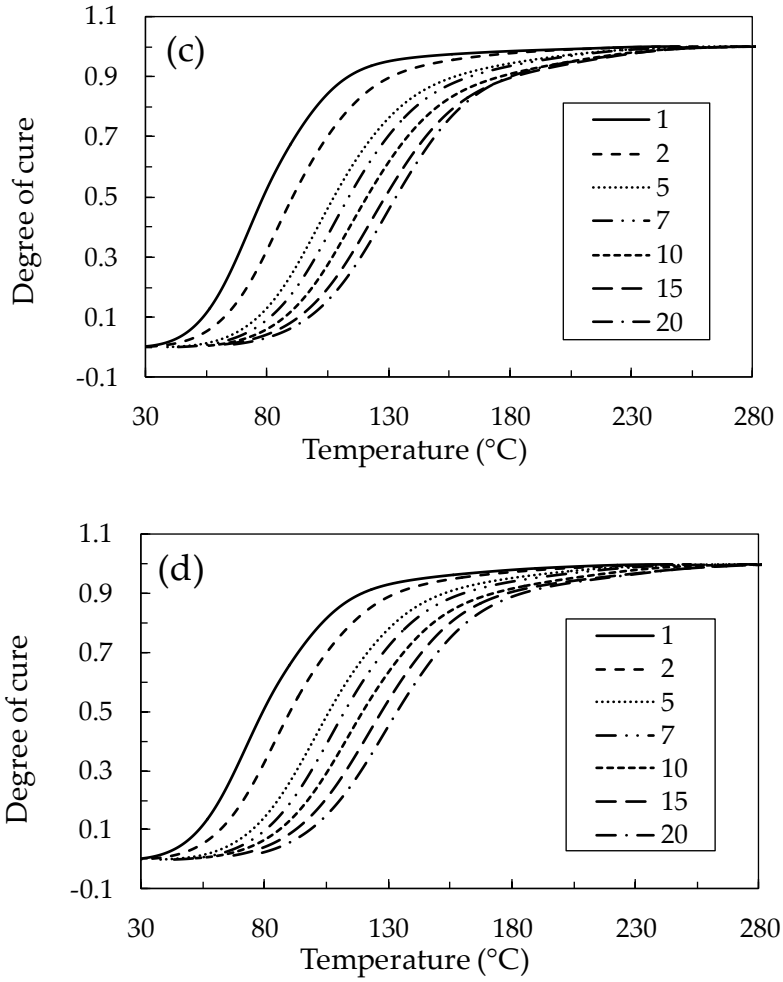

Figure 2-6: Degree of cure in DSC test runs with heating rates of 1, 2, 5, 7, 10, 15 and 20 °C/min for (a) pristine resin, (b) 0.5 wt%, (c) 1.0 wt% and (d) 1.5 wt% CNT contents (Continued from the previous page)

heating rates, while Figure 2-6 shows degree of cure for the same cases. These figures show that regardless of CNT concentration, a certain degree of cure is obtained at a higher temperature as heating rate increases. Furthermore, the temperature at which the rate of reaction reaches its highest value, T_m, increases by increasing the heating rate in DSC test.

Rate of curing reaction as well as degree of cure during a DSC test for a heating rate of 15 °C/min are shown in Figure 2-7. Rate and degree of cure for the rest of tests with different heating rates are reproduced in Appendix A and Appendix B, respectively. For clarity of the graphs in Appendix A, the scale of the vertical axis is adjusted according to the range of changes in the graphs. A noticeable trend in all the cases is that the values of both rate and degree of cure for samples with 1.5 wt% CNT content increase compared to those of the samples with 1.0 wt% CNT

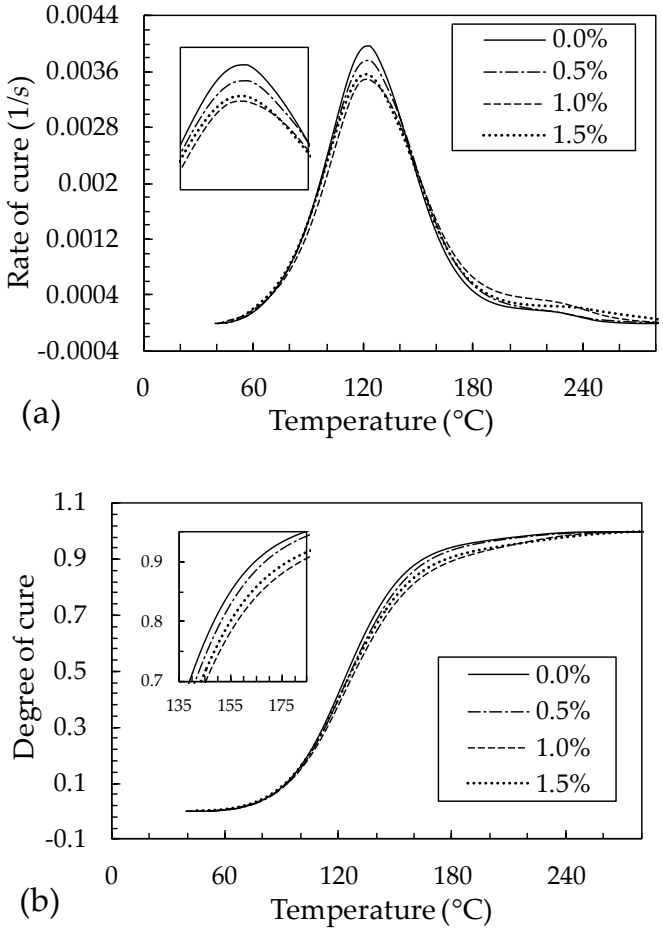

Figure 2-7: Comparison of (a) rate and (b) degree of cure of samples with different CNT contents in a DSC test with heating rate of 15 °C/min

content which do not follow the obvious decrease of these parameters from pristine resin to 1.0 wt% CNT concentration samples.

2.2.2. Heat capacity

Heat capacity measurements were conducted on the actual samples to be used in the computer code developed to model the temperature distribution which will be discussed in details in Chapter 3. For this purpose, a modulated differential scanning calorimetry (MDSC) machine was used which can alter the temperature by an adjustable amplitude while increasing the temperature with the given heating rate. This feature enables the machine to calculate the heat capacity of the sample in only one dynamic test run using mathematical models while the method using conventional DSC data needs several test runs.

To measure heat capacity, the samples were prepared as explained in Section 2.2.1 followed by a period to complete the curing according to the manufacturer recommendation: 24 hours at room temperature and 2 hours post-curing at 121°C. The program used for heat capacity measurements in MDSC machine was essentially a temperature ramp of 2 °C/min from 10°C to 200°C with modulation of ±0.32 °C/min. This procedure was repeated three times for each CNT concentration. Figure 2-8 illustrates the results between 40°C to 160°C

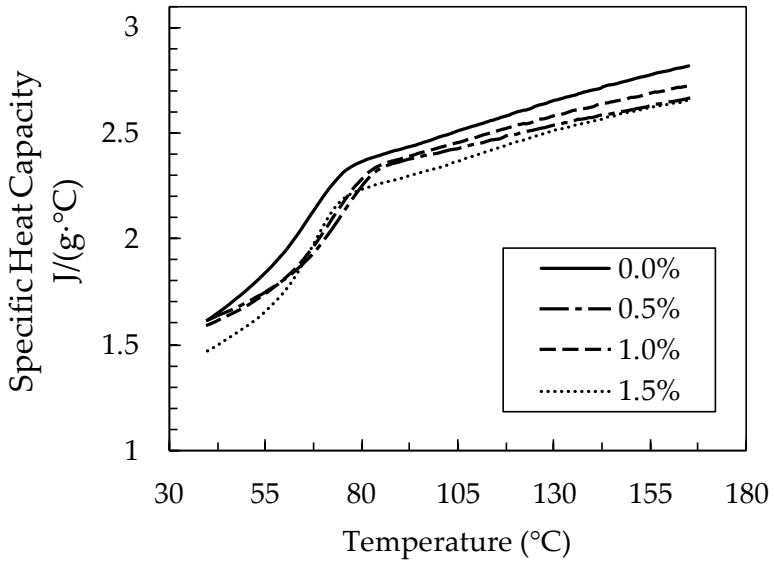

Figure 2-8: Specific heat capacity measurement using modulated DSC for different CNT concentrations

which is the range of operation temperature (see Section 2.3). Since the results of MDSC for heat capacity measurements were as repeatable as the DSC results discussed in Section 2.2.1, for cleanness of the graphs, the average of the three is shown. Note that the measured values for heat capacity are those of the cured samples and the heat capacity changes during the curing process were not taken into account.

To consider the variation of heat capacity with temperature in the computer code, each graph was split into two sections which can be distinguished by their different slopes. A quadratic polynomial was fitted on the first section and a line on the second one. Figure 2-9 shows the results of curve fitting on heat capacity measurements for samples with different CNT concentrations. The change in the

slope of the heat capacity variation with temperature is due to change in the molecular free volume. This change for the polymer happens around the glass transition temperature (T_g). According to the data sheet of the material provided by the manufacturer, T_g of EPON 862 is 90°C measured by Rheometrics dynamic mechanical tester at heating rate of 2 °C/min at 1.0 Hz for 0.1% of strain.

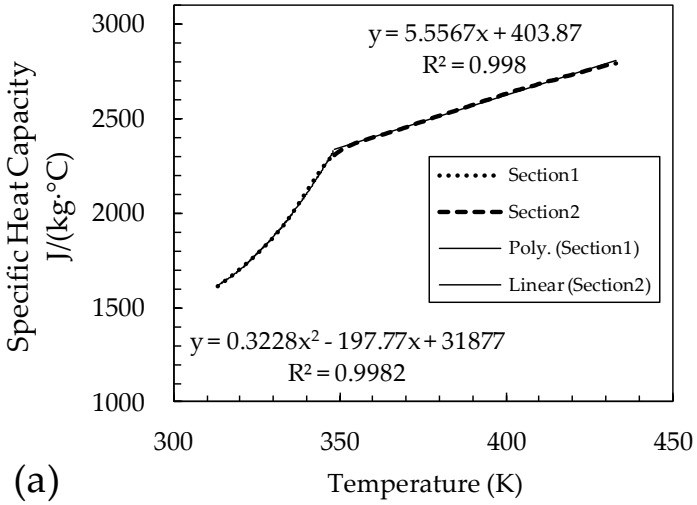

(a)

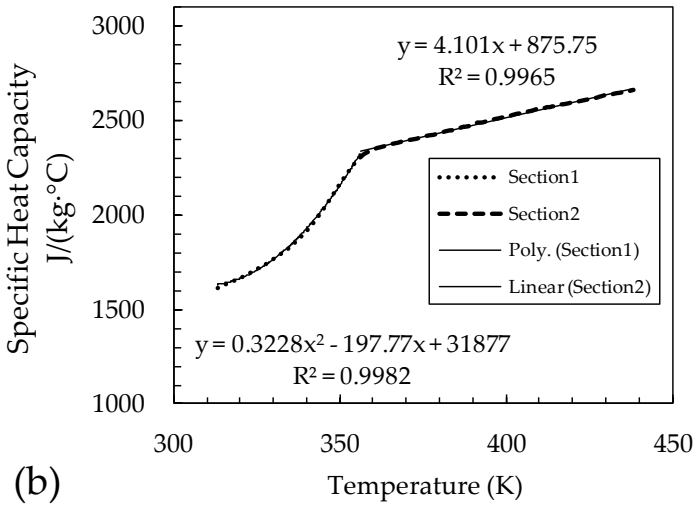

(b)

Figure 2-9: Curve fitting on the variations of heat capacity with temperature for samples of (a) neat resin, (b) 0.5 wt%, (c) 1.0 wt% and (d) 1.5 wt% CNT contents (to be continued)

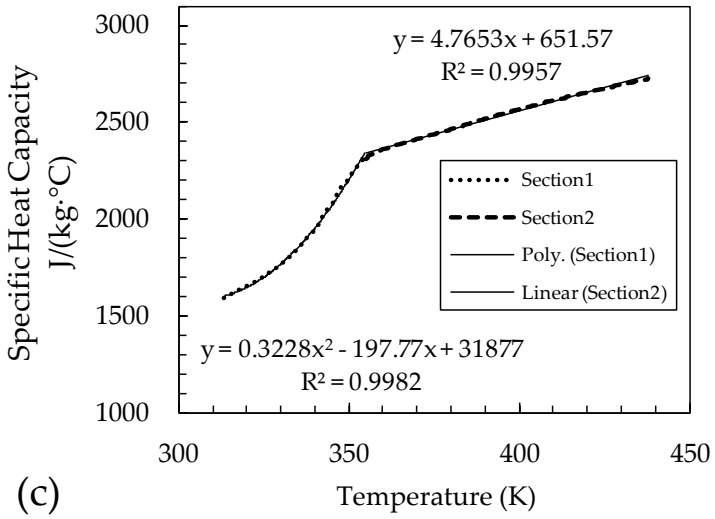

(c)

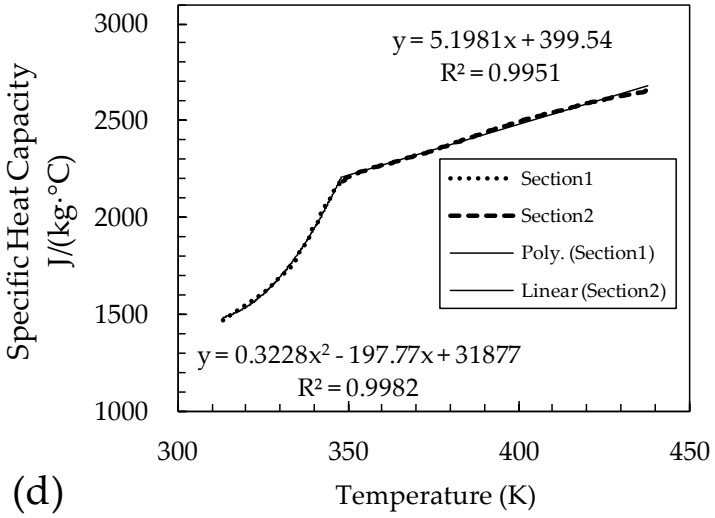

(d)

Figure 2-9: Curve fitting on the variations of heat capacity with temperature for samples of (a) neat resin, (b) 0.5 wt%, (c) 1.0 wt% and (d) 1.5 wt% CNT contents (Continued from the previous page)

2.2.3. Thermal diffusivity

A flash diffusivity measurement technique was used to measure the thermal conductivity of samples. The hardware providing this method was the LFA 447™ Nanoflash instrument which basically irradiates uniformly on one side of a

flat test sample using Xenon high energy flash tube pulse and measures the temperature rise on its opposite side as a function of time using an infrared detector. The magnitude of temperature rise and the amount of light energy are not required for thermal diffusivity determination; only the shape of the curve is used in the analysis (LFA 447 Nanoflash™ Instruction Manual 2002).

Measurement of the thermal diffusivity, λ, and having the values of heat capacity, C_p, as well as density, ρ, will allow to calculate the thermal conductivity, k, using Equation (2-5).

$$k = \lambda \rho C_p \tag{2-5}$$

According to LFA 447 Nanoflash™ Instruction Manual, flat test coupons were prepared within the thickness range of 0.5 to 2.0 mm with maximum non-uniformity up to 0.02 mm from all the carbon nanotubes concentrations. The samples were cured in molds with a rubber spacer to provide the desired thickness, according to the material provider's recommendation curing cycle: 24 hours at room temperature and 2 hours of post-curing at 121°C. Then, the required thickness uniformity was achieved using sandpaper. To enhance the absorption of flash energy and the emission of infrared radiation to the detector, a graphite coating is suggested which greatly increases the resulting signal-to-

noise ratio. According to LFA 447 Nanoflash™ Instruction Manual, the use of several thin layers of sprayed graphite, giving a total coating thickness of approximately 5 μm results in a durable and uniform coating. To do so, samples were laid down next to each other and graphite was sprayed across the row of the samples in two reciprocal passes. This coating was repeated 5 times on each side of the samples.

After having three samples ready for each CNT concentration, they were loaded into the instrument and the thermal diffusivity measurements were conducted at 40, 100 and 150°C. The average values are shown in Figure 2-10 and Table 2-4 as well as the standard deviations. Here, it is noticeable that thermal diffusivity

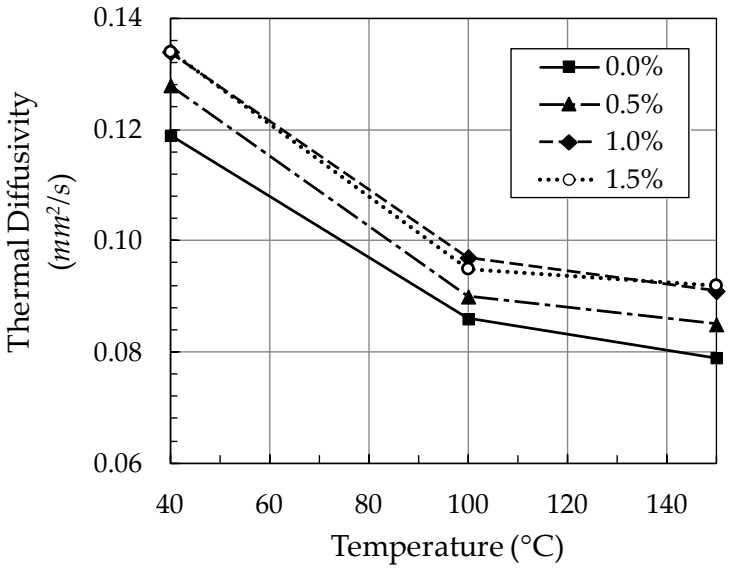

Figure 2-10: Thermal diffusivity of pristine resin and samples with 0.5, 1.0 and 1.5 wt% CNT content at 40, 100 and 150°C (lines just present the trends)

Table 2-4: Thermal diffusivity and corresponding standard deviation values for pristine resin and samples with 0.5, 1.0 and 1.5 wt% CNT content at 40, 100 and 150°C

CNT ($wt\%$)		Thermal diffusivity at (mm^2/s)		
		40°C	100°C	150°C
0.0	Value	0.119	0.086	0.079
	Std Dev	0.003	0.000	0.000
0.5	Value	0.128	0.090	0.085
	Std Dev	0.002	0.003	0.003
1.0	Value	0.134	0.097	0.091
	Std Dev	0.002	0.001	0.004
1.5	Value	0.134	0.095	0.092
	Std Dev	0.003	0.001	0.000

values of the samples with 1.5 wt% CNT content stop to increase opposing the trend observed from pristine resin samples to samples with 1.0 wt% CNT concentration.

In order for the variations of thermal diffusivity with temperature to be taken into consideration in the numerical model, a quadratic polynomial equation with the form of Equation (2-6) was fitted on the results for each CNT concentration, the coefficients of which are presented in Table 2-5.

$$\lambda = a_0 + a_1 T + a_2 T^2 \tag{2-6}$$

Table 2-5: Coefficients of quadratic equation fitted on thermal diffusivity measurement data for samples with different CNT contents

CNT ($wt\%$)	a_0	a_1	a_2
0.0	7.268×10^{-7}	-3.108×10^{-9}	3.727×10^{-12}
0.5	8.929×10^{-7}	-3.961×10^{-9}	4.848×10^{-12}
1.0	8.547×10^{-7}	-3.715×10^{-9}	4.515×10^{-12}
1.5	9.643×10^{-7}	-4.331×10^{-9}	5.364×10^{-12}

2.2.4. Density

To measure the density, flat coupons which were prepared for thermal diffusivity measurements (see Section 2.2.3) were weighed and the results were divided by the dimensions of the same coupons measured using a vernier calliper. These measurements were repeated three times for each samples. The average values as well as the standard deviation for each sample are presented in Table 2-6.

Table 2-6: Density of samples made of pristine resin and different CNT contents

CNT ($wt\%$)	**Density (kg/m^3)**	**Std Dev**
0.0	1159	2.5
0.5	1163	4.5
1.0	1175	3.6
1.5	1176	5.3

2.3. TEMPERATURE MEASUREMENTS AND RESULTS

The schematic view of the experimental setting can be seen in Figure 2-11. After dispersing carbon nanotubes in the epoxy, according to the procedure explained in Section 2.1, the mixture as well as the curing agent were preheated separately in the gravity convection oven at 40 ± 1°C for 20 minutes. Then, keeping the proportionality of curing agent to epoxy at 47:100 parts (according to the vendor's recommendation), curing agent was added to the mixture of epoxy and carbon nanotubes were stirred manually for 5 minutes and degassed in a vacuum oven at 40 ± 3°C for another 5 minutes. The final product was poured into a glass vial of diameter of 25 mm and cured in the gravity convection oven

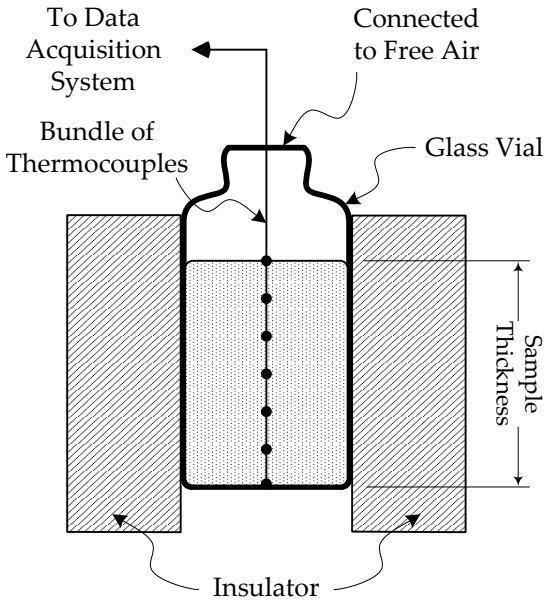

Figure 2-11: Schematic of temperature measurement experimental setting

at 40 ± 1°C. To examine the heat transfer mechanism in one dimension merely (across the thickness), the external circumferential surface of the vial was insulated by six layers of Ecoweaver 44 glass insulator. Care was taken so that the bottom part of the vial stay in direct contact with the air by inserting two spacer rods under the vial. Before mixing the curing agent with epoxy and starting the curing process, the vial, the insulator and the fixture used to hold the vial in the oven were preheated at 40 ± 1°C for 20 minutes.

K-type Nickel-Chromium thermocouples were used to measure the temperature at different points across the thickness of the samples during the curing process. The maximum temperature range for K-type thermocouples is -200 to 1250°C and their standard limits of error is 2.2°C or 0.75% above 0°C, whichever is greater. The thermocouples were mechanically attached together to make a bundle with desired numbers and tip-to-tip distance. Here, care was taken to prevent the wires of each individual thermocouple to make contact with the others by making sure that the insulator sheath on each thermocouple stays as close as possible to the tip of the thermocouple after welding the wires. As such, only the tip was exposed to the medium and the wires were protected from touching each other.

Samples with three different thicknesses of 0.5 ± 0.03, 1.0 ± 0.03 and 1.5 ± 0.03

inches for each of the carbon nanotube concentrations were investigated and each combination was repeated three times. For samples of 1.0″ and 1.5″ thickness, the temperature of seven equally-distanced points across the thickness was monitored during the curing process using a bundle of seven thermocouples. For samples with 0.5″ thickness, this bundle had five

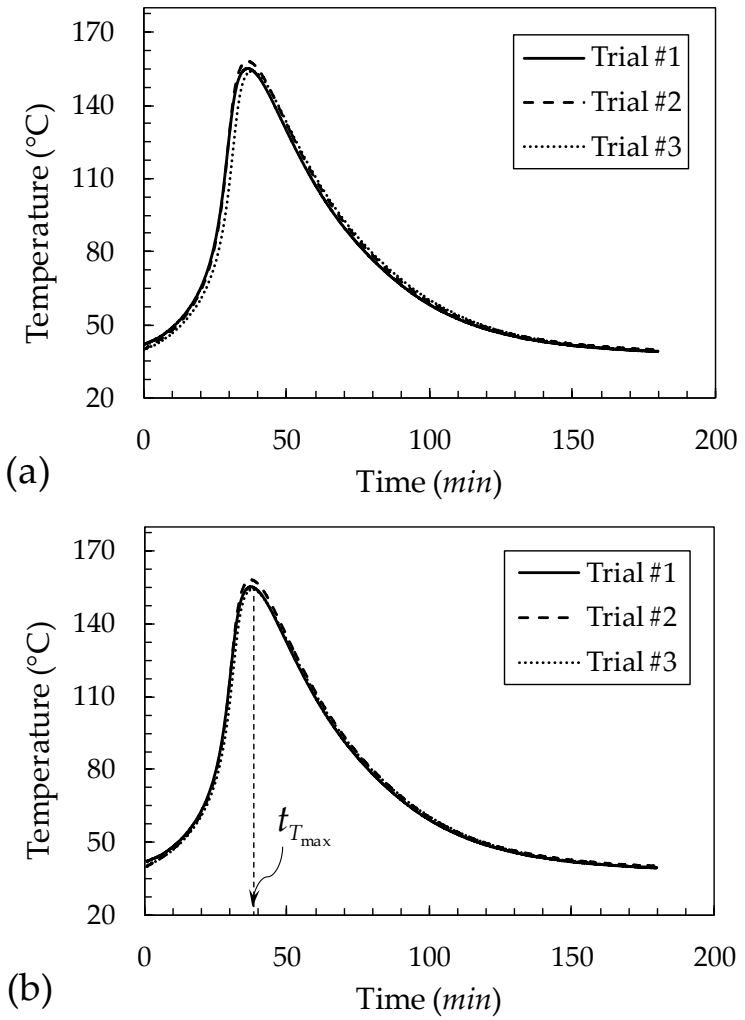

Figure 2-12: Change in the temperature of the midpoint during curing reaction for 1.5″-thick samples with 1.0 wt% CNT, in three repetitions (a) original positions, and (b) graphs shifted for their peaks to coincide at the same time

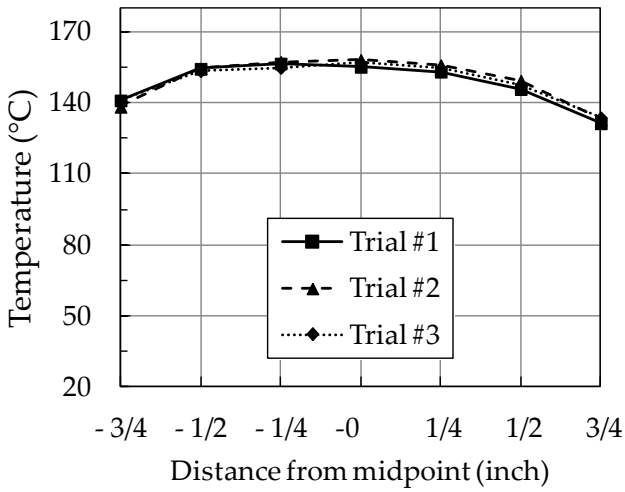

Figure 2-13: Temperature distribution across the thickness of 1.5″-thick samples with 1.0 wt% CNT when maximum temperature at midpoint occurs, in three repetitions (lines just present the trends)

thermocouples. Signals were recorded every nearly 5 seconds through a data acquisition system (National Instruments TBX-68) into a computer.

The abovementioned procedure was repeated three times for each sample with certain thickness and carbon nanotube content. Figure 2-12 shows three repetitions of temperature measurements at the midpoint for 1.5″-thick samples with 1.0 wt% carbon nanotube concentration during curing reaction. For the sake of comparison, the graphs are shifted on the time axis in order for their peak temperature to coincide at the same time which has been denoted as $t_{T_{max}}$ on the plot, Figure 2-12(b).

Temperature distribution across the thickness at $t_{T_{max}}$ is shown in Figure 2-13

from the same measurements. The case of 1.5″-thick samples with 1.0 wt% carbon nanotube concentration was randomly chosen to be shown among all the 12 investigated cases, i.e. four carbon nanotube concentrations (0.0, 0.5, 1.0 and 1.5 wt%) for three different thicknesses (0.5, 1.0 and 1.5″). The corresponding plots can be found in Appendix C. It is evident that the variation between the repetitions of the different runs of measurements is very small. Hence, for the

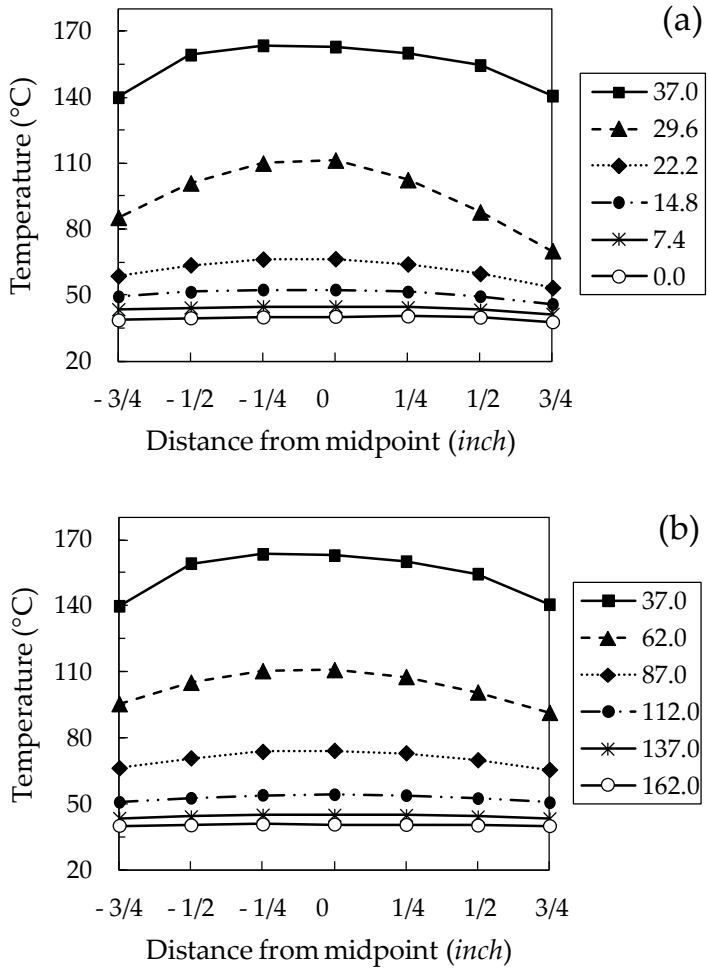

Figure 2-14: Temperature distribution across the thickness of 1.5″-thick neat resin sample (a) before the peak temperature, increments of 7.4 min, and (b) after the peak temperature, increments of 25.0 min (lines just present the trends – legend in minutes)

sake of clarity and neatness of the plots in the rest of this section, the average value of the three runs will be presented and the maximum standard deviation is mentioned, wherever larger than 5% of the mean value.

Figure 2-14 presents the temperature distribution across the thickness of 1.5″-thick neat resin sample at equal increments of time before and after the peak temperature occurs $t_{T_{max}}$. The numbers in the legends indicate the time at which the temperature distribution was recorded in minutes. For this case, maximum temperature occurred at 37.0 minutes. For the same sample, the change in the temperature for seven equally-distanced points across the thickness during the curing reaction is depicted in Figure 2-15. Further discussion about the results and figures can be found in Section 4.3.

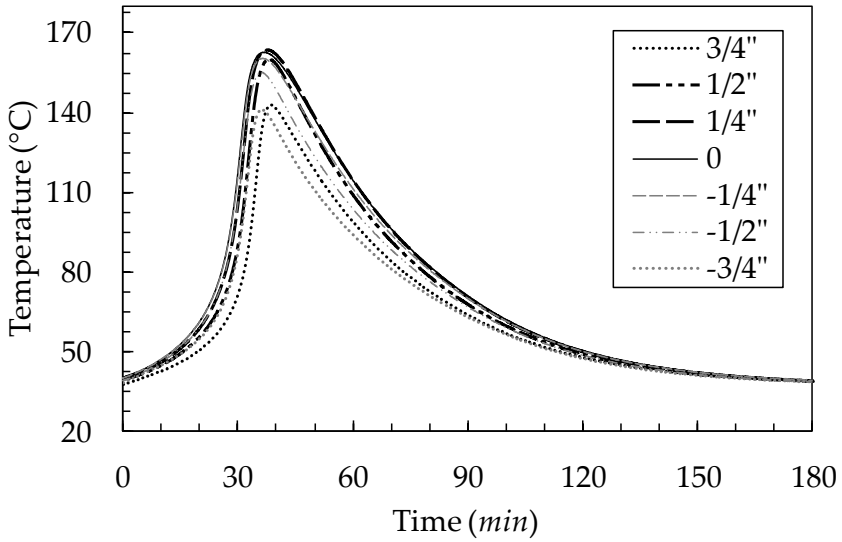

Figure 2-15: Change in the temperature at seven equally-distanced points across the thickness of pristine resin sample during curing reaction (legend: distance from the midpoint)

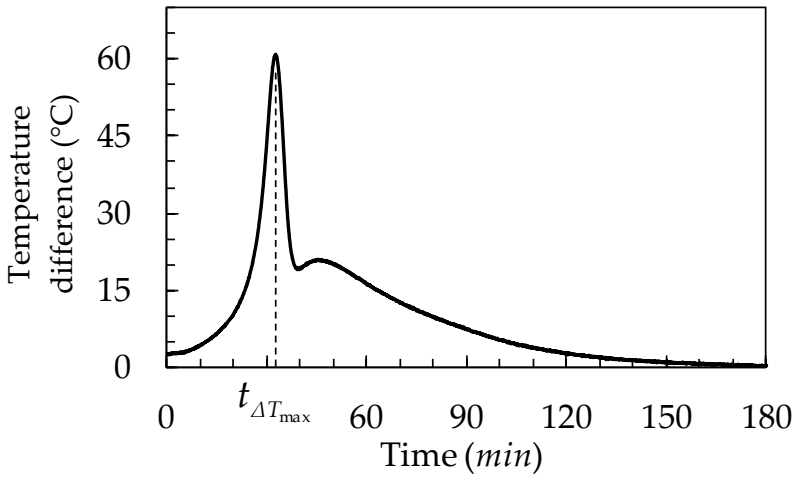

Figure 2-16: Change in temperature difference between the midpoint and the top surface of 1.5″-thick neat resin sample during curing reaction

The temperature difference between the midpoint and the outer surface of samples at any time during the curing process can be used as a useful indicator to show the severity of temperature gradient through the thickness of samples. This parameter is illustrated in Figure 2-16 for 1.5″-thick neat resin sample. The time at which this graph reaches its maximum, $t_{\Delta T_{max}}$, is of significant

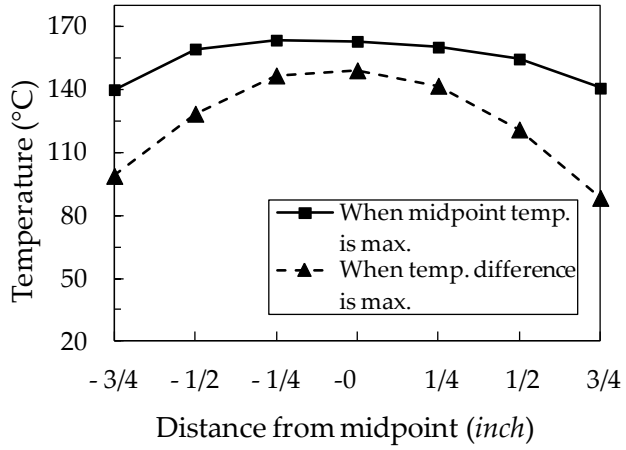

Figure 2-17: Temperature distribution across the thickness at $t_{\Delta Tmax}$ (▲), and t_{Tmax} (■) for the 1.5″-thick neat resin sample

importance. Temperature profiles across the thickness of the current sample at this time, $t_{\Delta T_{max}}$, as well as the moment at which the temperature of midpoint reaches its highest value, $t_{T_{max}}$, are shown in Figure 2-17. Although the peak temperature of the profile is higher at $t_{T_{max}}$, the difference between the temperature of the outer surface and the midpoint is larger at $t_{\Delta T_{max}}$. In other words, the temperature profile has its highest curvature for $t_{\Delta T_{max}}$. Since thermally induced residual stresses are more dependent on the temperature gradient rather than the value of the temperature itself, the moment of maximum gradient is more critical as compared to the time at which the maximum temperature occurs.

Figure 2-18 and Figure 2-19 respectively show the change in the midpoint temperature as well as the change in temperature difference between the midpoint and the outer surface for samples of different thicknesses containing different CNT concentrations during curing reaction. Temperature profile across the thickness at $t_{\Delta T_{max}}$ for those samples can be found in Figure 2-20. Results are discussed in Chapter 4.

2.4. SAMPLE SELECTION

While preparing the material, it was found that the viscosity increased

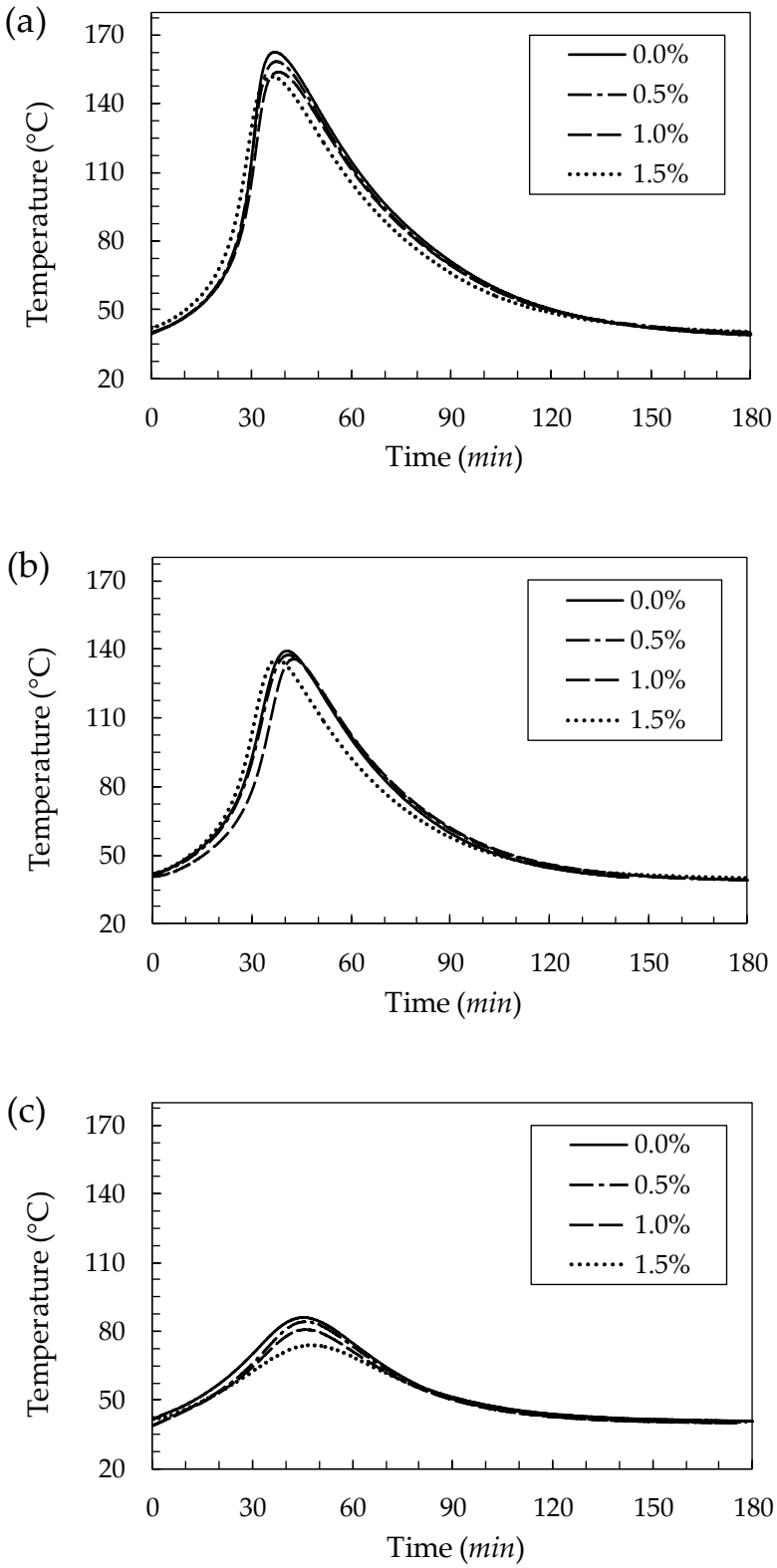

Figure 2-18: Change in the midpoint temperature of (a) 1.5″-, (b) 1.0″-, and (c) 0.5″-thick samples for different CNT concentrations during curing reaction

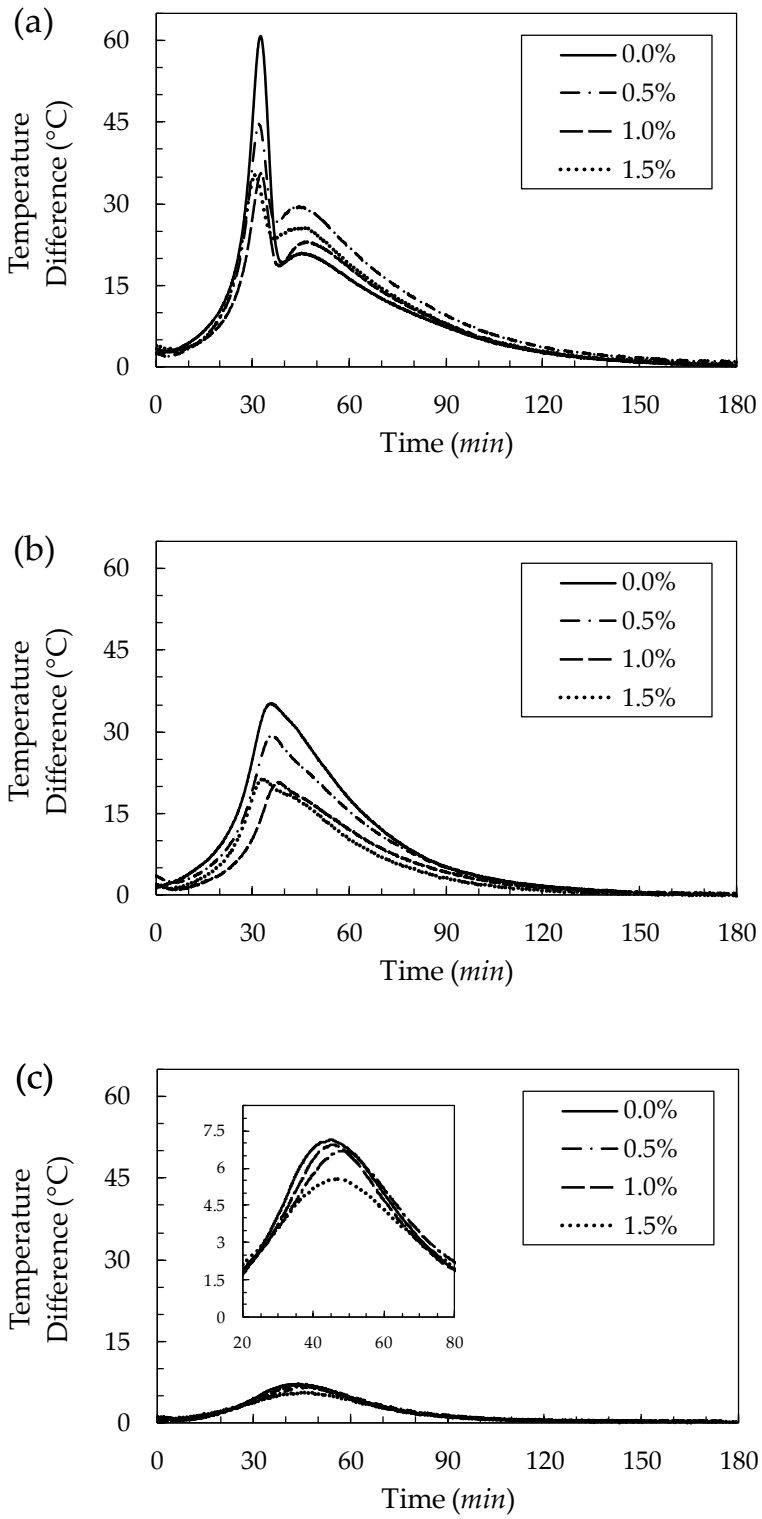

Figure 2-19: Change in temperature difference between the midpoint and the outer surface of (a) 1.5″-, (b) 1.0″-, and (c) 0.5″-thick samples for different CNT concentrations during curing reaction

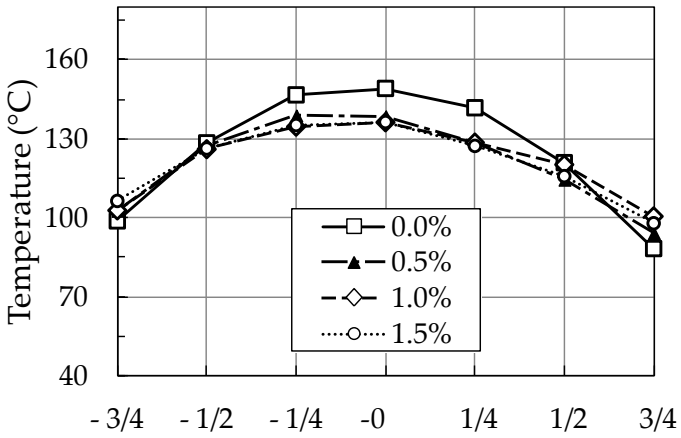

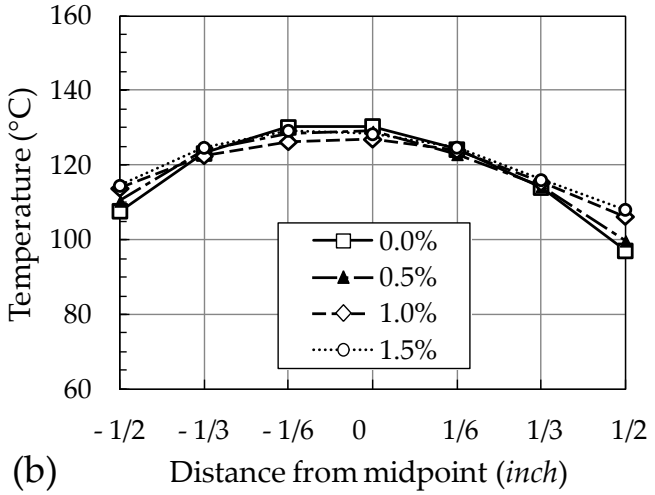

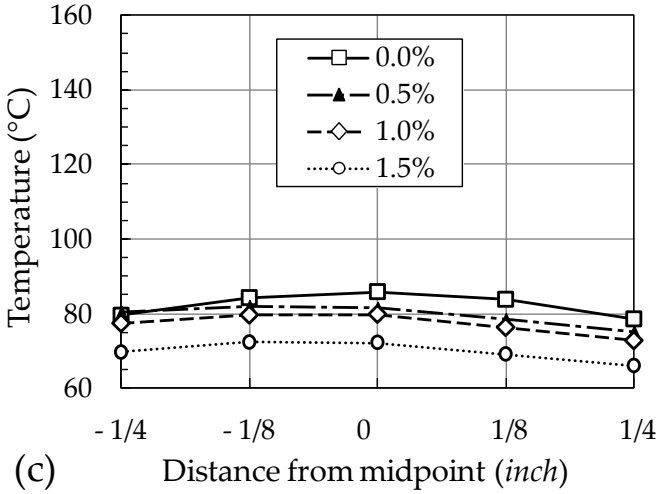

Figure 2-20: Temperature distribution across the thickness at $t_{\Delta T max}$ for (a) 1.5″-, (b) 1.0″-, and (c) 0.5″-thick samples with different CNT concentrations

dramatically when the concentration of carbon nanotubes in epoxy exceeded 1.0 wt%, making it very difficult to handle the material to prepare the samples and ensure a homogeneous mixture while blending with the curing agent. Particularly, preventing void formation while pouring the material in the glass vials for temperature measurements seemed to be impossible. However, all the measurements presented in this chapter were conducted on samples with 1.5 wt% CNT content as well.

In all of the measurements, the trends observed among the samples of neat resin, 0.5 and 1.0 wt% CNT were contradicting the trends for samples of 1.5 wt% CNT. For instance, Figure 2-10 shows a reduction of thermal diffusivity for samples with 1.5 wt% CNT concentration which is not expected since addition of a highly conductive material into a less conductive one should rise the overall thermal conductivity. Also, a comparatively large standard deviation in measurements of total heat of reaction for samples with 1.5 wt% CNT concentration can be seen in Table 2-3, showing high scattering which is in the same order of magnitude of the changes in total heat of reaction by increasing carbon nanotubes. High scattering in temperature profile measurements is also observed for samples with 1.5 wt% CNT contents as presented in Appendix C. The temperature profiles across the thickness of these samples are not smooth which suggest a poor and

non-homogeneous mixture of epoxy and curing agent.

Analogous dissimilarities between the measured values for samples with 1.5 wt% CNT compared to rest of the samples can be seen for heat capacity (Figure 2-8), activation energy (Table 2-2) and both rate and degree of cure (Figure 2-7 and Appendix B). Therefore, all the samples with 1.5 wt% CNT concentration will be dismissed from discussions in Chapter 4 due to the sample preparation difficulties and high uncertainties in the measurements.

Chapter 3: NUMERICAL MODEL AND RESULTS

3.1. INTRODUCTION

A computer code was developed to provide the comprehension of the effective parameters in the heat transfer problem and to model the heat generation during the curing process of the epoxy, using Maple software.

First, this chapter introduces the governing differential equation as well as the boundary conditions which describe the designed experimental setup (see Chapter 2). Subsequently, the finite difference method is used to derive the discretized form of the differential equation for nodes at different locations, i.e. interior, symmetric and boundary nodes. The numerical stability condition is also studied. The following section elaborates on the term of heat generation in the differential equation which is attributed to the exothermic chemical reaction during the curing process of the epoxy. Here, the thermo-chemical model that is used to evaluate the kinetics of the curing process will be introduced and discretized to be substituted in the discretized differential equation. The last section presents the results of temperature distribution modelling as well as the determined cure kinetics constants.

3.2. HEAT TRANSFER MODEL

3.2.1. Heat balance

To numerically model the experimental setup used in this study, Figure 3-1, the top and bottom surfaces of the sample are considered to be in direct contact with the air inside the oven. Although this is a simplification for the bottom of the sample because there is a thin layer of glass (vial) between the epoxy and air, the above assumption is valid since the bottom of the vial is rather thin (approximately 1 mm) compared to the thickness of the samples (0.5 to 1.5 inches). Obviously, assuming symmetric boundary conditions for the problem leads to symmetric temperature profile across the thickness of the sample, numerically. However, asymmetric experimental results are anticipated due to asymmetric boundary conditions.

For a control volume, the general form of the energy balance, assuming no mass transfer, is expressed by Equation (3-1) on the rate basis

$$\dot{E}_{in} + \dot{E}_{gen} = \dot{E}_{st} \tag{3-1}$$

where, $\dot{E}_{in}$ is the rate of input energy into the control volume from its surrounding, $\dot{E}_{gen}$ is the rate of energy generation at control volume and $\dot{E}_{st}$ is

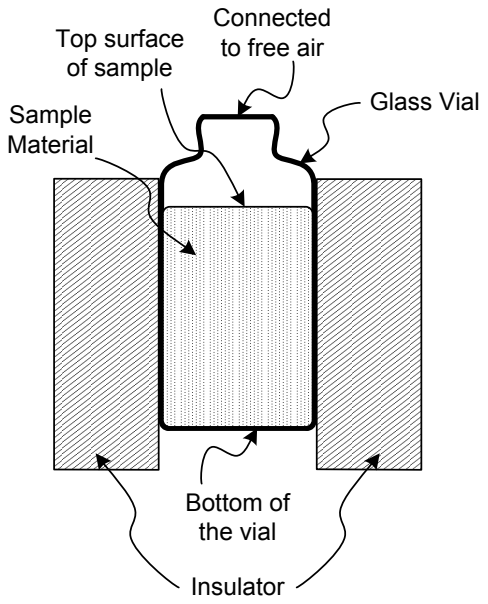

Figure 3-1: Schematic setup of the sample and insulator

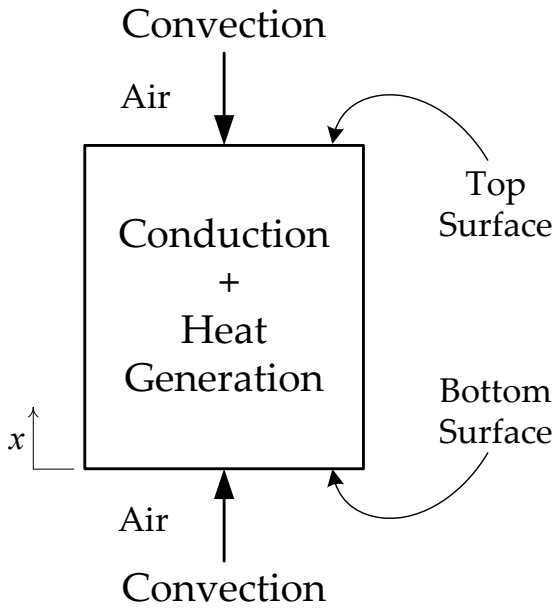

Figure 3-2: Schematics of heat transfer model used in the numerical code

the storage rate of energy at control volume.

The assumption of having top and bottom surfaces of the samples in direct contact with air leads the heat transfer to happen at the boundaries in the form of convection between the sample and the surrounding air. Figure 3-2 illustrates the schematic view of boundary conditions as well as the different heat transfer forms in the model. The differential equation expressing heat transfer across the thickness of this system (one-dimensional) is

$$k\,\frac{\partial^2 T}{\partial x^2} + \dot{q}_{gen} = \rho C_p \frac{\partial T}{\partial t}\ ; \qquad k\,\frac{\partial T}{\partial x}\Big|_{x=0\&L} = h\left(T_\infty - T_{Surf}\right) \tag{3-2}$$

in which, T is temperature of any point of the sample at any time, T_∞ is

temperature of the surrounding air in the oven, T_{Surf} is the temperature of the surface of the sample, k is coefficient of thermal conduction of composite, C_p is the specific heat capacity of composite, ρ is density of the resin system, h is convection heat transfer coefficient for air, x and t are independent spatial and time variables, respectively. The boundary condition ensures that the heat flux is continuous at the surfaces ($x = 0. \& L$). $\dot{q}_{gen}$, rate of heat generation per unit volume is related to $\dot{E}_{gen}$, the rate of heat generation during the chemical reaction by Equation (3-3).

$$\dot{E}_{gen} = \dot{q}_{gen}V = \rho V\left(\frac{\partial H_t}{\partial t}\right) \tag{3-3}$$

where $\partial H_t/\partial t$ is the rate of heat generation at a specific time in control volume with volume V. More elaboration on term of heat generation will be presented in Section 3.2.4.

3.2.2. Finite difference method – Explicit method

Since the problem has two independent variables, i.e. spatial x and time t variables, both the geometry and time domain need to be discretized for numerical solution. Here, n nodes distanced at Δx from each other are introduced through the thickness to discretize the spatial domain and p time steps are introduced with the interval of Δt to discretize the time domain, Figure 3-3

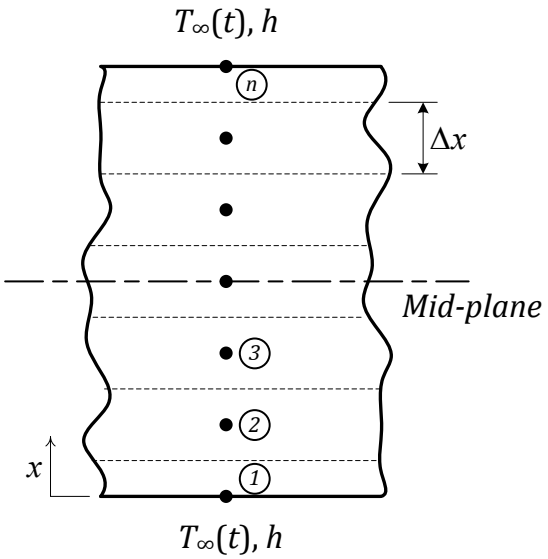

Figure 3-3: Typical discretized geometry and symmetric boundary conditions

Having the simplification of symmetrical boundary conditions ensures a symmetrical result with respect to the mid-plane of the sample. Therefore, only one half of the geometry needs to be analyzed since the other half will have the mirror results. Considering odd number of spatial nodes, three different types of nodes can be distinguished in Figure 3-3 based on their location across the thickness:

- nodes at the boundary (boundary nodes);
- the node on the mid-plane (symmetric nodes); and
- any nodes except the above-mentioned (interior nodes).

The heat transfer mechanisms for these three types of nodes are slightly different from each other due to the fact that the boundary nodes exchange energy in

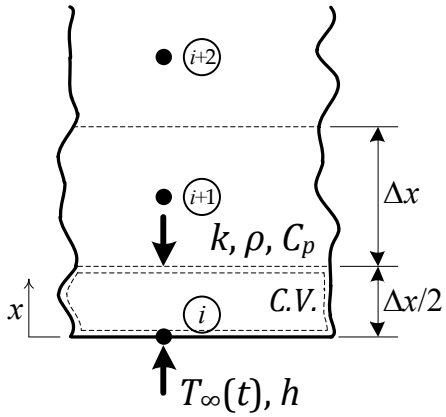

Figure 3-4: Heat transfer mechanisms for control volume surrounding the boundary node

convection with the surrounding air as well as in conduction with the adjacent node while the interior nodes merely conduct the energy to their adjacent nodes. As such, the form of equation of heat balance, Equation (3-1), the resulting differential equation and the discretized form of that are also slightly different for each type of nodes.

Figure 3-4 shows the heat transfer mechanisms for the control volume surrounding a boundary node. The specific governing differential equation for a boundary node is determined, Equation (3-4), by expanding Equation (3-1) for such a control volume.

$$hS(T_\infty - T_i) + kS\,\frac{\partial T}{\partial x} + \rho V\left(\frac{\partial H_t}{\partial t}\right) = \rho V C_p\,\frac{\partial T}{\partial t} \tag{3-4}$$

In which S is the cross section area perpendicular to the thickness of the sample. The same approach can be used to determine the specific form of heat balance

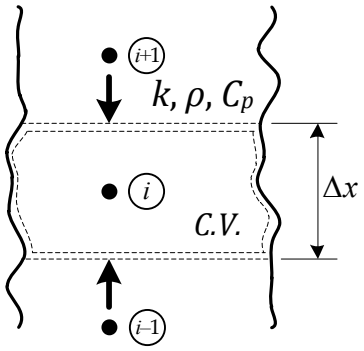

Figure 3-5: Heat transfer mechanisms for control volume surrounding a typical interior node

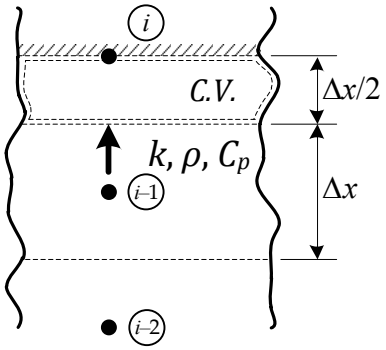

Figure 3-6: Heat transfer mechanisms for control volume surrounding a symmetric node

equation for interior and symmetric nodes. Figure 3-5 and Figure 3-6 respectively illustrate the control volume as well as the heat transfer mechanisms associated with a typical interior and symmetric node. Note that a symmetrical boundary condition is equivalent to have the boundary insulated. Energy balance for an interior and a symmetric node is also expressed by Equation (3-5). Obviously, interior nodes – including the symmetric node – do not have any contact with air which explains why the convection term in the energy balance equation disappears.

$$kS\,\frac{\partial T}{\partial x} + \rho V\left(\frac{\partial H_t}{\partial t}\right) = \rho V C_p \frac{\partial T}{\partial t} \tag{3-5}$$

To discretize Equations (3-4) and (3-5), the finite difference approximation to the spatial and time derivatives are expressed by

$$\left.\frac{\partial T}{\partial x}\right|_i^p \approx \frac{T_{i+1}^p - T_i^p}{\Delta x} \tag{3-6}$$

$$\left.\frac{\partial T}{\partial t}\right|_i^p \approx \frac{T_i^{p+1} - T_i^p}{\Delta t} \tag{3-7}$$

in which superscript i is the spatial counter and superscript p denotes time step. When the time derivative is a forward-difference approximation, the finite difference method is called *explicit*.

Substituting Equations (3-6) and (3-7) in Equations (3-4) and (3-5), the discrete forms of the energy balance equation for boundary nodes, interior nodes and symmetric node are determined as shown in Equations (3-8), (3-9) and (3-10), respectively.

$$hS\left(T_\infty^p - T_i^p\right) + kS\,\frac{T_{i+1}^p - T_i^p}{\Delta x} + \rho\left(S\frac{\Delta x}{2}\right)\left(\frac{\partial H_t}{\partial t}\right)_i^p = \rho C_p\left(S\frac{\Delta x}{2}\right)\frac{T_i^{p+1} - T_i^p}{\Delta t} \tag{3-8}$$

$$kS\,\frac{T_{i+1}^p - T_i^p}{\Delta x} + kS\,\frac{T_{i-1}^p - T_i^p}{\Delta x} + \rho(S\Delta x)\left(\frac{\partial H_t}{\partial t}\right)_i^p = \rho C_p(S\Delta x)\frac{T_i^{p+1} - T_i^p}{\Delta t} \tag{3-9}$$

$$kS\,\frac{T_{i-1}^p - T_i^p}{\Delta x} + \rho\left(S\frac{\Delta x}{2}\right)\left(\frac{\partial H_t}{\partial t}\right)_i^p = \rho C_p\left(S\frac{\Delta x}{2}\right)\frac{T_i^{p+1} - T_i^p}{\Delta t} \tag{3-10}$$

Rewriting these three equations for T_i^{p+1} leads to the final discretized energy balance equations:

$$T_i^{p+1} = \left[1 - 2\frac{\lambda\Delta t}{(\Delta x)^2} - 2\,\frac{h\Delta t}{\rho C_p \Delta x}\right] T_i^p + 2\frac{h\Delta t}{\rho C_p \Delta x} T_\infty^p + 2\frac{\lambda\Delta t}{(\Delta x)^2} T_{i+1}^p + \frac{\Delta t}{C_p}\left(\frac{\partial H_t}{\partial t}\right)_i^p \tag{3-11}$$

$$T_i^{p+1} = \left[1 - 2\frac{\lambda\Delta t}{(\Delta x)^2}\right] T_i^p + \frac{\lambda\Delta t}{(\Delta x)^2}\left(T_{i-1}^p + T_{i+1}^p\right) + \frac{\Delta t}{C_p}\left(\frac{\partial H_t}{\partial t}\right)_i^p \tag{3-12}$$

$$T_i^{p+1} = \left[1 - 2\frac{\lambda\Delta t}{(\Delta x)^2}\right] T_i^p + 2\frac{\lambda\Delta t}{(\Delta x)^2} T_{i-1}^p + \frac{\Delta t}{C_p}\left(\frac{\partial H_t}{\partial t}\right)_i^p \tag{3-13}$$

where λ is thermal diffusivity which is defined by Equation (3-14).

$$\lambda = \frac{k}{\rho C_p} \tag{3-14}$$

It is evident from Equation (3-11) to (3-13) that in explicit method, temperature of node i at any given time increment $(p+1)$ depends only on the temperature of the adjacent nodes at the time increment p, which are all known. That is the reason why the explicit method is known as a *marching solution*.

3.2.3. Numerical stability analysis

Explicit finite difference method is conditionally stable which means that for a given spatial increment length, Δx, time increment size should stay lower than a certain value to prevent numerical fluctuation and divergence of the solution.

According to von Neumann stability analysis or explicit finite difference solution, the initial error should not be amplified with the progress of solution.

Hence the error, ε_i^p, is defined as the difference between the solution of finite difference approximation, T_i^p, and the exact solution of the differential equation, $\hat{T}_i^p$, at ith node and pth time increment.

$$\varepsilon_i^p = T_i^p - \hat{T}_i^p \tag{3-15}$$

From Equation (3-13), the explicit finite difference solution for the symmetric node, T_i^{p+1} and $\hat{T}_i^{p+1}$ can be calculated.

$$T_i^{p+1} = [1 - 2Fo]T_i^p + 2FoT_{i-1}^p + \frac{\Delta t}{C_p}\left(\frac{\partial H_t}{\partial t}\right)_i^p + R_{E_i^{p+1}} \tag{3-16}$$

$$\hat{T}_i^{p+1} = [1 - 2Fo]\hat{T}_i^p + 2Fo\hat{T}_{i-1}^p + \frac{\Delta t}{C_p}\left(\frac{\partial H_t}{\partial t}\right)_i^p + T_{E_i^{p+1}} \tag{3-17}$$

In Equation (3-16) $R_{E_i^{p+1}}$ the numerical round-off and error and since exact solution of the differential equation should satisfy the discretized form of the solution as well, a truncation error, $T_{E_i^{p+1}}$, appears in Equation (3-17). Fourier number, Fo, is defined as follow:

$$Fo = \frac{\lambda \Delta t}{(\Delta x)^2} \tag{3-18}$$

Deducting Equation (3-17) from (3-16) leads to

$$\varepsilon_i^{p+1} - [1 - 2Fo]\varepsilon_i^p - 2Fo\ \varepsilon_{i-1}^p = R_{E_i^{p+1}} + T_{E_i^{p+1}} \tag{3-19}$$

which represents the propagation of the error during the numerical solution. Von Neumann considers the homogeneous form of Equation (3-19), the solution of which is

$$\varepsilon_i^p = ce^{\gamma p \Delta t} e^{j\xi i \Delta x} \tag{3-20}$$

Where $j = \sqrt{-1}$ and γ, c and ξ are constants.

The amplification factor of the initial error is determined by dividing the value of the error at $p = p_0 + 1$ by that of $p = p_0$. The *von Neumann condition for stability* states that amplification factor of initial error should stay less than unity in order for original error not to grow during the time of the solution, Equation (3-21).

$$\left|e^{\gamma \Delta t}\right| \leq 1 \tag{3-21}$$

To calculate the amplification factor, Equation (3-20) should be substituted into Equation (3-19) and rewritten for $e^{\gamma \Delta t}$:

$$e^{\gamma \Delta t} = 1 - 2Fo - 2Fo\, e^{-j\xi \Delta x} \tag{3-22}$$

Putting the modulus of this complex number into inequality (3-21), expanding Fourier number from Equation (3-18) and rearranging the result for Δt, the allowable range of Δt is determined in terms of material properties as well as the spatial increment length.

$$\Delta t \leq \frac{(\Delta x)^2}{2\lambda} \tag{3-23}$$

If the definition of Fourier number from Equation (3-18) is used, this equation can be expressed in terms of thermal numbers:

$$Fo \leq \frac{1}{2} \tag{3-24}$$

With a similar approach the von Neumann condition for stability can be determined for interior and boundary nodes, Equation (3-25) and (3-26), respectively.

$$Fo \leq \frac{1}{2} \tag{3-25}$$

$$Fo(1 + Bi) \leq \frac{1}{2} \tag{3-26}$$

In which Biot number, Bi, is defined as follow:

$$Bi = \frac{h\Delta t}{k} \tag{3-27}$$

Since Biot number is positive, whenever inequality (3-26) is true, it includes Equations (3-24) and (3-25) and consequently, the stability condition for all of the nodes is guaranteed.

3.2.4. Thermo-chemical constants (Kissinger's method)

The term of heat generation in Equation (3-2) denotes the exothermic chemical reaction which occurs between the molecules of epoxy and the curing agent during the curing process. According to the definition of *Degree of Cure*, α, stated by Equation (3-28), reaction rate, $\partial\alpha/\partial t$, is related to the rate of heat generation through Equation (3-29).

$$\alpha = \frac{H_t}{\Delta H_R} \tag{3-28}$$

$$\frac{\partial \alpha}{\partial t} = \frac{1}{\Delta H_R}\frac{\partial H_t}{\partial t} \tag{3-29}$$

In which H_t is the heat of reaction from time zero to the desired time and ΔH_R is the total heat of reaction.

To numerically evaluate this reaction, different models have been developed in literature for kinetics of curing process of polymers (Boey and Qiang 2000). One of the common models for epoxy is a two-parameter autocatalytic model which is formulated by Equation (3-30).

$$\frac{\partial \alpha}{\partial t} = Ae^{-\frac{E_a}{RT}}(1-\alpha)^n \alpha^m \tag{3-30}$$

where, A is frequency factor, E_a is activation energy, m and n are orders of

reaction and R is universal gas constant (8.314 $J/mol.K$). This model dictates that the value of rate of cure to be zero at the beginning and the end of the curing reaction which is compatible with the nature of curing of epoxy.

All the constants in this equation should be determined empirically using curve fitting on DSC data (Table 2-3). One of the methods to determine kinetic equation's constants is called Kissinger's method which has been validated for epoxy systems (Kissinger 1957, Boey and Qiang 2000, Prime 1997). According to Kissinger's method, DSC data of different heating rate tests is required. Then, having the heating rates, φ, and the temperature at which the maximum curing rate occurs, T_m, values of $\ln(\varphi/{T_m}^2)$ can be plotted versus $1/T_m$. Kissinger suggests that the slope of this graph is related to the activation energy by Equation (1-6).

Finally, the rest of the constants can be determined simultaneously by a multiple variable linear least square curve fitting on DSC data for the linearized form of Equation (3-30) (see Section 2.2.1).

Being able to calculate the value of rate of cure from Equation (3-30), the rate of heat generation can also be calculated from Equation (3-29) which eventually determines the term of $\dot{E}_{gen}$ in Equation (3-2). By substituting Equation (3-29)

into Equations (3-11) to (3-13) the final discretized form of the energy balance is concluded as follow:

$$T_i^{p+1} = \left[1 - 2\frac{\lambda\Delta t}{(\Delta x)^2} - 2\,\frac{h\Delta t}{\rho C_p \Delta x}\right] T_i^p + 2\frac{h\Delta t}{\rho C_p \Delta x} T_\infty^p + 2\frac{\lambda\Delta t}{(\Delta x)^2} T_{i+1}^p + \frac{(\Delta H_R)\Delta t}{C_p}\left(\frac{\partial\alpha}{\partial t}\right)_i^p \quad (3\text{-}31)$$

$$T_i^{p+1} = \left[1 - 2\frac{\lambda\Delta t}{(\Delta x)^2}\right] T_i^p + \frac{\lambda\Delta t}{(\Delta x)^2}\left(T_{i-1}^p + T_{i+1}^p\right) + \frac{(\Delta H_R)\Delta t}{C_p}\left(\frac{\partial\alpha}{\partial t}\right)_i^p \quad (3\text{-}32)$$

$$T_i^{p+1} = \left[1 - 2\frac{\lambda\Delta t}{(\Delta x)^2}\right] T_i^p + 2\frac{\lambda\Delta t}{(\Delta x)^2} T_{i-1}^p + \frac{(\Delta H_R)\Delta t}{C_p}\left(\frac{\partial\alpha}{\partial t}\right)_i^p \quad (3\text{-}33)$$

Since the value of degree of cure is required to calculate the curing rate at any time in Equation (3-30), as the solution progresses in time, the value of degree of cure should be calculated progressively. To do so, the value of degree of cure at ith node for any new time $(p+1)$ can be calculated using Equation (3-34).

$$\alpha_i^{p+1} = \alpha_i^p + \left(\frac{\partial\alpha}{\partial t}\right)_i^p \Delta t \quad (3\text{-}34)$$

3.3. COMPUTER CODE FLOWCHART

A computer code was developed using Maple software to model the heat generation and transfer during the curing process of the resin. The calculation procedure used in this model is as follow:

- Input thermo-chemical and thermo-physical properties;

- Input geometrical parameters, initial conditions and set required solution spatial and time resolution;
- Check the required numerical stability for the solution based on input parameters;
- Marching solution based on Equations (3-31) to (3-33) depending on the node type;
- Write the results in text files and plot them.

The code can be found in Appendix E.

3.4. SIMULATION RESULTS

As discussed in Section 2.4, samples with 1.5 wt% CNT contents were dismissed from this study due to the significant uncertainties in the measurements conducted. Therefore, these samples were not considered in the numerical simulations either and the results presented in this chapter consist of simulation results for neat resin, samples with 0.5 and 1.0 wt% CNT contents, only.

Figure 3-7 shows the numerical simulation results of changes in the midpoint temperature of samples with 1.5″, 1.0″, and 0.5″ thickness each one containing pristine resin, 0.5 and 1.0 wt% CNT concentrations during curing reaction. The simulation of change in temperature difference between the midpoint and the

outer surface of the same samples during curing reaction are illustrated in Figure 3-8. Temperature profile simulation at $t_{\Delta T_{max}}$ for all the abovementioned cases can be found in Figure 3-9.

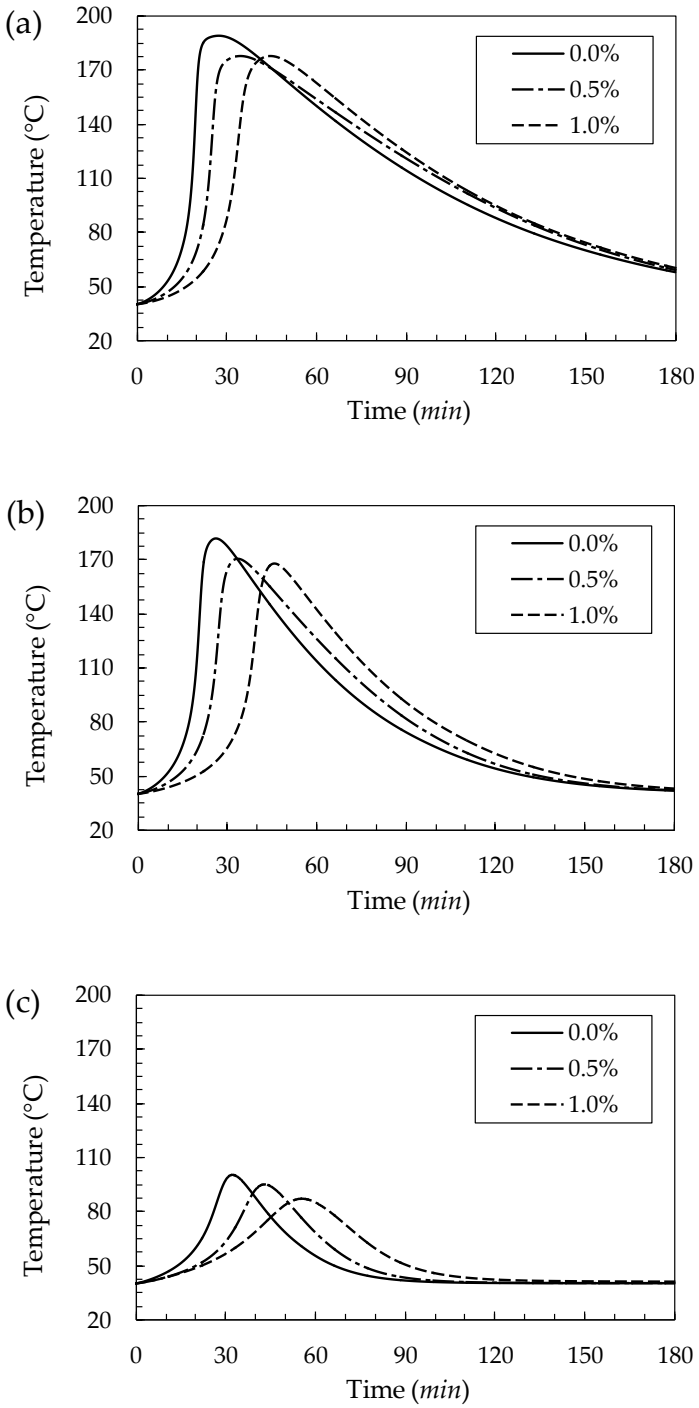

Figure 3-7: Numerical simulation of changes in the midpoint temperature of (a) 1.5″-, (b) 1.0″-, and (c) 0.5″-thick samples for different CNT concentrations during curing reaction

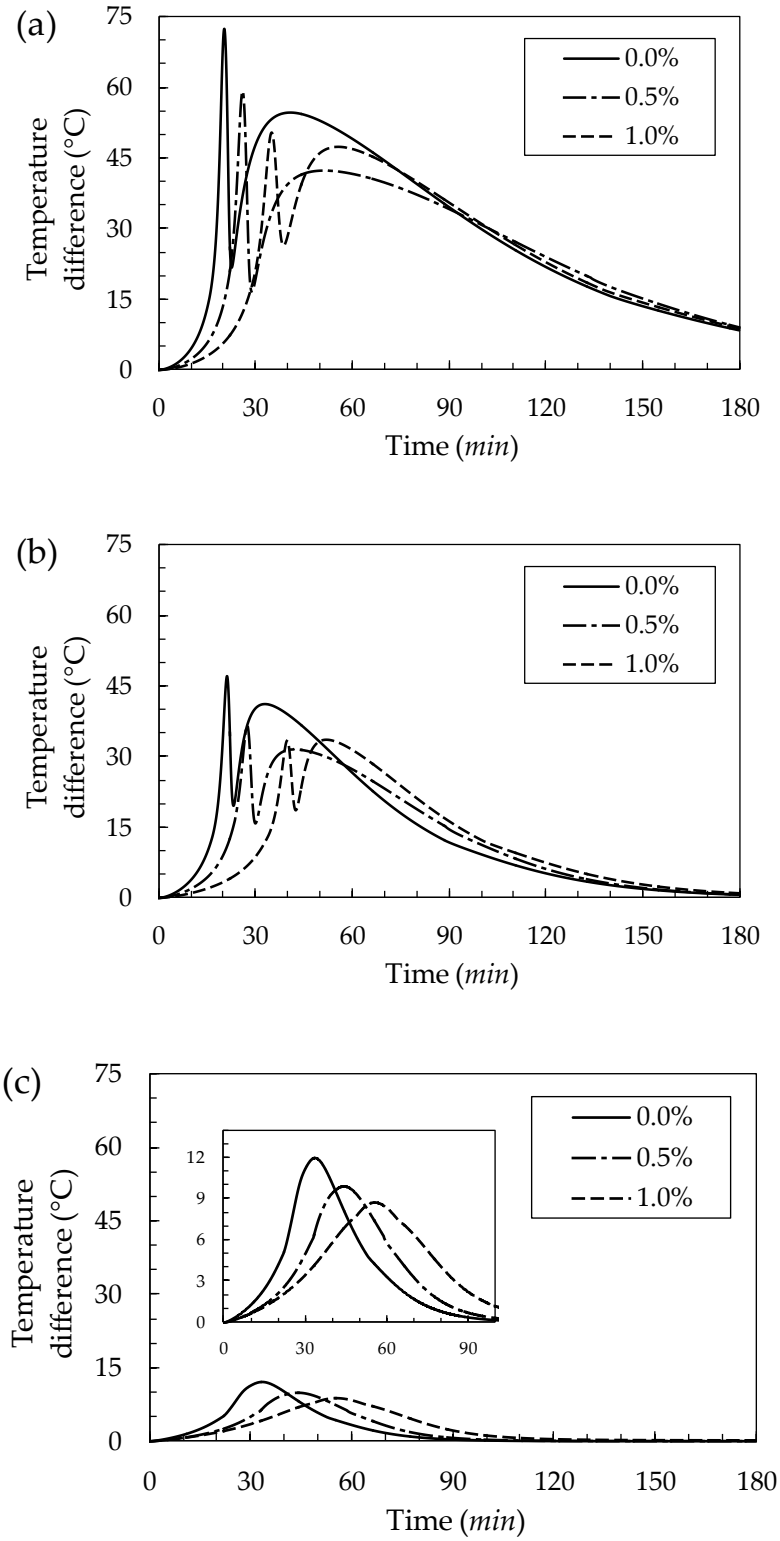

Figure 3-8: Numerical simulation of changes in temperature difference between the midpoint and the outer surface of (a) 1.5″-, (b) 1.0″-, and (c) 0.5″-thick samples for different CNT concentrations during curing reaction

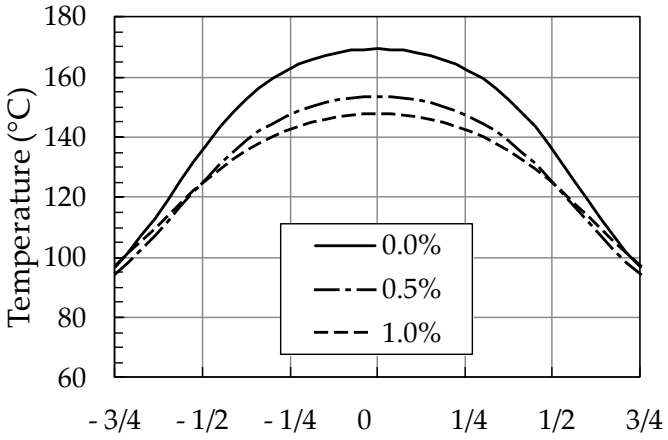

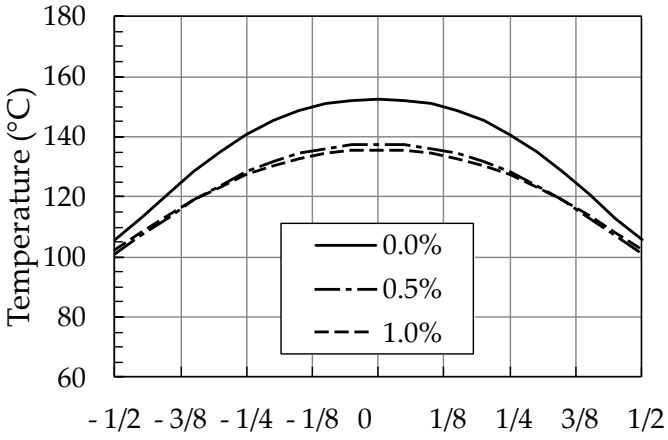

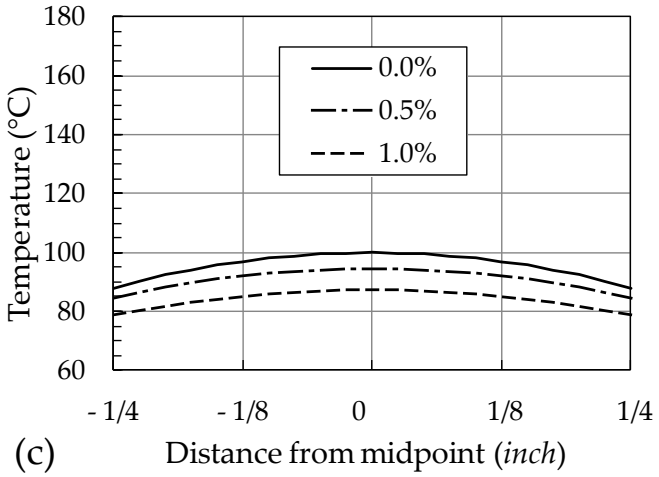

Figure 3-9: Numerical simulation of temperature distribution across the thickness at $t_{\Delta Tmax}$ for (a) 1.5″-, (b) 1.0″-, and (c) 0.5″-thick samples with different CNT concentrations

Chapter 4: DISCUSSION

4.1. INTRODUCTION

This chapter will discuss the experimental and numerical results presented in Chapter 2 and Chapter 3.

First, the results from measurements of material thermal properties are discussed. The following section will discuss the experimental results from temperature measurements. Finally, the computer simulation will be discussed and compared with the experimental results.

As explained in Section 2.4, the discussion will not include samples with 1.5 wt% carbon nanotube concentration.

4.2. MATERIAL PROPERTIES MEASUREMENTS

4.2.1. Cure kinetics

Figure 4-1 depicts the change in the constants of cure kinetic equation, Equation (3-30), by adding carbon nanotubes. The measurement method of these constants as well as related results were presented in Section 2.2.1. The increase in the pre-exponential factor (A) is more significant than the other parameters by adding

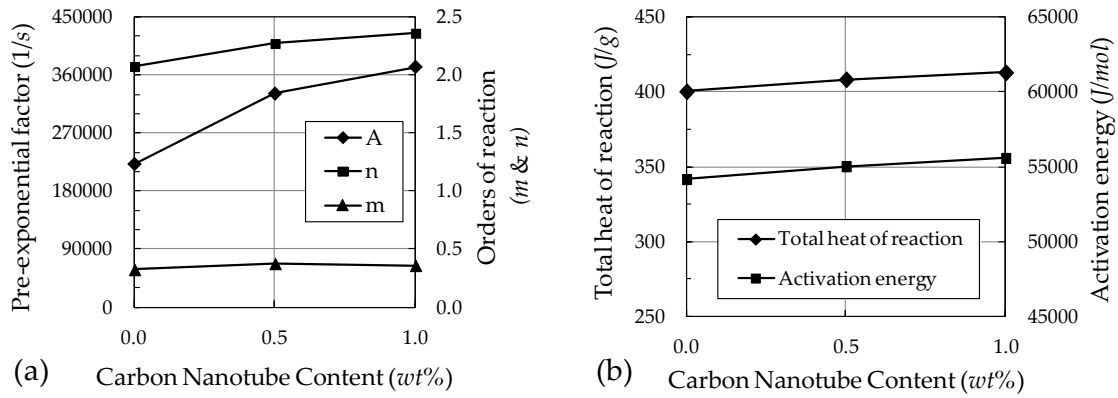

Figure 4-1: Change in (a) pre-exponential factor as well as orders of reaction, and (b) total heat of reaction and activation energy by adding CNTs (lines just present trends)

CNT. An increase in activation energy suggests a delay in the kickoff the reaction. However, the slight raise in the total heat of reaction implies higher released energy during the curing process. Figure 2-7(b) and the plots in Appendix B show less degree of cure at a certain temperature for samples containing carbon nanotubes compared to that of the pristine resin. This trend can also be observed in Figure 2-7(a) and Appendix A for the rate of cure, suggesting an overall hindering effect of carbon nanotubes on curing of epoxy. Carbon nanotubes can be considered as obstacles between molecules of epoxy and curing agent for making bonds which reduces the speed of the reaction, however, by increasing the temperature which reduces the viscosity, the molecules can bypass the carbon nanotubes and eventually make bonds. The opposite results, however, have been reported previously for resin systems with high viscosity which can be explained by mobility of the molecules (Figure 1-9).

The effect of increasing the viscosity by adding CNT into a resin system is less pronounced for highly viscose systems compared to systems with lower viscosity. As the curing reaction begins, while the temperature is rising the decrease in viscosity is less pronounced in highly viscose systems compared to systems with lower viscosity. Therefore, in systems with higher viscosity, carbon nanotubes can conduct energy from an already cured spot in the resin to other uncured parts while there are very small movements in the molecules of the system due to high viscosity. However, for low viscosity resin systems, the same increase in temperature results in more mobility of the system's molecules as well as the carbon nanotubes which leads the carbon nanotubes to be more effective in hindering the curing reaction because they can easier be present between molecules of epoxy and curing agent. This results in a reduction in the rate of cure.

Figure 2-7(b) can be reproduced from the cure kinetic model by substituting the calculated constants of the cure kinetic equation from Table 2-2 and Table 2-3 into Equation (3-30) and integrating the result numerically using the Runge-Kutta method. The results in Figure 4-2 show the same abovementioned trend of decelerating the cure reaction.

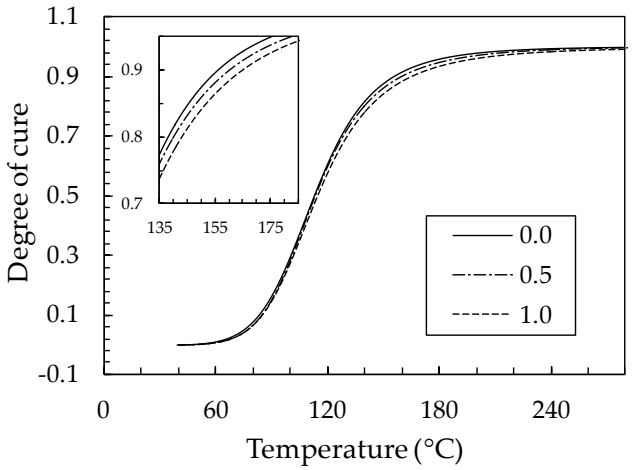

Figure 4-2: Results of numerical integration from Equation (3-30) for samples with different CNT contents in a DSC test with heating rate of 15 °C/min

4.2.2. Thermal diffusivity

Figure 2-10 illustrates the change in thermal diffusivity by adding carbon nanotubes into the epoxy resin at three temperatures, i.e. 40, 100 and 150°C. About 13% increase in thermal diffusivity is noticeable at all temperatures by addition of 1.0 wt% carbon nanotubes, which suggests an enhancement in the effectiveness of the samples containing carbon nanotubes to transfer energy by conduction compared to their energy storage capacity. The idea that adding a more thermally conductive material, in this case carbon nanotubes, into a less conductive material, here to be epoxy, will increase the overall thermal conductivity can explain the enhancement in thermal diffusivity.

4.2.3. Density

It is well known that epoxy exhibits a considerable shrinkage during the curing process. However, to simplify the computer code, the variations of density during the cure was not taken into account in the numerical simulations of this study. Density of the cured samples was measured according to the procedure described in Section 2.2.4 and the values are reported in Table 2-6. Density of samples increases slightly by adding carbon nanotubes which is conceivable due to higher density of carbon nanotubes compared to epoxy/curing agent mixture.

4.3. TEMPERATURE MEASUREMENTS

As discussed in Section 2.3 (Figure 2-17) temperature profile across the thickness has its most critical situation at $t_{\Delta T_{max}}$. Figure 2-20 shows the temperature distribution across the thickness for all of the samples. As anticipated in Section 3.2.1, asymmetries between the temperature of each point from one side of the midpoint, e.g. top, and its corresponding point on the other side of the midpoint, e.g. bottom, are evident in all of the graphs. This is due to the unsymmetrical boundary conditions in the experimental settings, that is the direct contact of top surface of samples with air while having a thin layer of glass (almost 1 mm) at the bottom of the vial, Figure 2-11. The increase in thermal

resistance at the bottom of the sample leads to a slight increase in temperature of the material closer to that boundary compared to mirror side of that region with respect to the midpoint.

As shown in Figure 2-18, the peak temperature of the midpoint of the samples with different thicknesses during the curing process tends to decrease by increase in carbon nanotube contents. This trend can be seen in Figure 4-3 for the investigated samples. The slight drop of the peak temperature is attributed to the hindrance effect of carbon nanotubes on the rate of curing reaction discussed in Section 4.2.1. Since heat is released at a lower speed in the samples containing carbon nanotubes compared to pristine resin, the material has more time to dissipate the energy. Also, enhancement in thermal diffusivity of the composite by adding carbon nanotube helps the material to be more efficient in dissipating

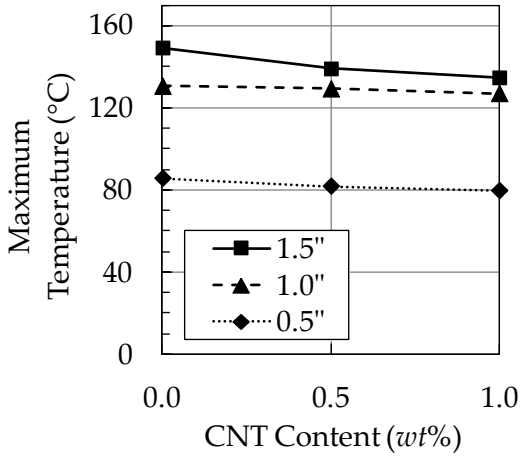

Figure 4-3: Change in midpoint peak temperature of samples with different thicknesses during the curing process by adding CNT (lines just present trends)

heat. Therefore, the temperature at the center of the sample rises slightly less.

Figure 2-19 shows the change in the temperature difference between the midpoint and the outer surface of samples with different CNT concentrations during curing reaction. For 1.5″-thick samples, two peaks are noticeable in the temperature difference between the midpoint and the outer surface of samples. The first peak is a large and sharp increase which is due to the accelerating effect of heat generation on the curing reaction. To understand the sharp drop after the first peak as well as the second peak, the rate of change in temperature of midpoint and surface of the samples should be compared. When midpoint temperature starts to decrease, temperature of the surface is still rising which leads to an opposing rate of change in the temperature and an abrupt decrease in the temperature difference between the midpoint and the outer surface of sample. Shortly after this drop, surface temperature begins to reduce too, but since there is a significant difference between temperature of the surface (T_{surf}) and the ambient temperature (T_{∞}), rate of heat transfer in convection tends to be one order of magnitude higher than that of the conduction near the center of the sample, although convection thermal resistance at the surface can be greater than conduction thermal resistance inside the material. This can be better understood by the following numerical example for the case of pristine resin with 1.5″

thickness:

The rate of heat transfer per unit area in conduction and convection is expressed by Equation (4-1) and (4-2), respectively.

$$q" = k\frac{\partial T}{\partial x} \tag{4-1}$$

$$q" = h\left(T_{\infty} - T_{Surf}\right) \tag{4-2}$$

The ambient temperature is 40°C while the surface temperature of the sample when the midpoint temperature reaches its maximum value is about 140°C. The temperature gradient in Equation (4-1) can be estimated roughly by Equation (4-3) in which Δx is the distance between the midpoint and the adjacent thermocouple.

$$\frac{\partial T}{\partial x} \approx \frac{T_{midpoint} - T_{adjacent\ thermocouple}}{\Delta x} \tag{4-3}$$

Midpoint temperature is 162°C and the temperature of the adjacent point is 160°C. Considering $h = 20\ W/m^2K$ and $k = 0.3\ W/mK$, the heat transfer rate per unit area in conduction is calculated to be about 94 W/m^2 while this value for the convection at the surface is 2000 W/m^2.

Higher cooling rate at the surface of the sample compared to that of the midpoint

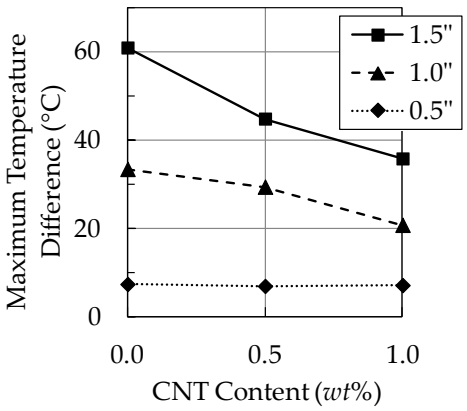

Figure 4-4: Change in the peak of temperature difference between the midpoint and the outer surface of samples with different thicknesses by adding carbon nanotubes (lines just present trends)

leads to a smooth raise in the temperature difference between the midpoint and the outer surface of sample and forms the second peak in the graphs shown in Figure 2-19(a). For 1.0″- and 0.5″-thick samples, Figure 2-19(b) and (c), the second peak does not occur since the temperature difference between the surface of the samples and the ambient air is not large enough to accelerate the cooling rate of the surface.

Figure 4-4 shows the change in the peak of temperature difference between the midpoint and the outer surface of samples with different carbon nanotube contents. 41% reduction in maximum temperature difference between the midpoint and the outer surface of 1.5″-thick samples is observed which is attributed to both slower heat generation and thermal diffusivity enhancement of epoxy by addition of carbon nanotubes. The reduction in maximum temperature

Table 4-1: Graphical aspect ratio of temperature distribution profiles across the thickness of all the investigated samples

CNT (*wt%*)	Graphical Aspect Ratio (°C/in)		
	1.5″	**1.0″**	**0.5″**
0.0	40.5	33.3	14.6
0.5	29.8	29.3	13.7
1.0	23.8	20.7	14.1

difference between the midpoint and the outer surface of 1.0″- and 0.5″-thick samples is 38% and 5%, respectively. Evidently, introduction of carbon nanotubes is more effective in flattening the temperature profile through the thickness of thicker samples.

To visualise the effectiveness of carbon nanotubes in flattening the temperature profile across the thickness of samples a graphical aspect ratio can be defined as the ratio between the length and the height of the temperature distribution profiles across the thickness for each sample, Figure 4-5. The values of this

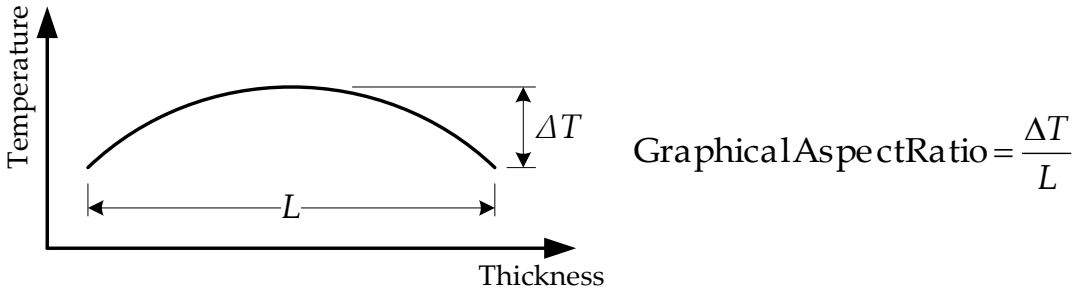

Figure 4-5: Schematic representation of through-the-thickness temperature distribution profile graphical aspect ratio

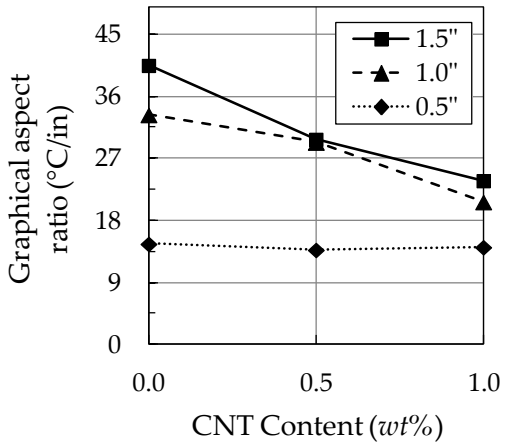

Figure 4-6: Graphical aspect ratio values of temperature distribution profile measurements across the thickness of the investigated samples (lines just present trends)

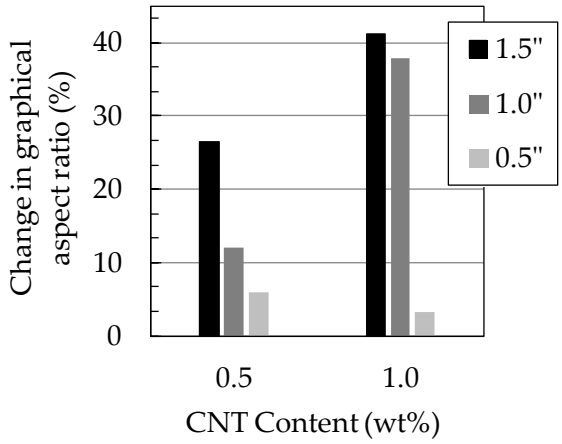

Figure 4-7: Change in the graphical aspect ratio of temperature profile measurements across the thickness for samples containing CNT compared to that of the pristine resin

graphical aspect ratio are presented in Table 4-1 and Figure 4-6. The changes in the graphical aspect ratio of temperature profile across the thickness of samples containing CNT are compared to that of the pristine resin in Figure 4-7.

4.4. HEAT TRANSFER SIMULATION RESULTS

Figure 3-7 and Figure 3-8 respectively illustrate the numerical simulation results for changes in the midpoint temperature and the temperature difference between the midpoint and the outer surface of samples with different thicknesses, during curing reaction by increasing carbon nanotube content. These figures should be compared to Figure 2-18 and Figure 2-19, respectively, which show the measurement results of the same parameters. Figure 4-8 shows this comparison

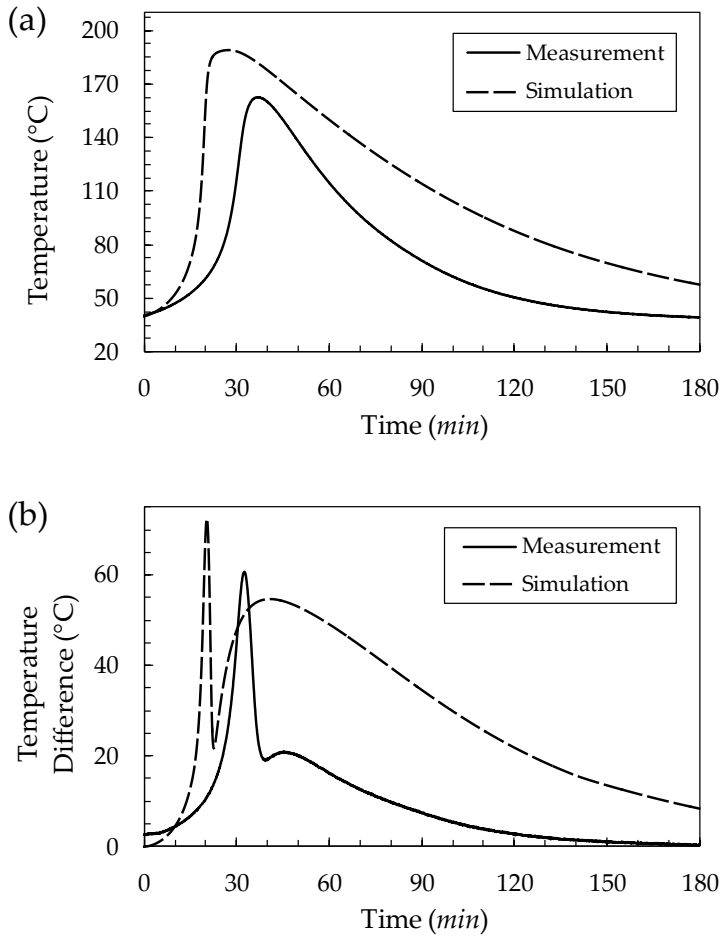

Figure 4-8: Comparing the simulation and measurement of changes in (a) the midpoint temperature and (b) temperature difference between the midpoint and the outer surface of 1.5″-thick sample made of neat resin during curing reaction

only for the 1.5″-thick, neat resin sample. Similar graphs for all of the investigated samples are presented in Appendix D.

The same trend of reduction in measured midpoint peak temperature of the samples with different thicknesses by adding carbon nanotubes which was observed in Figure 2-18 can be seen in Figure 3-7 (as well as figures in Appendix D with index "1"). Nevertheless, the values of maximum temperature are

overestimated by the simulation. This is also evident in Figure 4-8(a). The reason is that the developed model does not consider the mass transfer and changes in the viscosity with temperature while these can influence the reduction of the maximum temperature at the center of the samples. The same reasons can explain steeper increase in the temperature of the midpoint in simulation compared to that of the measurement. Figure 4-9 depicts the simulated values of maximum temperature at midpoint of the investigated samples versus carbon nanotube content as well as those already shown in Figure 4-3. A similar reasoning can explain the higher peaks in Figure 3-8 compared to Figure 2-19 (also Figure 4-8(b) and figures in Appendix D with index "2"). The change in the peak of temperature difference between the midpoint and the outer surface of

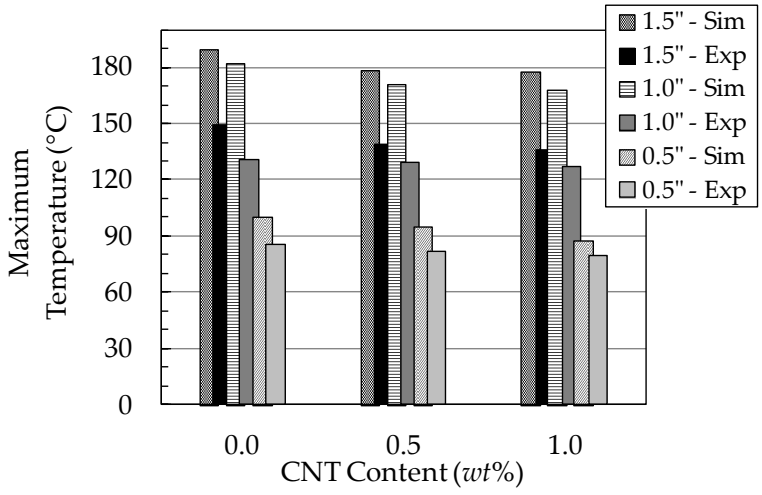

Figure 4-9: Comparison of experimental (Exp) and simulation (Sim) results of change in midpoint peak temperature of samples with different thicknesses during the curing process by adding CNT

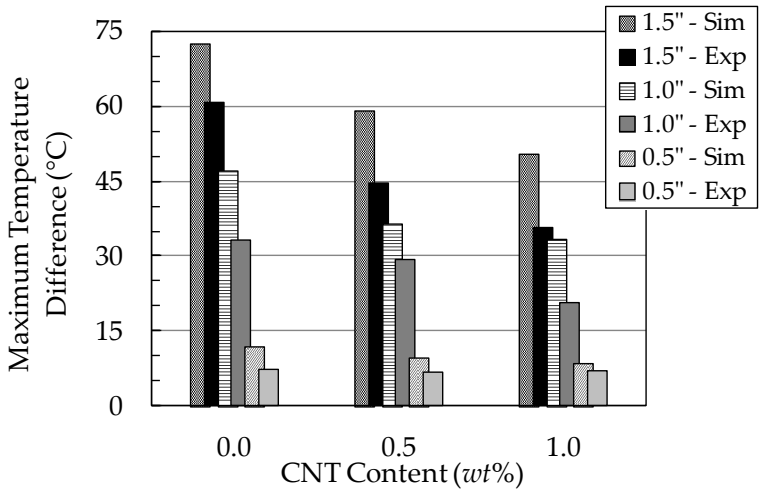

Figure 4-10: Comparison of experimental (Exp) and simulation (Sim) results for change in the peak of temperature difference between the midpoint and the outer surface of samples with different thicknesses by adding carbon nanotubes

samples with different thicknesses by adding carbon nanotubes is compared between the measurement and simulation in Figure 4-10.

Figure 3-7 and Figure 3-8 show shift of graphs on time axis to the right side by increasing carbon nanotube contents which is not observed clearly in the experimental results, i.e. Figure 2-18 and Figure 2-19. This delay in the temperature raise can be attributed, in general, to the overall slowdown of the cure reaction, and in particular, to the increase in activation energy, by adding carbon nanotubes. Nonetheless, the shifting of curves on the time axis is practically difficult to observe since it can be affected by the initial temperature of samples in the measurements which is not perfectly repeatable and has a margin of 6°C (see Section 2.3).

In Figure 3-8(a) and (b) the second peak in the graphs is more pronounced compared to the experimental results, Figure 2-19(a) and (b) because the numerical simulation does not consider variations in the convection heat transfer coefficient, h, of adjacent air to the surface of samples with temperature. In the computer code, this parameter was assumed to be $h = 20\ W/m^2K$. However, variations of convection heat transfer coefficient with temperature is significant and, of course this, in turn, can affect the convection thermal resistance value, drastically.

By substituting the boundaries of variation range of convection heat transfer coefficient as well as the density into the computer code, the sensitivity of the problem to these two parameters can be studied. The published range of variations in convection heat transfer coefficient for free convection is 5 to 25 W/m^2K (Incropera and DeWitt 1985) and Typically, there is 5% shrinkage in epoxy after curing (Hoa, Ouellette and Ngo 2009). For the case of 1.5″-thick pristine resin, when convection heat transfer coefficient and density have their minimum values, the simulated value of the second peak was about 13.3°C while this value for upper limits of convection heat transfer coefficient and density calculated to be more than 35.5°C. Combination of lower limit of convection heat transfer coefficient and upper limit of density yields to 12.8°C for the simulated

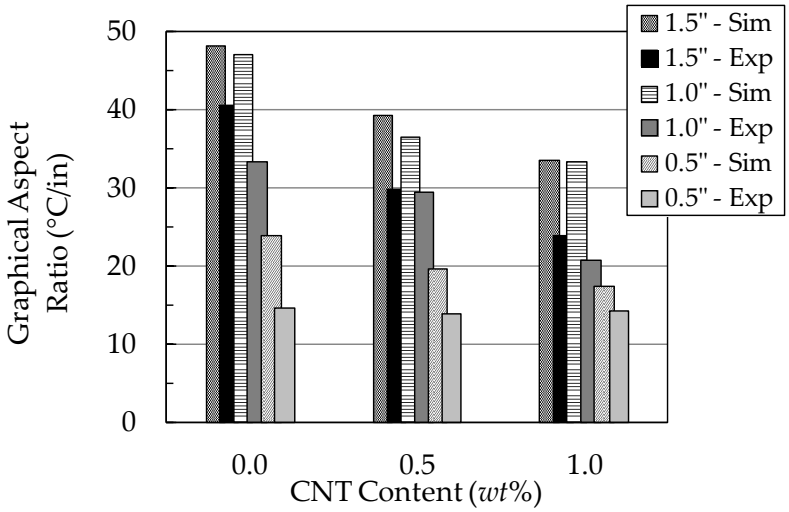

Figure 4-11: Comparison of experimental (Exp) and simulation (Sim) results for graphical aspect ratio values of temperature distribution profile across the thickness of the investigated samples

value of the second peak while the opposite combination of them leads to 35.7°C. Up to 280% change in the value of the second peak within the variation range of convection heat transfer coefficient and density suggests that in order for simulation results to be more realistic, the variations in convection coefficient and density with temperature are critical and need to be taken into account.

Finally, by defining a graphical aspect ratio (GAR) for the simulated temperature distribution profiles, Figure 3-9, similar to that of the experimental measurements (see Section 4.3), the simulated flattening effect of carbon nanotubes on temperature profiles across the thickness of thick thermosets can be examined. Figure 4-11 shows these values obtained from measurements and simulation. Furthermore, the reduction in graphical aspect ratio is compared in

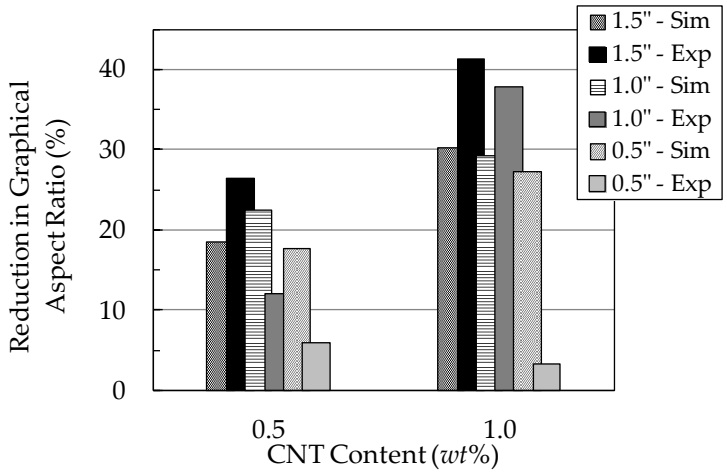

Figure 4-12: Experimental (Exp) and simulation (Sim) results for reduction in the graphical aspect ratio of temperature profile across the thickness for samples containing CNT compared to that of the pristine resin

Figure 4-12 with that of the pristine resin samples for samples containing 0.5 and 1.0 wt% carbon nanotubes which was calculated using Equation (4-4).

$$Change\ in\ GAR = \left|\frac{GAR_{samples\ with\ CNT} - GAR_{Neat\ Resin}}{GAR_{Neat\ Resin}}\right| \tag{4-4}$$

It is evident that the addition of CNTs reduces the graphical aspect ratio for all the cases compared to that of pristine resin.

Chapter 5: CONCLUSION, CONTRIBUTION AND FUTURE WORK

5.1. CONCLUSION

Through-the-thickness temperature distributions of 1.5″-, 1.0″- and 0.5″-thick epoxy EPON 862/EPIKURE 3046 samples made of pristine resin and with 0.5 and 1.0 wt% multiwall carbon nanotube content were measured during their curing process. Results depicted a decrease of 8% in the maximum value of temperature at the midpoint due to adding up to 1.0 wt% of carbon nanotubes to the neat resin. More significantly, the maximum temperature difference between the midpoint and the surface of 1.5″-thick samples dropped by 41% for the same sample (flattening the temperature distribution profile).

Dynamic DSC tests with different heating rates were performed on the samples made of pristine resin and with 0.5 and 1.0 wt% multiwall carbon nanotube content. Here, constants of two-parameter autocatalytic kinetic model for curing reaction were determined using Kissinger's method and least square curve fitting. The results showed a hindrance effect of carbon nanotubes in curing reaction.

Variations of heat capacity and thermal diffusivity with both temperature and carbon nanotube contents were measured. It was shown that by adding up to 1 wt% CNT thermal diffusivity increased by 13% while heat capacity decreased on average about 7%.

The determined cure kinetic equation as well as variation of heat capacity and thermal diffusivity were implemented in an explicit finite difference code to model the transient heat transfer problem. The simulation results showed agreement between the numerical model and the experimental data trends. However, the exact measured values for temperature could not be reproduced well by the computer code. Causes discussed and recommendations for a more precise model were presented.

5.2. CONTRIBUTION

The suggested method to flatten the temperature distribution profile across the thickness of thick thermosets promises potentials in developing manufacturing of structures with varying thickness, from thin to thick in one component which have to be cured in autoclave or room temperature. A very small amount of carbon nanotubes can be added to the thick parts in order for the temperature gradient to stay more uniform through the thickness of the whole component,

which in turn, can minimize warpage and residual stress.

5.3. RECOMMENDATIONS FOR FUTURE WORK

Mass transfer and variation in viscosity with temperature seem to have important roles in a more accurate numerical model.

Density tends to vary significantly during the curing process of epoxy. More precise measurements of that can promise a more accurate model.

Variations in convection heat transfer coefficient of air adjacent to the surface of the samples can affect the convection thermal resistance at the boundary of the problem extensively. This, in turn, can help to predict the changes in the temperature difference between the midpoint and the surface of samples with higher precision.

A more sophisticated computer code can be developed based on the introduced approach in this study to model the heat transfer in two or three spatial dimensions in order to obtain a more realistic values for the temperature distribution.

Although addition of carbon nanotubes was shown to be effective in flattening the temperature distribution across the thickness of thick structures, further

investigation is required to determine the carbon nanotube content impact on mechanical properties. An optimum carbon nanotube concentration can be found to maximize the temperature profile flattening effect, yet to have minimal negative influences on mechanical properties.

BIBLIOGRAPHY

ASTM E 2041. "Standard Method for Estimating Kinetic Parameters by Differential Scanning Calorimetry Using the Borchardt and Daniels Method." West Conshohocken, 2008.

ASTM E 2070. "Standard Test Method for Kinetic Parameters by Differential Scanning Calorimetry Using Isothermal Methods." West Conshohocken, 2008.

Berber, Savas, Young-Kyun Kwon, and David Tománek. "Unusually High Thermal Conductivity of Carbon Nanotubes." *Phys.Rev.Lett.* 84, no. 20 (2000): 4613-4616.

Biercuk, MJ, MC Llaguno, M. Radosavljevic, JK Hyun, AT Johnson, and JE Fischer. "Carbon nanotube composites for thermal management." *Applied Physics Letters* 80, no. 15 (2002): 2767-2769.

Boey, F. Y. C., and W. Qiang. "Experimental modeling of the cure kinetics of an epoxy-hexaanhydro-4-methylphthalicanhydride (MHHPA) system." *Polymer* 41, no. 6 (2000): 2081–2094.

Bogetti, Travis A., and John W. Gillespie. "Process-Induced Stress and Deformation in Thick-Section Thermoset Composite Laminates." *Journal of Composite Materials* 26, no. 5 (1992): 626-660.

Bogetti, Travis A., and John W. Gillespie. "Two-Dimensional Cure Simulation of Thick Thermosetting Composites." *Journal of Composite Materials* 25, no. 3

(1991): 239-273.

Calius, Emilio P., Soo-Yong Lee, and George S. Springer. "Filament Winding Cylinders: II. Validation of the." *Journal of Composite Materials* 24, no. 12 (1990): 1299-1343.

Choi, Jin Ho, and Dai Gil Lee. "Expert Cure System for the Carbon Fiber Epoxy Composite Materials." *Journal of Composite Materials* 29, no. 9 (1995): 1181-1200.

Criado, J.M., and A. Ortega. "Non-isothermal transformation kinetics: Remarks on the Kissinger method." *Journal of Non-Crystalline Solids* 87, no. 3 (1986): 302-311.

Davé, Raju. "A Unified Approach to Modeling Resin Flow During Composite Processing." *Journal of Composite Materials* 24, no. 1 (1990): 22-41.

Dusi, Mark R., Woo I. Lee, Peter R. Ciriscioli, and George S. Springer. "Cure Kinetics and Viscosity of Fiberite 976 Resin." *Journal of Composite Materials* 21, no. 3 (1987): 243-261.

Gojny, Florian H., et al. "Evaluation and identification of electrical and thermal conduction mechanisms in carbon nanotube/epoxy composites." *Polymer* 47, no. 6 (2006): 2036-2045.

Guo, Zhan-Sheng, Shanyi Du, and Boming Zhang. "Temperature field of thick thermoset composite laminates during cure process." *Composites Science and Technology* 65, no. 3-4 (2005): 517-523.

Gutowski, Timothy G., Tadahiko Morigaki, and Zhong Cai. "The Consolidation

of Laminate Composites." *Journal of Composite Materials* 21, no. 2 (1987): 172-188.

Han, Zhidong, and Alberto Fina. "Thermal conductivity of carbon nanotubes and their polymer nanocomposites: A review." *Progress in Polymer Science* 36, no. 7 (2011): 914-944.

Hoa, S.V., P. Ouellette, and T.D. Ngo. "Determination of Shrinkage and Modulus Development of Thermosetting Resins." *Journal of Composite Materials* 43, no. 7 (2009): 783-803.

Hojjati, M., and S.V. Hoa. "Curing simulation of thick thermosetting composites." *Composites Manufacturing* 5, no. 3 (1994): 159-169.

Hong, Wen-Tai, and Nyan-Hwa Tai. "Investigations on the thermal conductivity of composites reinforced with carbon nanotubes." *Diamond and Related Materials* 17, no. 7-10 (2008): 1577-1581.

Incropera, Frank P., and David P. DeWitt. *Introduction to heat transfer.* New York: John Wiley & Sons, Inc., 1985.

Jin, Zhaoxia, K.P. Pramoda, Guoqin Xu, and Suat Hong Goh. "Dynamic mechanical behavior of melt-processed multi-walled carbon nanotube/poly(methyl methacrylate) composites." *Chemical Physics Letters* 337, no. 1-3 (2001): 43-47.

Joshi, S.C., X.L. Liu, and Y.C. Lam. "A numerical approach to the modeling of polymer curing in fibre-reinforced composites." *Composites Science and Technology* 59, no. 7 (1999): 1003-1013.

Kalra, Lokesh, Mark J. Perry, and L.James Lee. "Automation of Autoclave Cure of Graphite-Epoxy Composites." *Journal of Composite Materials* 26, no. 17 (1992): 2567-2584.

Kim, Cheol, Hong Teng, Charles L. Tucker, and Scott R. White. "The Continuous Cuing Process for Thermoset Polymer Composites. Part 1: Modeling and Demonstration." *Journal of Composite Materials* 29, no. 9 (1995): 1222-1253.

Kim, Jin Soo, and Dai Gil Lee. "Development of an Autoclave Cure Cycle with Cooling and Reheating Steps for Thick Thermoset Composite Laminates." *Journal of Composite Materials* 31, no. 22 (1997): 2264-2282.

Kim, Si Hwan, Woo Il Lee, and Joung Man Park. "Assessment of dispersion in carbon nanotube reinforced composites using differential scanning calorimetry." *Carbon* 47, no. 11 (2009): 2699-2703.

Kissinger, H. E. "Reaction Kinetics in Differential Thermal Analysis." *Anal. Chem.* 29, no. 11 (1957): 1702–1706.

LFA 447 Nanoflash™ Instruction Manual. Burlington: NETZSCH Instruments Inc., 2002.

Loos, Alfred C., and George S. Springer. "Curing of Epoxy Matrix Composites." *Journal of Composite Materials* 17, no. 2 (1983): 135-169.

Málek, J., J. šesták, F. Rouquerol, J. Rouquerol, J.M. Criado, and A. Ortega. "Possibilities of two non-isothermal procedures (temperature- or rate-controlled) for kinetical studies." *Journal of Thermal Analysis and Calorimetry* 38, no. 1 (1992): 71-87.

Mamunya, Ye., A. Boudenne, N. Lebovka, L. Ibos, Y. Candau, and M. Lisunova. "Electrical and thermophysical behaviour of PVC-MWCNT nanocomposites." *Composites Science and Technology* 68, no. 9 (2008): 1981-1988.

Mantell, S.C., P.R. Ciriscioli, and G. Almen. "Cure Kinetics and Rheology Models for ICI Fiberite 977-3 and 977-2 Thermosetting Resins." *Journal of Reinforced Plastics and Composites* 14, no. 8 (1995): 847-865.

Moisala, A., Q. Li, I.A. Kinloch, and A.H. Windle. "Thermal and electrical conductivity of single- and multi-walled carbon nanotube-epoxy composites." *Composites Science and Technology* 66, no. 10 (2006): 1285-1288.

Monthioux, Marc, and Vladimir L. Kuznetsov. "Who should be given the credit for the discovery of carbon nanotubes?" *Carbon* 44, no. 9 (2006): 1621-1623.

Oh, Je Hoon, and Dai Gil Lee. "Cure Cycle for Thick Glass/Epoxy Composite Laminates." *Journal of Composite Materials* 36, no. 1 (2002): 19-45.

Park, Hoon Cheol, and Sung W. Lee. "Cure Simulation of Thick Composite Structures Using the Finite Element Method." *Journal of Composite Materials* 35, no. 3 (2001): 188-201.

Parthasarathy, Sanjay, Susan C. Mantell, and Kim A. Stelson. "Estimation, Control and Optimization of Curing in Thick-Sectioned Composite Parts." *Journal of Dynamic Systems, Measurement, and Control* (ASME) 126, no. 4 (2004): 824-833.

Pop, Eric, David Mann, Qian Wang, Kenneth Goodson, and Hongjie Dai. "Thermal Conductance of an Individual Single-Wall Carbon Nanotube above

Room Temperature." *Nano Letters* 6, no. 1 (2006): 96-100.

Prime, R. B. "Thermosts." In *Thermal characterization of polymeric materials*, by E. A. Turi, 435–569. New York: Academic Press, 1997.

Puglia, D., L. Valentini, and J.M. Kenny. "Analysis of the cure reaction of carbon nanotubes/epoxy resin composites through thermal analysis and Raman spectroscopy." *Journal of Applied Polymer Science* 88, no. 2 (2003): 452-458.

Roşu, D., C.N. Caşcaval, F. Mustaţă, and C. Ciobanu. "Cure kinetics of epoxy resins studied by non-isothermal DSC data." *Thermochimica Acta* 383, no. 1-2 (2002): 119-127.

Sbirrazzuoli, N., Y. Girault, and L. Elégant. "The Málek method in the kinetic study of polymerization by differential scanning calorimetry." *Thermochimica Acta* 249 (1995): 179-187.

Shin, D.D., and H.T. Hahn. "A consistent cure kinetic model for AS4/3502 graphite/epoxy." *Composites Part A: Applied Science and Manufacturing* 31, no. 9 (2000): 991-999.

Song, Young Seok, and Jae Ryoun Youn. "Influence of dispersion states of carbon nanotubes on physical properties of epoxy nanocomposites." *Carbon* 43, no. 7 (2005): 1378-1385.

Sourour, S., and M.R. Kamal. "Differential scanning calorimetry of epoxy cure: isothermal cure kinetics." *Thermochimica Acta* 14, no. 1–2 (1976): 41-59.

Tao, Kun, et al. "Effects of carbon nanotube fillers on the curing processes of epoxy resin-based composites." *Journal of Applied Polymer Science* 102, no. 6

(2006): 5248-5254.

Thostenson, Erik T., and Tsu-Wei Chou. "Processing-structure-multi-functional property relationship in carbon nanotube/epoxy composites." *Carbon* 44, no. 14 (2006): 3022-3029.

Thostenson, Erik T., Zhifeng Ren, and Tsu-Wei Chou. "Advances in the science and technology of carbon nanotubes and their composites: a review." *Composites Science and Technology* 61, no. 13 (2001): 1899-1912.

Twardowski, T.E., S.E. Lin, and P.H. Geil. "Curing in Thick Composite Laminates: Experiment and Simulation." 27, no. 3 (1993): 216-250.

Um, Moon-Kwang, Isaac M. Daniel, and Byung-Sun Hwang. "A study of cure kinetics by the use of dynamic differential scanning calorimetry." *Composites Science and Technology* 62, no. 1 (2002): 29-40.

Velasco-Santos, Carlos, Ana L. Martínez-Hernández, Frank T. Fisher, Rodney Ruoff, and Victor M. Castaño. "Improvement of Thermal and Mechanical Properties of Carbon Nanotube Composites through Chemical Functionalization." *Chemistry of Materials* 15, no. 23 (2003): 4470-4475.

White, S.R., and Y.K. Kim. "Staged curing of composite materials." *Composites Part A: Applied Science and Manufacturing* 27, no. 3 (1996): 219-227.

Woo, Il Lee, Alfred C. Loos, and George S. Springer. "Heat of Reaction, Degree of Cure, and Viscosity of Hercules 3501-6 Resin." *Journal of Composite Materials* 16, no. 6 (1982): 510-520.

Xiangqiao Yan. "Finite Element Simulation of Cure of Thick Composite:

Formulations and Validation Verification." *Journal of Reinforced Plastics and Composites* 27, no. 4 (2008): 339-355.

Xie, Hongfeng, Binghua Liu, Zuanru Yuan, Jianyi Shen, and Rongshi Cheng. "Cure kinetics of carbon nanotube/tetrafunctional epoxy nanocomposites by isothermal differential scanning calorimetry." *Journal of Polymer Science Part B: Polymer Physics* 42, no. 20 (2004): 3701-3712.

Xu, Donghua, and Zhigang Wang. "Role of multi-wall carbon nanotube network in composites to crystallization of isotactic polypropylene matrix." *Polymer* 49, no. 1 (2008): 330-338.

Yi, Sung, and Harry H. Hilton. "Effects of Thermo-Mechanical Properties of Composites on Viscosity, Temperature and Degree of Cure in Thick Thermosetting Composite Laminates during Curing Process." *Journal of Composite Materials* 32, no. 7 (1998): 600-622.

Yi, Sung, H.H. Hilton, and M.F. Ahmad. "A finite element approach for cure simulation of thermosetting matrix composites." *Computers & Structures* 64, no. 1-4 (1997): 383-388.

Yu, Aiping, Palanisamy Ramesh, Xiaobo Sun, Elena Bekyarova, Mikhail E. Itkis, and Robert C. Haddon. "Enhanced Thermal Conductivity in a Hybrid Graphite Nanoplatelet - Carbon Nanotube Filler for Epoxy Composites." *Advanced Materials* 20, no. 24 (2008): 4740-4744.

APPENDICES

APPENDIX A: Rate of cure versus temperature for DSC tests

Rate of cure of pristine resin samples as well as those with 0.5, 1.0 and 1.5 wt% CNT contents in DSC tests for heating rates of (a) 1, (b) 2, (c) 5, (d) 7, (e) 10, (f) 15 and (g) 20 °C/min.

Note: For clarity, the scale of the vertical axis adjusted according to the range of changes in the graphs.

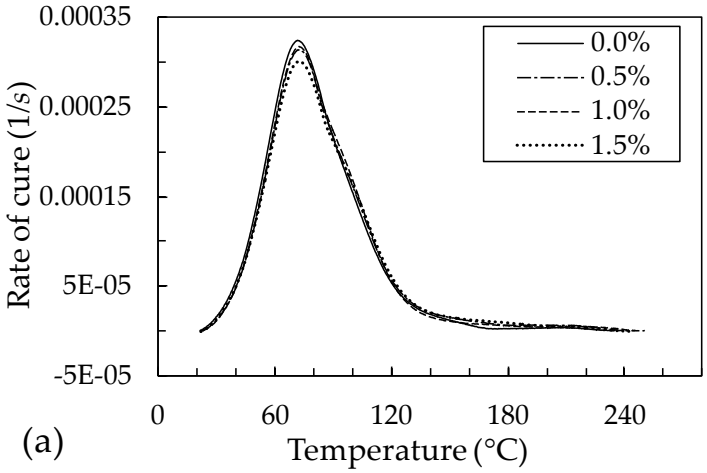

(a)

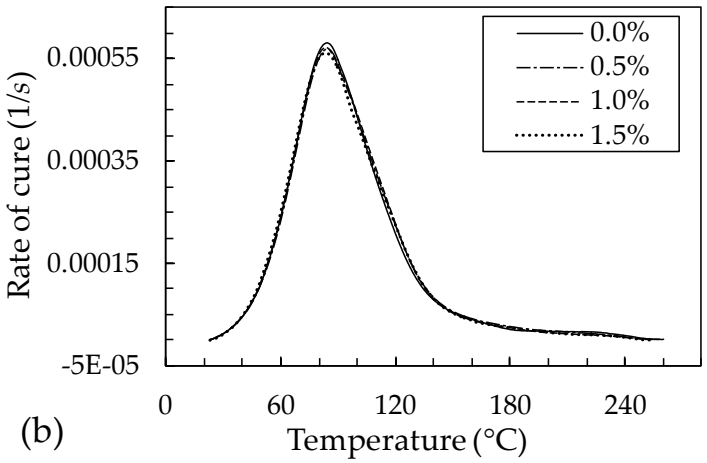
0.0%
0.5%
1.0%
1.5%
Rate of cure (1/s)
0.00055
0.00035
0.00015
-5E-05
0
60
120
180
240
Temperature (°C)

(b)

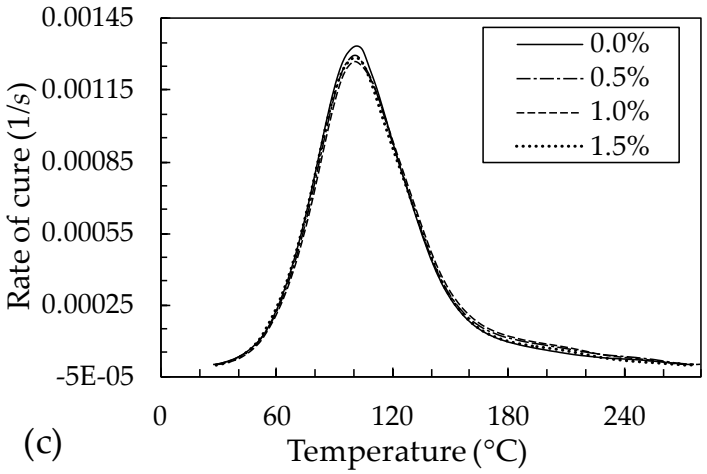
0.0%
0.5%
1.0%
1.5%
Rate of cure (1/s)
0.00145
0.00115
0.00085
0.00055
0.00025
-5E-05
0
60
120
180
240
Temperature (°C)

(c)

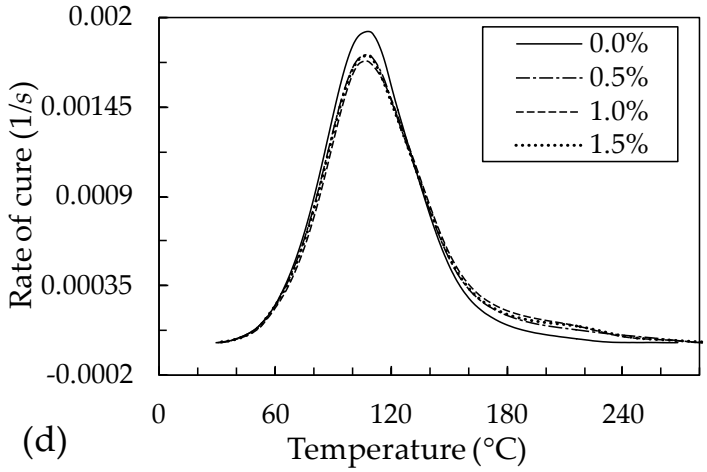
0.0%
0.5%
1.0%
1.5%
Rate of cure (1/s)
0.002
0.00145
0.0009
0.00035
-0.0002
0
60
120
180
240
Temperature (°C)

(d)

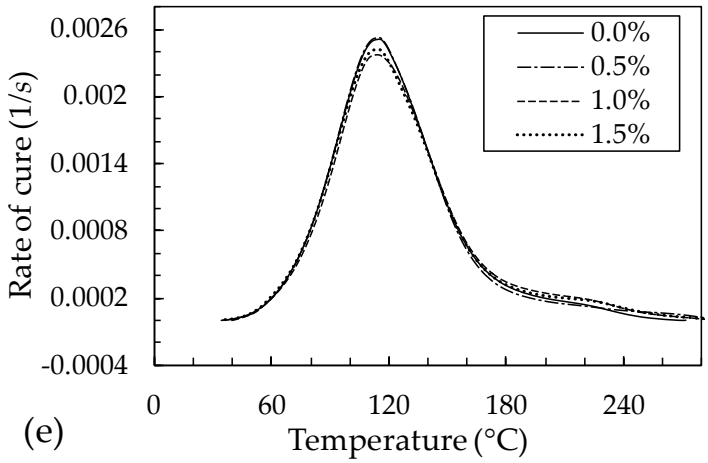
0.0026
0.002
0.0014
0.0008
0.0002
-0.0004
Rate of cure (1/s)
0
60
120
180
240
Temperature (°C)
0.0%
0.5%
1.0%
1.5%

(e)

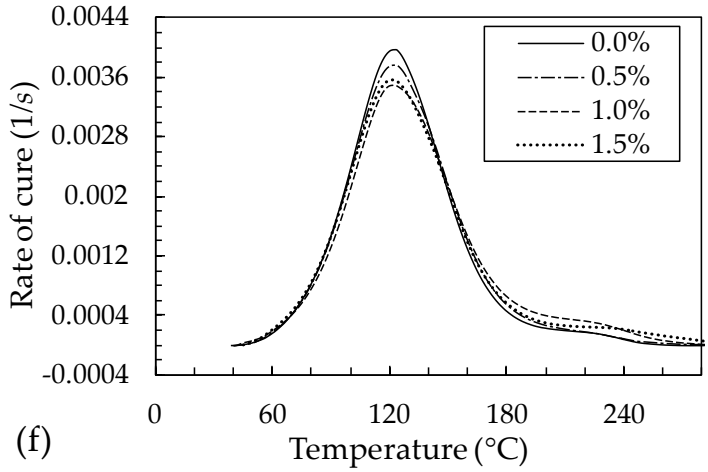
0.0044
0.0036
0.0028
0.002
0.0012
0.0004
-0.0004
Rate of cure (1/s)
0
60
120
180
240
Temperature (°C)
0.0%
0.5%
1.0%
1.5%

(f)

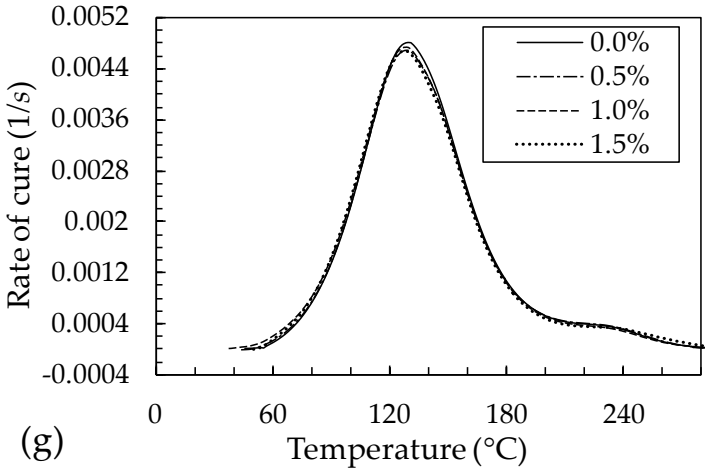
0.0052
0.0044
0.0036
0.0028
0.002
0.0012
0.0004
-0.0004
Rate of cure (1/s)
0
60
120
180
240
Temperature (°C)
0.0%
0.5%
1.0%
1.5%

(g)

APPENDIX B: Degree of cure versus temperature for DSC tests

Degree of cure of pristine resin samples as well as those with 0.5, 1.0 and 1.5 wt% CNT contents in DSC tests for heating rates of (a) 1, (b) 2, (c) 5, (d) 7, (e) 10, (f) 15 and (g) 20 °C/min.

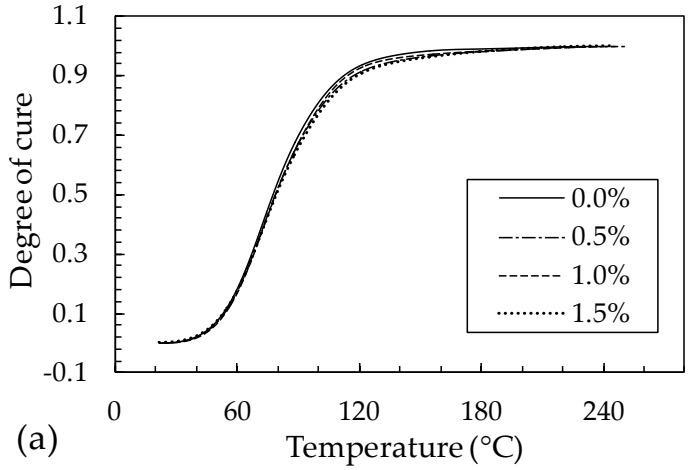

(a)

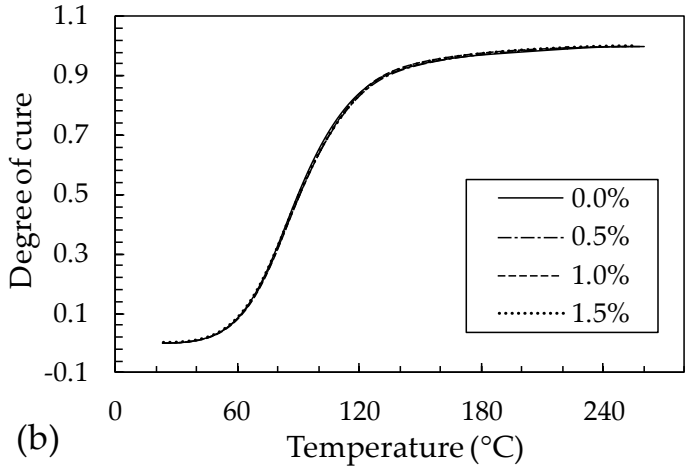

(b)

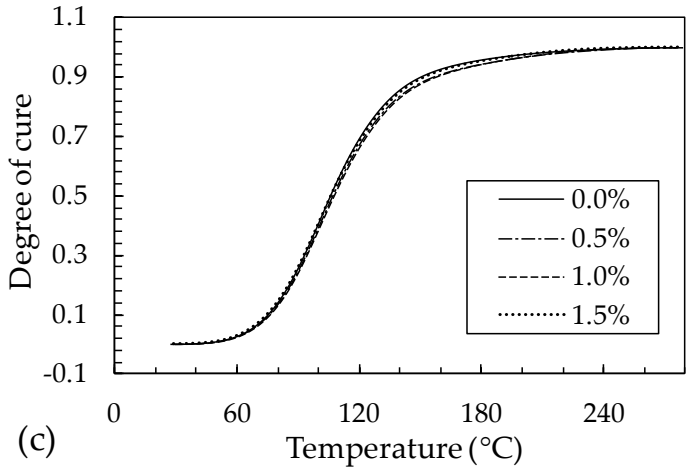
1.1
0.9
0.7
0.5
0.3
0.1
-0.1
Degree of cure
0.0%
0.5%
1.0%
1.5%
0
60
120
180
240
Temperature (°C)

(c)

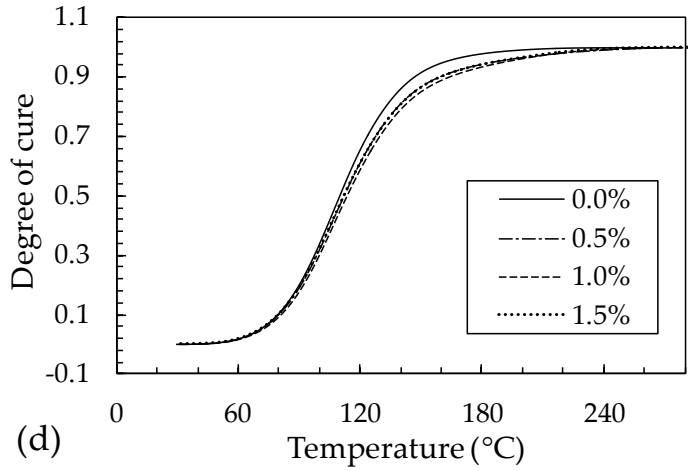
1.1
0.9
0.7
0.5
0.3
0.1
-0.1
Degree of cure
0.0%
0.5%
1.0%
1.5%
0
60
120
180
240
Temperature (°C)

(d)

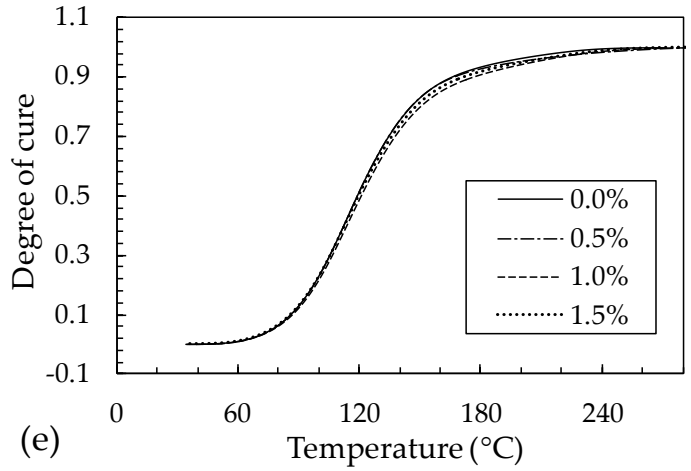
1.1
0.9
0.7
0.5
0.3
0.1
-0.1
Degree of cure
0.0%
0.5%
1.0%
1.5%
0
60
120
180
240
Temperature (°C)

(e)

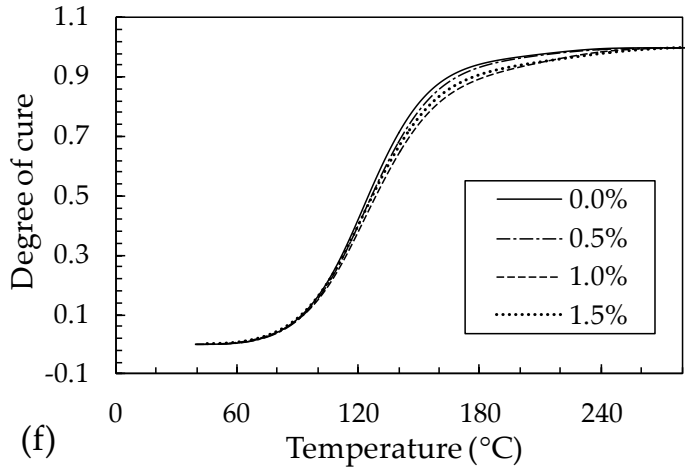
1.1
0.9
0.7
0.5
0.3
0.1
-0.1
Degree of cure
0
60
120
180
240
Temperature (°C)
0.0%
0.5%
1.0%
1.5%

(f)

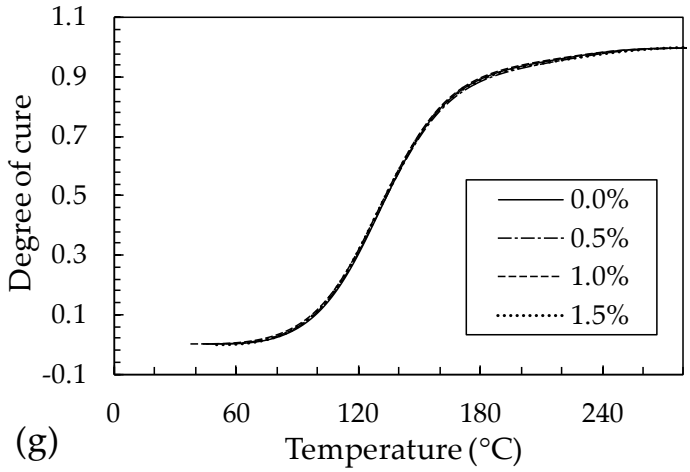
1.1
0.9
0.7
0.5
0.3
0.1
-0.1
Degree of cure
0
60
120
180
240
Temperature (°C)
0.0%
0.5%
1.0%
1.5%

(g)

APPENDIX C: Measured temperature profile across the thickness

Temperature profile at $t_{\Delta T_{max}}$ in three repetitions of measurements across the thickness of each sample:

(lines are just to present the trend)

- (a) Neat resin - 1.5″
- (b) Neat resin - 1.0″
- (c) Neat resin - 0.5″
- (d) 0.5 wt% CNT - 1.5″
- (e) 0.5 wt% CNT - 1.0″
- (f) 0.5 wt% CNT - 0.5″
- (g) 1.0 wt% CNT - 1.5″
- (h) 1.0 wt% CNT - 1.0″
- (i) 1.0 wt% CNT - 0.5″
- (j) 1.5 wt% CNT - 1.5″
- (k) 1.5 wt% CNT - 1.0″
- (l) 1.5 wt% CNT - 0.5″

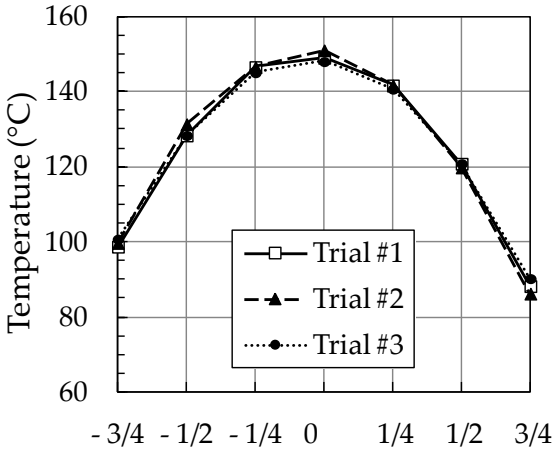
160
140
120
100
80
60
Temperature (°C)
Trial #1
Trial #2
Trial #3
- 3/4 - 1/2 - 1/4 0 1/4 1/2 3/4
Distance from midpoint (*inch*)

(a)

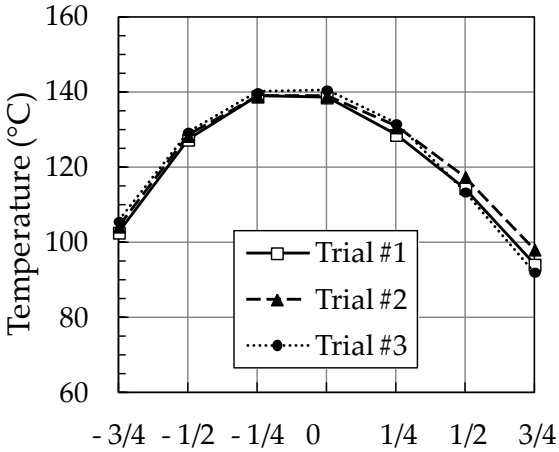
160
140
120
100
80
60
Temperature (°C)
Trial #1
Trial #2
Trial #3
- 3/4 - 1/2 - 1/4 0 1/4 1/2 3/4
Distance from midpoint (*inch*)

(d)

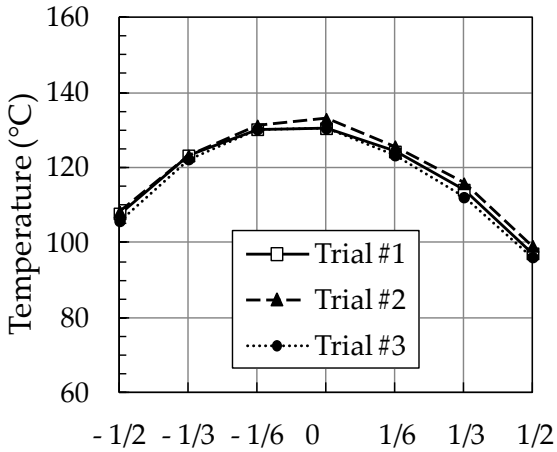
160
140
120
100
80
60
Temperature (°C)
Trial #1
Trial #2
Trial #3
- 1/2 - 1/3 - 1/6 0 1/6 1/3 1/2
Distance from midpoint (*inch*)

(b)

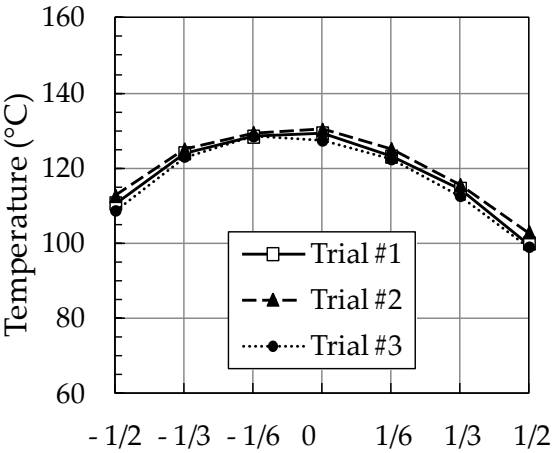
160
140
120
100
80
60
Temperature (°C)
Trial #1
Trial #2
Trial #3
- 1/2 - 1/3 - 1/6 0 1/6 1/3 1/2
Distance from midpoint (*inch*)

(e)

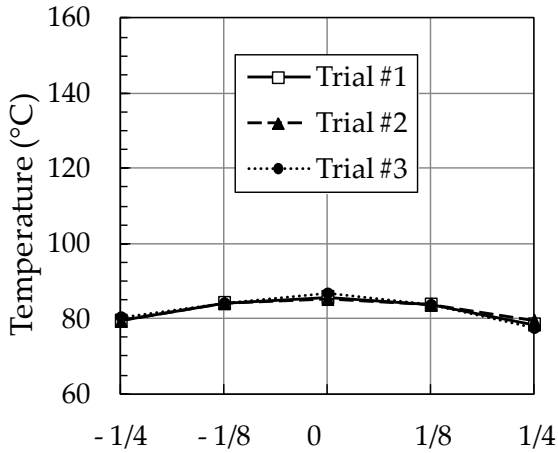
160
140
120
100
80
60
Temperature (°C)
Trial #1
Trial #2
Trial #3
- 1/4 - 1/8 0 1/8 1/4
Distance from midpoint (*inch*)

(c)

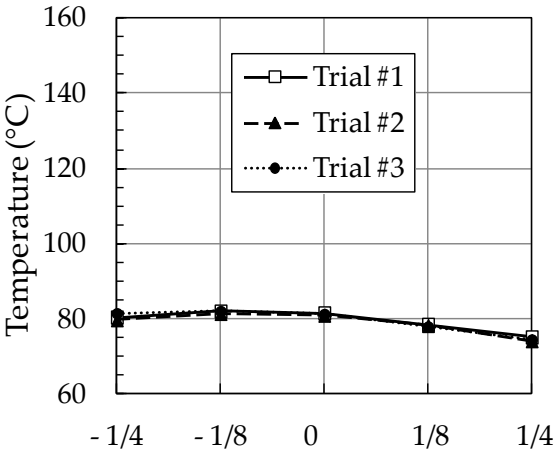
160
140
120
100
80
60
Temperature (°C)
Trial #1
Trial #2
Trial #3
- 1/4 - 1/8 0 1/8 1/4
Distance from midpoint (*inch*)

(f)

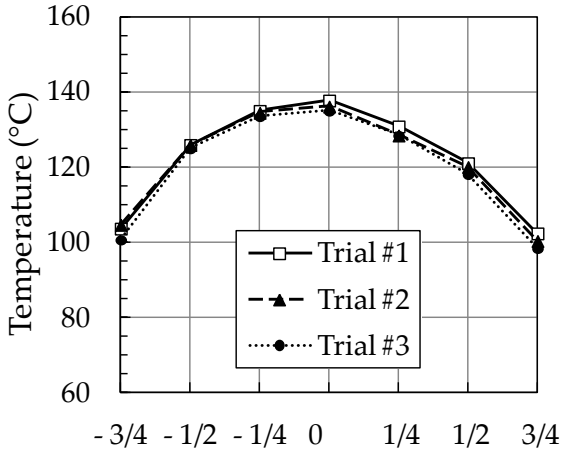
160
140
120
100
80
60
Temperature (°C)
Trial #1
Trial #2
Trial #3
- 3/4 - 1/2 - 1/4 0 1/4 1/2 3/4
Distance from midpoint (*inch*)

(g)

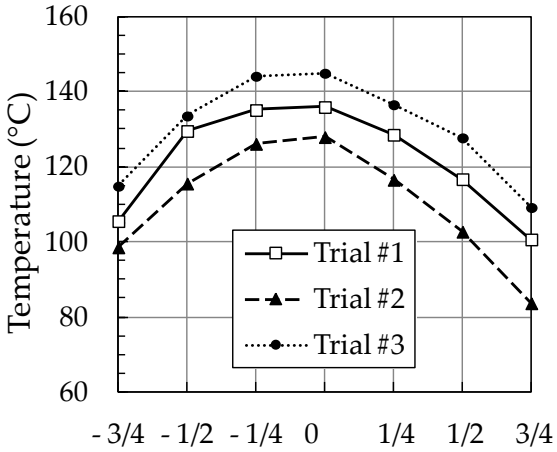
160
140
120
100
80
60
Temperature (°C)
Trial #1
Trial #2
Trial #3
- 3/4 - 1/2 - 1/4 0 1/4 1/2 3/4
Distance from midpoint (*inch*)

(j)

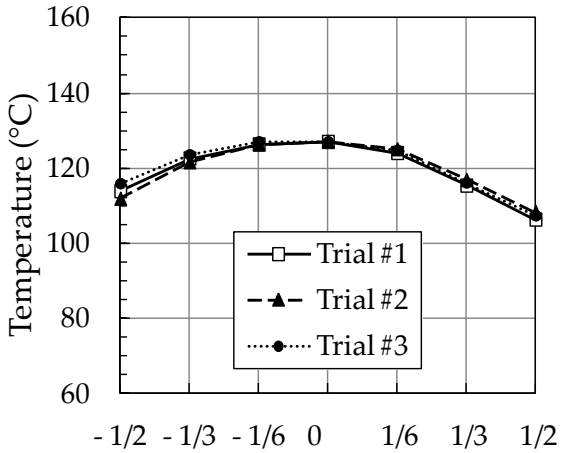
160
140
120
100
80
60
Temperature (°C)
Trial #1
Trial #2
Trial #3
- 1/2 - 1/3 - 1/6 0 1/6 1/3 1/2
Distance from midpoint (*inch*)

(h)

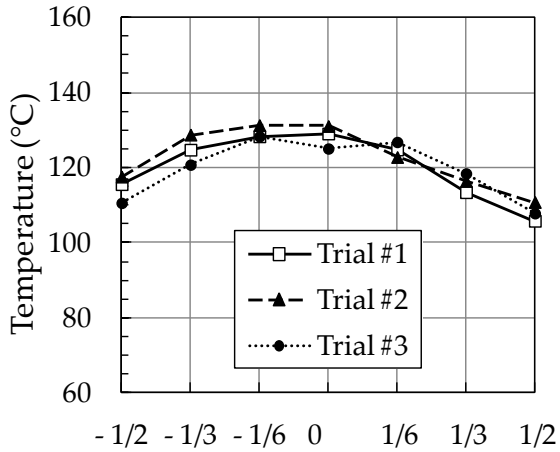
160
140
120
100
80
60
Temperature (°C)
Trial #1
Trial #2
Trial #3
- 1/2 - 1/3 - 1/6 0 1/6 1/3 1/2
Distance from midpoint (*inch*)

(k)

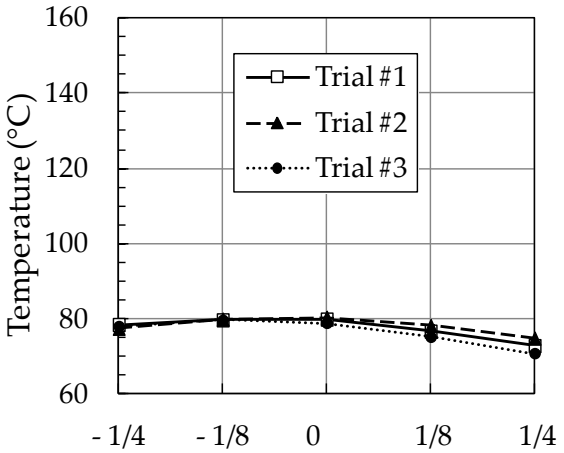
160
140
120
100
80
60
Temperature (°C)
Trial #1
Trial #2
Trial #3
- 1/4 - 1/8 0 1/8 1/4
Distance from midpoint (*inch*)

(i)

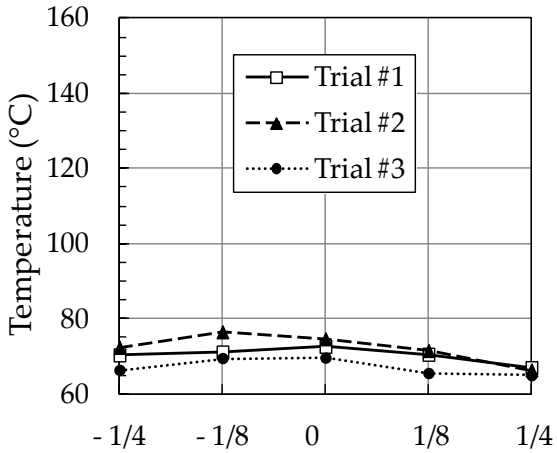
160
140
120
100
80
60
Temperature (°C)
Trial #1
Trial #2
Trial #3
- 1/4 - 1/8 0 1/8 1/4
Distance from midpoint (*inch*)

(l)

APPENDIX D: Variations of midpoint temperature and temperature difference (simulation and measurement)

Comparison of the simulation and measurement of changes in the midpoint temperature (figure numbers with index 1) and temperature difference between the midpoint and the outer surface (figure numbers with index 2) during curing reaction for the following samples:

- (a) 1.5″ - Neat resin
- (b) 1.5″ - 0.5 wt% CNT
- (c) 1.5″ - 1.0 wt% CNT
- (d) 1.0″ - Neat resin
- (e) 1.0″ - 0.5 wt% CNT
- (f) 1.0″ - 1.0 wt% CNT
- (g) 0.5″ - Neat resin
- (h) 0.5″ - 0.5 wt% CNT
- (i) 0.5″ - 1.0 wt% CNT

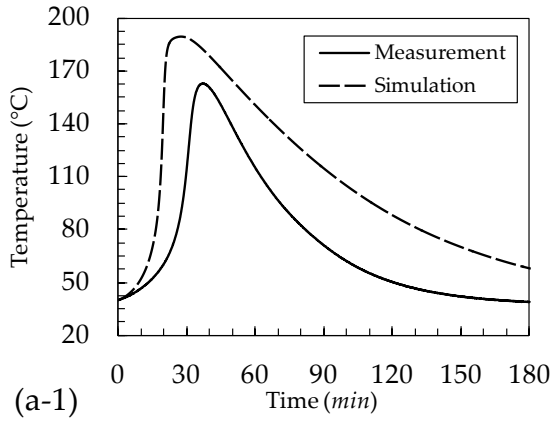

(a-1)

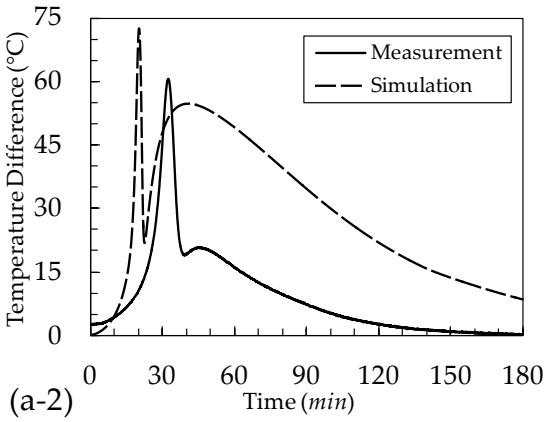

(a-2)

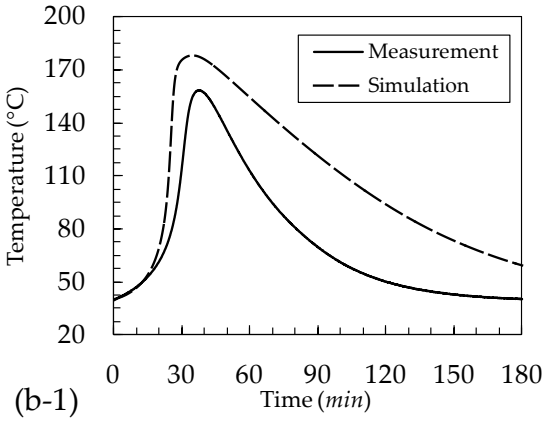

(b-1)

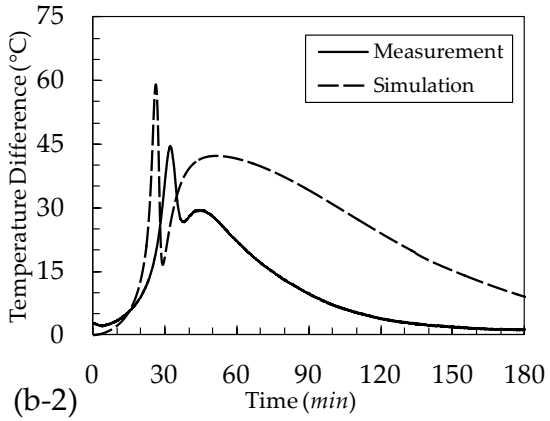

(b-2)

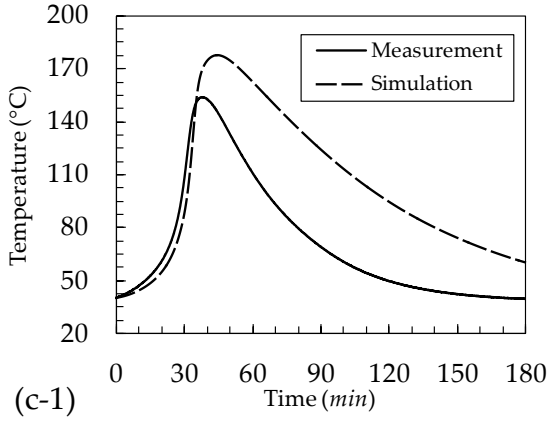

(c-1)

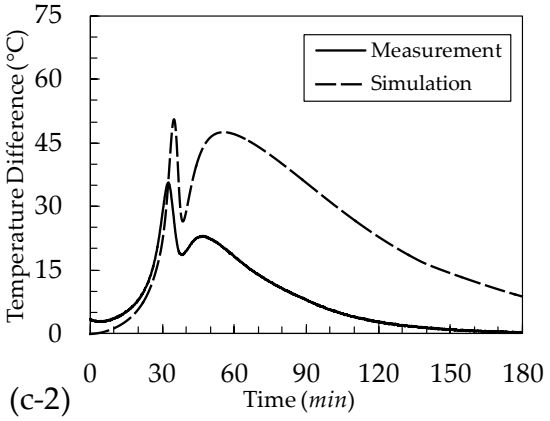

(c-2)

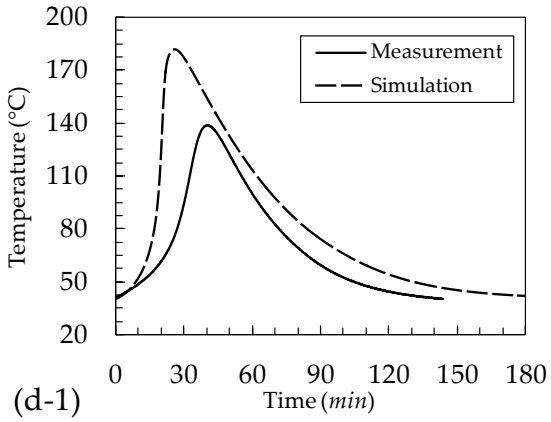

(d-1)

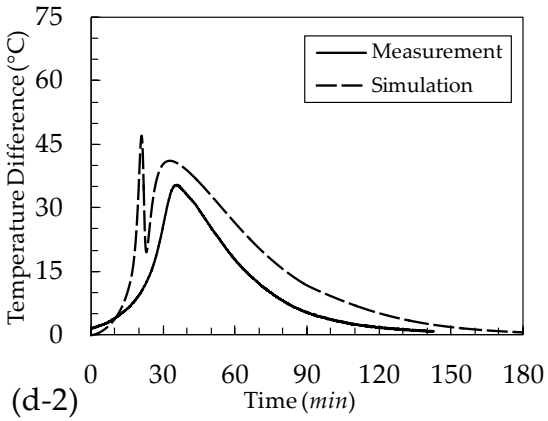

(d-2)

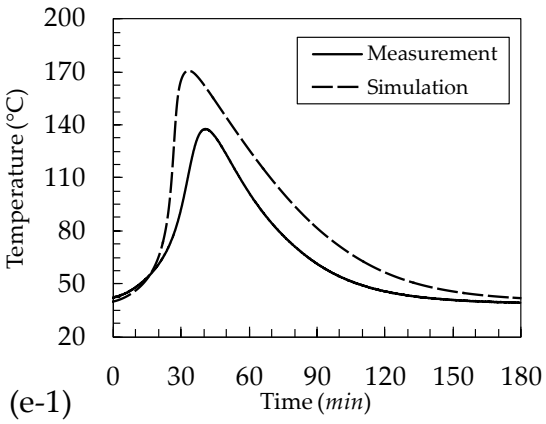

(e-1)

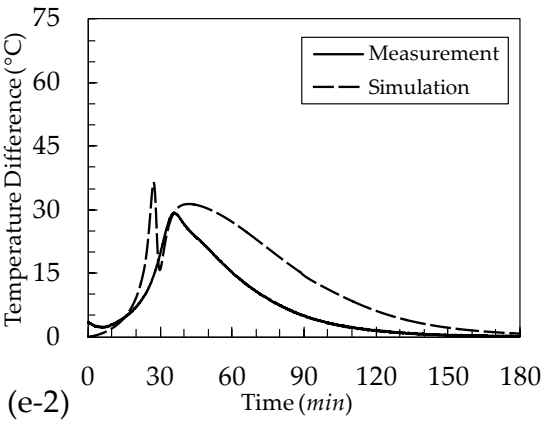

(e-2)

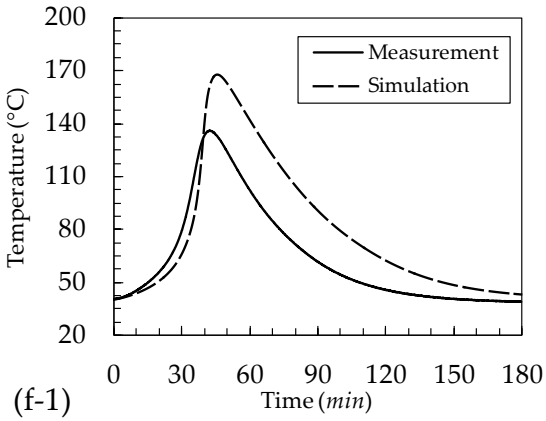

(f-1)

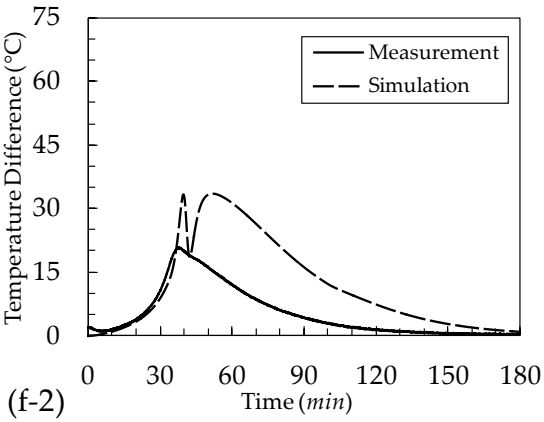

(f-2)

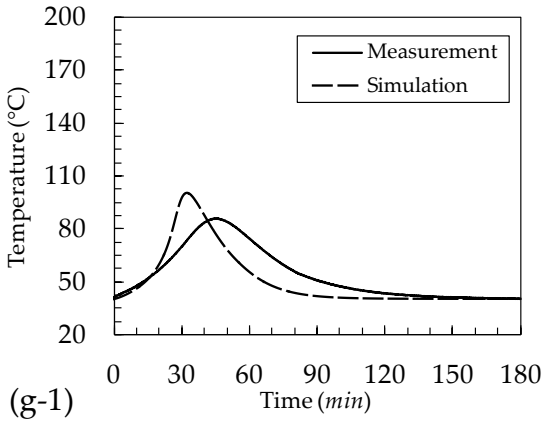

(g-1)

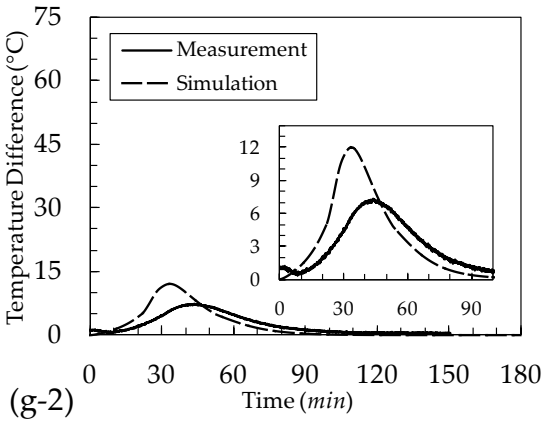

(g-2)

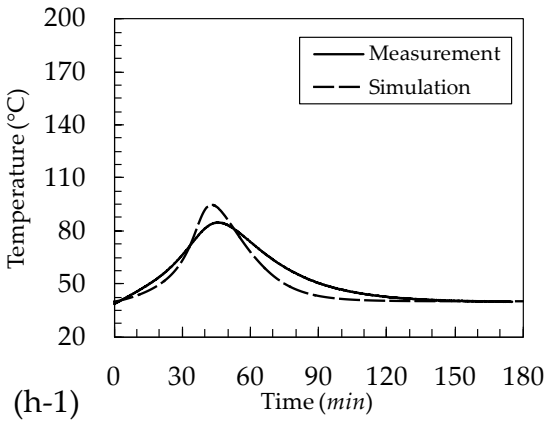

(h-1)

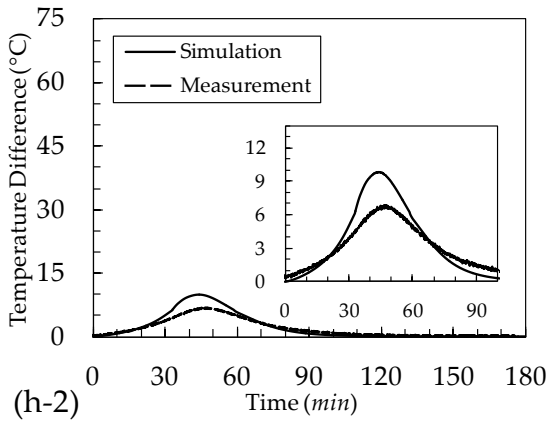

(h-2)

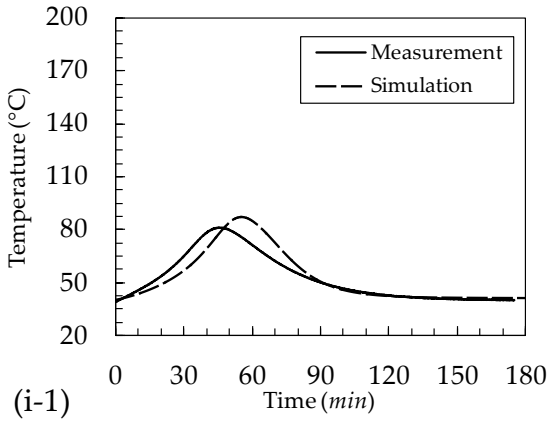

(i-1)

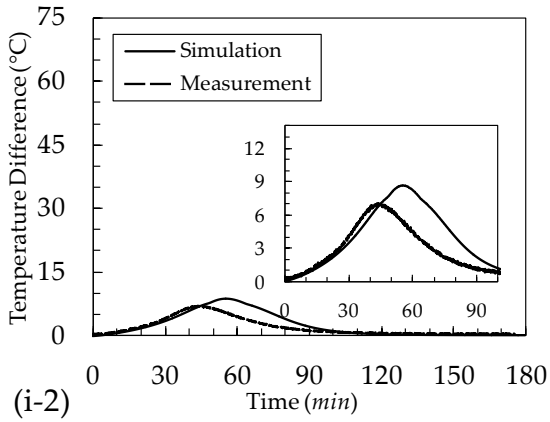

(i-2)

APPENDIX E: Computer code

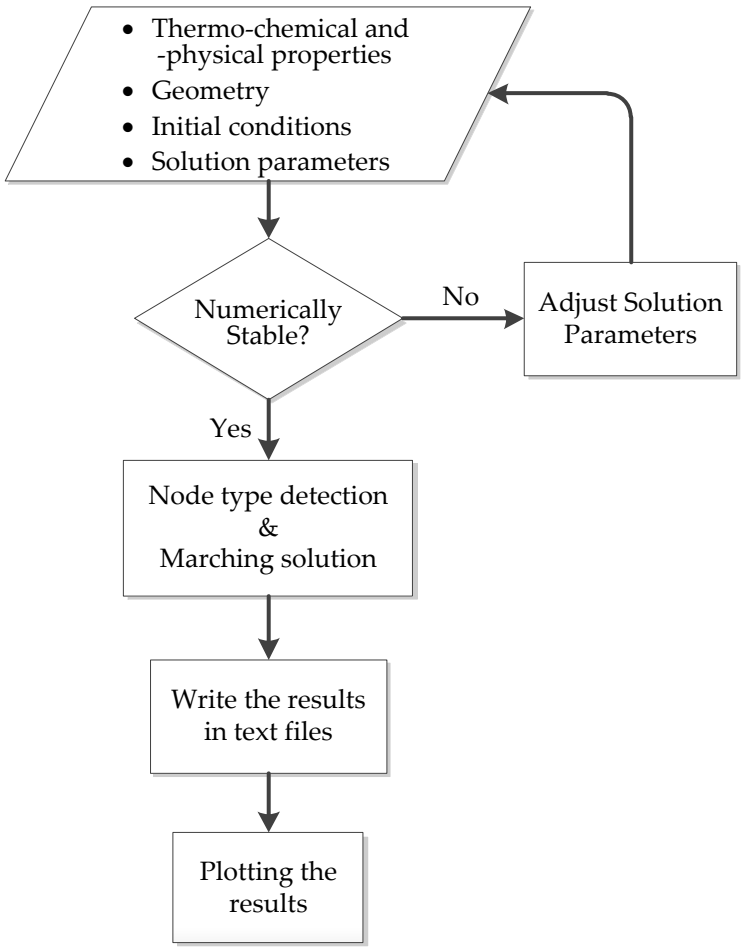

Computer code for the case of 1.5"-thick samples for neat resin:

0% CNT - 1.5"

```
> restart:
  with(plots):
  with(plottools):
  Digits := 20:
```

Material Properties

```
Resin
> k  := 0.329:              #(W/m.K)
  ro := 1159.:       #(kg/m^3)
  Cp := 1612.8:             #(J/kg.K)
  Cp1 := T -> 0.2708 * T^2 - 158.7 * T + 24755.:
  Cp2 := T -> 5.5567 * T + 403.87:
```

```
lambda := 0.119e-6:
ThDi := T -> 3.7272727273E-12 * T^2 - 0.0000000031080272727 * T +
0.00000072677148386:

Ambient
> h := 20.0:        #(W/m^2.K)
```

Cure Kinetics

```
Constants
> A1 := 221822.2:          #(1/s)
  R  := 8.314:             #(kJ/kmol.K)
  E1 := 54169.9 / R:       #(J/mol)
  HR := 400.4:             #(J/g) Total heat of reaction
  m := 0.322:
  n := 2.073:


Kinetic Equation
> Dalpha   := (T, alpha) -> A1 * exp(-E1/T) * (1 - alpha)^n * alpha^m:
```

Curing Cycle

```
> Troom := 40 + 273.15:
  Tac := 40 + 273.15:
```

Geometry and Solution Parameters

```
Meshing and Solution Variable Initialization
> Tik := 1.5 * 2.54e-2:    #Total thickness (m)
  TD  := 40:               #Number of desired divisions across the
                            thickness (necessarily an EVEN number)
  SP  := 180:              #Desired solution period (min)
  TSL := 2:                #Time step length(s)
  Dt  := TSL:
  Dx  := Tik / TD:  #Spatial mesh length
  p   := SP * 60 / TSL:    #Number of time increments
  N   := TD/2 + 1:  #Number of Spatial increments (symmetric
                    condition)
  Temp:= Matrix(p, N):
  DoC := Matrix(p, N):
  RoC := Matrix(p, N):
```

Constant Numbers and Stability Conditions

```
Constant Numbers
> Fo := k * Dt / (ro * Cp * Dx^2);
  Bi := h * Dx / k:
  Fo * (1 + Bi);


Stability Condition
> convert(Fo <= 1/2, 'truefalse');
  convert(Fo * (1 + Bi) <= 1/2, 'truefalse');

  if (convert(Fo <= 1/2, 'truefalse')) = false
  or (convert(Fo * (1 + Bi) <= 1/2, 'truefalse')) = false then     print(`Error:
Unstable Solution`) end if;
```

Solution

```
Resin initial temperature, degree of cure and rate of cure
> TextFile1 := fopen("Temp.txt", WRITE):
```

```
  TextFile2 := fopen("DoC.txt", WRITE):
  TextFile3 := fopen("RoC.txt", WRITE):

  fprintf(TextFile1, "%g\t", 0):
  fprintf(TextFile2, "%g\t", 0):
  fprintf(TextFile3, "%g\t", 0):

for i from 1 to N do
       Temp[1, i] := Troom:
       DoC [1, i] := 0.001:
       RoC [1, i] := Dalpha(Temp[1, i], DoC[1, i]):

       if i = N then
              fprintf(TextFile1, "%g\n", Temp[1, i]):
              fprintf(TextFile2, "%g\n", DoC[1, i]):
              fprintf(TextFile3, "%g\n", RoC[1, i]):
       else
              fprintf(TextFile1, "%g\t", Temp[1, i]):
              fprintf(TextFile2, "%g\t", DoC[1, i]):
              fprintf(TextFile3, "%g\t", RoC[1, i]):
       end if:

end do:

Resin temperature, degree of cure and rate of cure
> for i from 2 to p do:
       fprintf(TextFile1, "%g\t", (i-1)*Dt/60):
       fprintf(TextFile2, "%g\t", (i-1)*Dt/60):
       fprintf(TextFile3, "%g\t", (i-1)*Dt/60):

       for j from 1 to N do:
              if j = 1 then
              Temp[i, j]   := (1 - 2 * (lambda*Dt/Dx^2) - 2 * (h*Dt/(ro*Cp*Dx)))
* Temp[i-1, j]
                     + 2 * (lambda*Dt/Dx^2) * Temp[i-1, j+1]
                     + 2 * (h*Dt/(ro*Cp*Dx)) * Tac
                     + (Dt * HR * 1000 / Cp) * Dalpha(Temp[i-1, j], DoC[i-1,j]):
              fprintf(TextFile1, "%g\t", Temp[i, j]):

              elif j = N then
              Temp[i, j]   := (1 - 2 * (lambda*Dt/Dx^2)) * Temp[i-1, j]
                     + 2 * (lambda*Dt/Dx^2) * Temp[i-1, j-1]
                     + (Dt * HR * 1000 / Cp) * Dalpha(Temp[i-1, j], DoC[i-1,j]):
              fprintf(TextFile1, "%g\n", Temp[i, j]):

              else
              Temp[i, j]   := (1 - 2 * (lambda*Dt/Dx^2)) * Temp[i-1, j]
                     + (lambda*Dt/Dx^2) * (Temp[i-1, j-1] + Temp[i-1, j+1])
                     + (Dt * HR * 1000 / Cp) * Dalpha(Temp[i-1, j], DoC[i-1,j]):
              fprintf(TextFile1, "%g\t", Temp[i, j]):
              end if:

              DoC[i, j] := DoC[i-1, j] + Dalpha(Temp[i-1, j], DoC[i-1, j]) * Dt:
              RoC[i, j] := Dalpha(Temp[i, j], DoC[i, j]):

              if j = N then
                     fprintf(TextFile2, "%g\n", DoC[i, j]):
                     fprintf(TextFile3, "%g\n", RoC[i, j]):
              else
                     fprintf(TextFile2, "%g\t", DoC[i, j]):
                     fprintf(TextFile3, "%g\t", RoC[i, j]):
```

```
            end if:

if Temp[i, j] < (75+273.15) then
      Cp := Cp1(Temp[i, j]):
else
      Cp := Cp2(Temp[i, j]):
end if:

lambda := ThDi(Temp[i, j]):

      end do:
end do:

fclose(TextFile1):
fclose(TextFile2):
fclose(TextFile3):
```

Expanded Text Files

```
> ExpTextFile1 := fopen("ExpTemp.txt", WRITE):
  ExpTextFile2 := fopen("ExpDoC.txt", WRITE):
  ExpTextFile3 := fopen("ExpRoC.txt", WRITE):

for i from 1 to p do
      fprintf(ExpTextFile1, "%g\t", (i-1)*Dt/60):
      fprintf(ExpTextFile2, "%g\t", (i-1)*Dt/60):
      fprintf(ExpTextFile3, "%g\t", (i-1)*Dt/60):

      for j from 1 to 2*(N-1)+1 do

            if j <> 2*(N-1)+1 then
                  if j<=N then
                        fprintf(ExpTextFile1, "%g\t", Temp[i, j] - 273.15):
                        fprintf(ExpTextFile2, "%g\t", DoC[i, j]):
                        fprintf(ExpTextFile3, "%g\t", RoC[i, j]):
                  else
                        fprintf(ExpTextFile1, "%g\t", Temp[i, 2*N-j] -
273.15):
                        fprintf(ExpTextFile2, "%g\t", DoC[i, 2*N-j]):
                        fprintf(ExpTextFile3, "%g\t", RoC[i, 2*N-j]):
                  end if:
            else
                  fprintf(ExpTextFile1, "%g\n", Temp[i, 2*N-j] - 273.15):
                  fprintf(ExpTextFile2, "%g\n", DoC[i, 2*N-j]):
                  fprintf(ExpTextFile3, "%g\n", RoC[i, 2*N-j]):
            end if:
      end do:
end do:

fclose(ExpTextFile1):
fclose(ExpTextFile2):
fclose(ExpTextFile3):
```

Ploting

Temperature of midpoint vs. the time of solution

```
> desired_point := N:      #th node through the thickness
  x_Const := Matrix(p, 2):

for i from 1 to p do
      x_Const[i, 1] := (i-1) * Dt / 60:
      x_Const[i, 2] := Temp[i, desired_point] - 273.15:
```

```
end do:

pointplot(x_Const, labels = [`Time (min)`, `Temperature (C)`],
labeldirections=[horizontal, vertical], symbol = point, labelfont =
[PalatinoLinotype, 17], font = [PalatinoLinotype, 14]);

desired_point := 1: #th node through the thickness
x_Const1 := Matrix(p, 2):

for i from 1 to p do
       x_Const1[i, 1] := (i-1) * Dt / 60:
       x_Const1[i, 2] := Temp[i, desired_point] - 273.15:
end do:

pointplot(x_Const1, labels = [`Time (min)`, `Temperature (C)`],
labeldirections=[horizontal, vertical], symbol = point, labelfont =
[PalatinoLinotype, 17], font = [PalatinoLinotype, 14]);

Temperature difference between the outer surface and midpoint of the sample vs.
the time of solution
> desired_point := N:      #th node through the thickness
  del_temp := Matrix(p, 2):

for i from 1 to p do
       del_temp[i, 1] := (i-1) * Dt / 60:
       del_temp[i, 2] := Temp[i, N] - Temp[i, 1]:
end do:

pointplot(del_temp, labels = [`Time (min)`, `Temperature Difference (C)`],
labeldirections=[horizontal, vertical], symbol = point, labelfont =
[PalatinoLinotype, 14], font = [PalatinoLinotype, 14]);

Temperature profile when the maximum temperature difference between the outer
surface and midpoint of the sample occurs
> del := 0.:
for i from 1 to p do
       if del_temp[i, 2] > del then
              del := del_temp[i, 2]:
              desired_time := del_temp[i, 1]
       end if:
end do:


3D plot: Temperature versus time through the thickness
TempExp := Matrix(p, 2*(N-1)+1):
for i from 1 to p do
       for j from 1 to 2*(N-1)+1 do
              if j<=N then
                     TempExp[i, j] := Temp[i, j] - 273.15
              else
                     TempExp[i, j] := Temp[i, 2*N-j] - 273.15
              end if:
       end do:
end do:

ee := matrixplot(TempExp, labels = [`Time (Time-step #)`, `Thickness (Node #)`,
`Temperature (K)`], axes = box, style = point, color = black):
scaling := scale(ee, Dt/60, Dx*1000, 1):
display(scaling, labels = [`Time (min)`, `Thickness (mm)`, `Temperature (C)`],
labelfont = [Verdana, bold, 12], labeldirections = [horizontal, horizontal,
vertical], font = [Verdana, bold, 12], orientation = [-50, 68]);
```